U.PORTO
FEUP FACULDADE DE ENGENHARIA
UNIVERSIDADE DO PORTO

U.PORTO
INSTITUTO DE CIÊNCIAS
BIOMÉDICAS ABEL SALAZAR
UNIVERSIDADE DO PORTO

Printable brain

A bioprinting approach to mimic the astrocytic extracellular environment

Master Dissertation

Integrated Master in Bioengineering

Specialization in Molecular Biotechnology

Author:

Mariana Martins Costa e Silva

Supervisor:

Prof. Ana Paula Pêgo

Co-Supervisor:

Eva Maia Carvalho

Porto, November 2020

Printable brain

A bioprinting approach to mimic the astrocytic extracellular environment

Mariana Martins Costa e Silva

Dissertation submitted to Faculdade de Engenharia da Universidade do Porto and to Instituto de Ciências Biomédicas Abel Salazar to obtain the degree of

Masters in Bioengineering

Final version

Porto, November 2020

Institutional Acknowledgements

The work presented in this dissertation was financially supported by:

- Project NORTE-01-0145-FEDER-000008 and NORTE-01-0145-FEDER-000012, supported by Norte Portugal Regional Operational Programme (NORTE 2020), under the PORTUGAL 2020 Partnership Agreement, through the European Regional Development Fund (ERDF) and FEDER - Fundo Europeu de Desenvolvimento Regional funds through the COMPETE 2020 - Operacional Programme for Competitiveness and Internationalisation (POCI), Portugal 2020;
- Portuguese funds through FCT/MCTES in the framework of the project "Institute for Research and Innovation in Health Sciences" (POCI-01-0145-FEDER-007274);
- National Funds through FCT – Fundação para a Ciência e a Tecnologia (UTAPEXPL/NTec/0057/2017).

The authors acknowledge the support of the i3S Scientific Platform Bioimaging, member of the national infrastructure PPBI - Portuguese Platform of Bioimaging (PPBI-POCI-01-0145-FEDER-022122).

The liquid handler (JANUS with a 4 Tip dispensing arm and a Modular Dispense Technology™) could be used thanks to the Portuguese Network for Screening (PT-OPENSCREEN).

Acknowledgements

Durante estes cincos anos do Mestrado Integrado em Bioengenharia cresci muito como pessoa, e a nível profissional. Foram anos que me ensinaram muito sobre a importância da ciência de base, mas também da sua aplicação no mundo real, e como essa aplicação reflete quem somos a nível individual e da sociedade.

Primeiramente, gostaria de agradecer à professora Ana Paula Pêgo, pela oportunidade de aprender e trabalhar para a minha tese no nBTT, e pelo apoio presentado durante a sua realização. Obrigada, também, por salientar que a bioengenharia tem muitas aplicações para lá da academia, e que a ciência não está confinada apenas nas Universidades, mas acontece também na Indústria, e que há espaço para nós nos dois ambientes.

À Eva Carvalho, pelo incansável apoio, paciência e positivismo durante estes meses, mesmo quando eu própria começava a duvidar. Obrigada por me teres acolhido neste projeto que te é tão querido, e por me teres mostrado a importância das células da glia. Obrigada ao Miguel Morais pela ajuda no trabalho laboratorial, principalmente quando COVID veio tornar difícil acabar o trabalho todo no meu turno.

A todos os membros do nBTT, pelo caloroso acolhimento apesar das circunstâncias e disponibilidade para ajudar. Em particular, obrigada à Beatriz Custódio pelo desenvolvimento das placas de 24 poços para o printing; e à Sofia Guimarães por me ter ajudado a acabar as experiências quando tive de entrar em isolamento profilático.

Ao António Pombinho, do serviço Biosciences Screening, pela disponibilidade para a criação do protocolo do printing, da sua otimização e pelo manuseamento do equipamento; bem como pelo interesse mostrado e pelas sugestões para melhorar o trabalho. Agradeço também à María Lázaro, do serviço Bioimaging, pela ajuda com o microscópio confocal, e ao Ricardo Vidal Silva, do serviço Biointerfaces and Nanotechnology, pela ajuda com o reómetro.

À professora Cristina Barrias e ao Marco Araújo, do grupo Bioengineered 3D Microenvironments, pelo desenvolvimento dos alginatos e por os terem cedido para o desenvolvimento deste projeto.

A um nível mais pessoal, gostaria de agradecer às pessoas que me acompanharam ao longo destes anos.

À Francisca, Leonor, Sofia, Beatriz, Andreia, Joana e a Renata que tornaram estes anos mais alegres e memoráveis. E a todos os meus colegas que também estiveram no i3s, obrigada pelos

pequenos momentos de conversa durante o trabalho, que em muito ajudaram a quebrar o stress do dia-a-dia.

Aos meus pais, Marília e Mário, e ao meu irmão, Luís, por me ouvirem quando precisava de desabafar, e por sempre me encorajarem a seguir em frente e a lutar pelos meus sonhos.

Abstract

Demyelinating diseases, like multiple sclerosis (MS), are related with the loss of the myelin sheath and subsequently neurodegeneration. At the early stages of these diseases, there are cycles of myelin loss (demyelination) and production of new myelin (remyelination). However, at a certain point the remyelination process fails and the reasons underneath are still not fully understood.

While remyelination is performed by oligodendrocyte progenitor cells (OPCs), other glial cells also play an important role throughout the process of de- and remyelination. Astrocytes, specifically, are peculiarly affected during the processes that lead to demyelination. These cells switch their phenotype and start oversecreting a series of factors and extracellular matrix (ECM) proteins in a process named astrogliosis. At the same time, astrocytes are responsible for the creation of a glial scar, a structure with completely altered biophysical and mechanical properties. These changes in the stiffness of the lesioned site might be the missing key to understand remyelination failure. Our working hypothesis is that by targeting the mechanical properties changes during demyelination one would be able to promote remyelination. This may provide a novel therapeutic approach for the development of efficient treatments against demyelinating diseases.

One of the major hurdles in addressing the role of the ECM mechanical properties on demyelination is the lack of suitable models that uncouple the biochemical signals from cellular functions. Current models to mimic the glial scar are either oversimplified 2D models or animal models which do not allow the specific study of matrix alterations without the biochemical signalling impact.

Here, a novel tissue engineered platform to mimic the ECM environment of astrogliosis and at the same time to allow for the high-throughput screening of biological and therapeutical targets is explored. Briefly, this platform is composed by an alginate matrix where primary rat astrocytes were embedded. Hydrogel formation and cellular behavior were evaluated both manually and automatically recurring to an extrusion-based dispenser to mimic 3D bioprinting processes. Alginate was used either in its pure state or as a mix of modified alginate with a cell adhesion (RGD, at 40 μM) and a matrix metalloproteinase sensitive peptide (PVGLIG) at two distinct concentrations (200 and 400 μM).

In this work it is shown that all cell laden alginate formulations had a stiffness similar with the brain parenchyma. Additionally, the modified alginates presented delayed gelation times which constitutes an advantage towards the development of a printing-like protocol to produce

alginate discs. More importantly, astrocytes cultured in modified alginates discs had increased cellular metabolic activity, unaffected viability, and a morphology similar to that observed *in vivo.*

Due to technical problems in the customized alginate bioprinter fabrication, an adapted system using a liquid dispenser was created as a setup to test the polymer printability and its effects on astrocytes. Under the tested conditions the printing process had a significant impact on the cellular viability and survival. Nevertheless, astrocytes remain functional as observed by the expression of their characteristic marker (glial fibrillary acidic protein, GFAP) and the process extension on modified alginates. The successful printing of the hydrogels is an initial proof that it is possible to bioprint astrocytes in the tested alginate formulations. Moreover, these results are the motto to pursue with further studies on bioprinting approaches for the development of central nervous system (CNS) biological relevant *in vitro* models.

We present a pioneer bioprinting-like approach to automatically create 3D alginate-based matrices for the growing of astrocytes. Overall, the work presented in this dissertation constitutes a technical advance in the development of high-throughput platforms for screening therapeutical targets involved in astrogliosis processes and consequently in demyelinating diseases.

Keywords: demyelination; glial scar; astrocytes; alginate; 3D model; bioprinting; tissue engineering

Sumário

As doenças desmielinizantes, como a esclerose múltipla, estão relacionadas com a perda da bainha de mielina, e subsequente neurodegeneração. Nas fases inicias destas doenças, existem ciclos de perda (desmielinização) e produção de nova mielina (remielinização). No entanto, num certo momento o processo de remielinização falha, e as razões por detrás disso ainda não estão completamente entendidas.

Embora a remielinização é feita pelas células progenitoras de oligodendróticos, as outras células da glia também têm um papel importante no processo de des- e remielinização. Os astrócitos, em particular, são especialmente afetados durante o processo que leva à desmielinização. Estas células mudam o seu fenótipo, e passam a secretar, em grandes quantidades, uma série de fator e proteínas da matriz extracelular, num processo chamado de astrogliose. Ao mesmo tempo, os astrócitos são responsáveis pela criação da cicatriz glial, uma estrutura com propriedades biofísicas e mecânicas alteradas. Esta alteração da rigidez das lesões pode ser a informação que faltava para perceber a falha da remielinização. A nossa hipótese é que agindo sobre as propriedades mecânicas alteradas durante a desmielinização, é possível promover a remielinização. Isto constituiria uma nova opção terapêutica para o desenvolvimento de tratamento eficazes contra as doenças desmielinizantes.

Um dos maiores obstáculos no estudo do papel das propriedades da matriz extracelular na desmielinização é a falta de modelos adequados, que separam os sinais bioquímicos das funções celulares. Os modelos atuais que mimetizam a cicatriz glial são, ou modelos 2D muito simplicados, ou modelos animais, que não permitem o estudar especificamente as alterações da matriz sem o impacto da sinalização bioquímica.

Aqui, é explorada uma nova plataforma de engenharia de tecidos que permita mimetizar o ambiente da matriz extracelular em astrogliose e, ao mesmo tempo, o rastreio de alto rendimento de alvos biológicos e terapêuticos. Sumariamente, esta plataforma é constituída por uma matriz de alginato, onde astrócitos primários de rato são inseridos. A formação dos hidrogeis e o comportamento celular foram avaliados, quer manualmente, quer automaticamente, recorrendo a um dispensador baseado na extrusão para aproximar o processo de bioimpressão 3D. O alginato foi usado quer no seu estado puro, quer misturado com alginato modificado com péptidos para adesão celular (RGD, a 40 μM) e sensíveis a metaloproteinases da matriz (PVGLIG), em duas concentrações distintas (200 e 400 μM).

Neste trabalho, é mostrado que todas as formulações de alginato têm uma rigidez semelhante à do parênquima cerebral. Além disso, os alginatos modificados apresentaram tempos de

gelificação maiores, o que constitui uma vantagem aquando do desenvolvimento de um protoloco de impressão para produzir discos de alginato. Os astrócitos cultivados no alginato modificado tinham maiores níveis de atividade metabólica, não tiveram a sua viabilidade afetada, e apresentaram uma morfologia semelhante àquela que é observada *in vivo*.

Devido a problemas técnicos relacionadas com a produção de uma bioimpressora de alginato personalizada, um sistema adaptado usando um dispensador de líquidos foi desenvolvido para testar a possibilidade de imprimir o polímero e os seus efeitos nos astrócitos. Nestas condições, o processo de impressão teve um impacto significativo na atividade metabólica e sobrevivência das células. Mesmo assim, os astrócitos mantiveram-se funcionais, como se observa pela expressão do seu marcador característico (proteína glial fibrilar ácida, GFAP), e a presença, nos alginatos modificados, de extensões de processos. O sucesso na impressão dos hidrogéis, é uma prova inicial que é possível bioimprimir os astrócitos nas formulações testadas. Além do mais, estes resultados são uma base para estudos futuros de bioimpressão para o desenvolvimento de modelos biológicos *in vitro* relevantes do sistema nervoso central.

Aqui apresentamos uma aproximação pioneira a um sistema de bioimpresão, para criar automaticamente matrizes 3D baseadas em alginato, que permitam o crescimento de astrócitos. De uma forma geral, o trabalho apresentado nesta dissertação constitui um avanço técnico no desenvolvimento de plataformas de rastreio de alto rendimento para a procura de alvos terapêuticos envolvidos na astrogliose e, consequentemente, em doenças desmielinizantes.

Palavras-chave: desmielinização; cicatriz glial; astrócitos; alginato; modelo 3D; bioimpressão; engenharia de tecidos

Table of contents

List of Images

List of Tables

List of Abbreviations

ANOVA ANalysis of VAriance

BBB	Blood-Brain Barrier
BDNF	Brain-Derived Neurotrophic Factor
BSA	Bovine Serum Albumin
CIS	Clinically Isolated Syndrome
CNS	Central Nervous System
CNTF	Ciliary Neurotrophic Factor
CNTs	Carbon Nanotubes
CSPGS	Chondroitin Sulfate Proteoglycans
DMEM	Dulbecco's Modified Eagle's Medium
DMSO	Dimethyl Sulfoxide
DRG	Dorsal Root Ganglions
EAE	Experimental Autoimmune Encephalomyelitis
ECM	Extracellular Matrix
Eph	Ephrins
ESCs	Embryonic Stem Cells
EtBr	Ethidium Bromide
FBS	Foetal Bovine Serum
FDM	Fused Deposition Modelling
FGF-2	Fibroblast Growth Factor 2
GAG	Glycosaminoglycan
GDL	δ- Gluconolactone
GDNF	Glial Cell-Derived Neurotrophic Factor
GelMA	Methacryloyl-Modified Gelatin
GFAP	Glial Fibrillary Acidic Protein

HA	Hyaluronic Acid
HBSS	Hank's Balanced Salt Solution
HEPES	4-(2-hydroxyethyl)-1-piperazineethanesulfonic acid
hiPSCs	Human Induced Pluripotent Stem Cells
IFNγr	Interferon Gamma Receptor
IFN-γ	Interferon Gamma
IGF-1	Insulin-Like Growth Factor-1
IL	Interleukin
iPSCs	Induced Pluripotent Stem Cells
LPC	Lysophosphatidylcholine (Lysolecithin)
LPS	Lipopolysaccharide
LVR	Linear Viscoelastic Region
MeDex	Methacrylated Dextran
MeHp	Methacrylated Heparin
MGCs	Mixed Glial Cultures
MMPs	Matrix Metalloproteinases
MOG	Myelin Oligodendrocyte Glycoprotein
MP-PFA	Microtubule Protecting Paraformaldehyde
MS	Multiple Sclerosis
MW	Molecular Weight
MWCNT	Multiwalled Carbon Nanotubes
NDS	Normal Donkey Serum
NG2	Neuron-Glial Antigen 2
NOS	Nitric Oxide Synthase
NPCs	Neural Progenitor Cells
NSCs	Neural Stem Cells
NT3	Neurotrophin-3

OLs	Oligodendrocytes
OPCs	Oligodendrocyte Precursor Cells
P/S	Penicillin/Streptavidin
PμSL	Projection Micro-Stereolithography
PBS	Phosphate Buffered Saline
PDGF	Platelet-Derived Growth Factor
PDMS	Poly(dimethyl)siloxane
PEDOT	Poly(3,4-ethylenedixoxythiophene)
PEDOT:PSS	Poly(3,4-ethylenedixoxythiophene):Poly(styrene sulfonate)
PEG	Poly(ethylene glycol)
PEGDA	Poly(ethylene glycol) Diacrylate
PEGDMA	Poly(ethylene glycol) dimethacrylate
PET	Poly(ethylene terephthalate)
PIPES	Piperazine-N,N'-Bis(2-ethanesulfonic acid)
PLL	Poly(L-lysine)
PNS	Peripheral Nervous System
PP	Poly(propylene)
PPMS	Primary Progressive Multiple Sclerosis
PPy	Poly(pyrrole)
RRMS	Relapsing-Remitting Multiple Sclerosis
RT	Room Temperature
SPMS	Secondary Progressive Multiple Sclerosis
TBS	Tris-Buffered Saline
TCPS	Tissue Culture Poly(styrene)
TGF	Transforming Growth Factor
TIMPs	Tissue Inhibitors of Metalloproteinases
TLR	Toll-like Receptor

TMEV	Theiler's Murine Encephalomyelitis Virus
TNF	Tumor Necrosis Factor
TrkB	Tropomyosin-Related Kinase
UV	Ultraviolet
VEGF	Vascular Endothelial Growth Factor
Vim	Vimentin

List of Symbols

G*	Complex shear modulus
G’	Shear modulus storage (elastic component)
G’’	Shear modulus loss (viscous component)
E	Young’s modulus
δ	Phase angle
ν	Poisson’s ratio
ξ	Mesh size

Chapter 1- Introduction

1.1. De- and re-myelination processes in the central nervous system (CNS)

Multiple sclerosis (MS) is a chronic inflammatory disease of the central nervous system (CNS) associated with the loss of the myelin sheath, and subsequently neurodegeneration [1]. In 2016, there were an estimated 2,2 million MS cases worldwide, and around 18 thousand deaths associated with the majority of cases being reported in Northern Europe and North America (Fig. 1) [2]. MS is a disease whose first symptoms manifest normally when the patient is around 30 years old, evolving in the coming decades. As such, the symptoms are felt during a significant portion of the patients life, and include optic neuritis, diplopia, sensory loss, limb weakness, gait ataxia, loss of bladder control, and cognitive dysfunction [2].

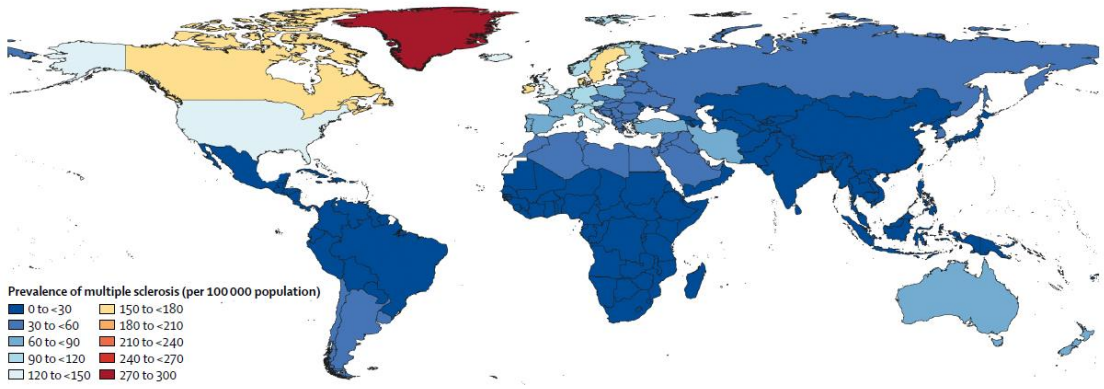

Figure 1 - Multiple sclerosis (MS) prevalence worldwide, per 100 000, in 2016 (age-standardized, both sexes). Adapted with permission from The Lancet Neurology [2].

The myelin sheath is a lipid-rich membrane, with around 30% of proteins, that surrounds the neurons' axons, and is associated with faster speed of axonal conduction [3]. In the CNS, myelin is produced by oligodendrocytes (OLs), so insults to these cells cause disturbances in the

myelination process. In turn, generally, the loss of the myelin sheath results in problems of electrical signal conduction, and a higher chance of neuronal degeneration [4, 5].

Although each MS patient can develop a specific disease course, the National MS Society defined four MS different types with its own distinctive characteristics: i) relapsing-remitting MS (RRMS), in which there are recurring demyelination cycles that alternate with periods of total or partial recovery where the symptoms are absent; ii) secondary progressive MS (SPMS), in which the cycles are present, but eventually there is an uninterrupted demyelination phase and the clinical symptoms slowly cause progressive deterioration over a period of many years; iii) primary progressive MS (PPMS), that is progressive since the beginning, without cycles of demyelination/remyelination; and iv) clinically isolated syndrome (CIS), which is the first incident of demyelination or inflammation that culminates in the appearance of symptoms that last 24 hours, and it may or may not develop into the other stages of MS [1, 4, 6]. MS pathogenesis is also associated with focal inflammatory lesions, particularly during the demyelination phase [7]. Nevertheless, these are not always the same, leading to different lesions classifications. As such, they can be: i) active (acute); ii) inactive (chronic); iii) chronic active, where there is an inactive core, with evidence of ongoing or recent activity, usually at the peripheral rim; and iv) early or pre-active lesions, where no plaques are present, but breakdown of the blood-brain barrier (BBB), mild perivascular inflammatory reaction, and reactive astrocytes are present [8]. In RRMS there are active or chronic, while inactive lesions appear in SPMS or PPMS patients [8].

The observed myelination cycles in some MS types are a consequence of the CNS capacity of replacing myelin following acute demyelination. While mature OLs present in the lesion cannot myelinate *de novo* spared axons, as OLs are in a post-mitotic state [9], in the adult CNS there are pools of oligodendrocyte precursor cells (OPCs) and neural progenitor cells (NPCs) that, after demyelination, can migrate to the injured site and differentiate into OLs [5, 9] (Fig. 2). However, the new myelin sheaths produced are thinner and shorter than those on axons that did not lose their myelin sheaths, which leads to slower conduction speed across the axon [4]. Despite differences in the produced myelin, it is believed that the processes used by OPCs to remyelinate the axons are similar to the ones occurring during developmental myelination. This idea is known as the “recapitulation hypothesis”, as the stages of OPCs migration and proliferation, and later differentiation and maturation in OLs are identical [10]. Notwithstanding, the processes underneath remyelination failure are still not truly understood.

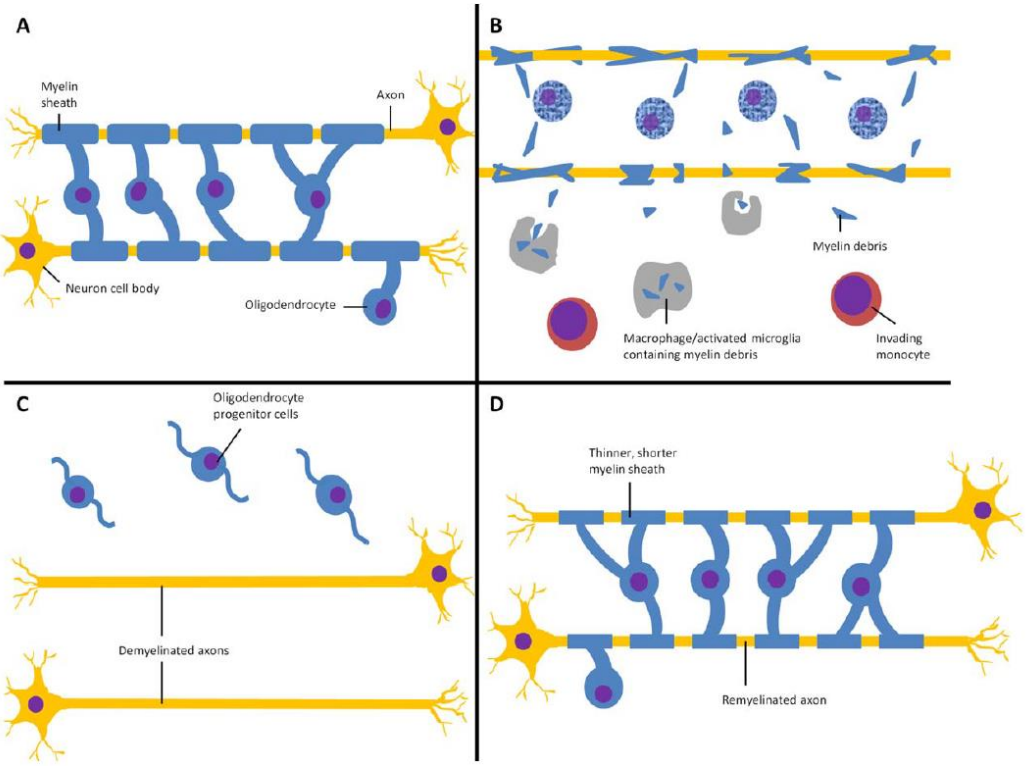

Figure 2 - Schematic representation of a cycle of demyelination and remyelination in demyelinating diseases. In homeostasis scenarios the majority of the central nervous system (CNS) axons are myelinated by oligodendrocytes (OLs) (A). Once demyelination starts the myelin sheath is destroyed, and the debris is removed by infiltrating macrophages and microglia (B). Later oligodendrocyte progenitor cells (OPCs) are activated and migrate to the demyelinated axon site (C). Finally, the axon is remyelinated by mature OLs (D). Used with permission from Journal of Neuroscience Research [4].

As a consequence of the destruction of the myelin sheath, in MS lesion sites there is myelin debris whose clearance is achieved by activated microglia, the CNS resident inflammatory cells [11]. The over expression of pro-inflammatory factors as interleukin (IL)-12, IL-23 or reactive oxygen species leads to CNS lymphocytic infiltration of T-cells, contributing to the inflammatory milieu of the lesion. If efficient, myelin debris clearance contributes to a permissive environment for remyelination. Nonetheless, with disease progression microglia is not capable to efficiently clear the myelin debris and this contributes to the inhibitory environment within the lesion site [9, 11, 12].

Astrocytes also play a pivotal role throughout demyelinating diseases, as these are the first cells to be recruited to the lesion sites. During the disease course, these cells became reactive in a process termed astrogliosis, overproducing many altered extracellular matrix (ECM) proteins that contribute to the formation of a glial scar [13]. While the glial scar is a neuroprotective mechanism that CNS uses to avoid the invasion of the inflammatory cells or pathogens into the surrounding tissue, it is also a barrier to regeneration, as MS progresses. This duality of effects is in line with the role played by astrocytes in the pathology, as both useful and an obstacle to recovery [14]. On one hand, astrocytes are responsible for the creation of a permissive environment that promotes remyelination by, for instance, upregulating genes associated with neuroprotection [13]. On the other hand, astrocytes contribute to the demyelination process

and subsequent axonal degeneration by the releasing in cytotoxic factors and ECM components associated with OL differentiation inhibition in significant quantities [13].

Many factors released by astrocytes have been identified as regulators of OPC differentiation. OPC proliferation and survival is increased by the over secretion of fibroblast growth factor 2 (FGF-2) by astrocytes as well as glycosaminoglycan (GAG) hyaluronan, which interacts with the CD44 receptor on the OPC membrane [13]. During astrogliosis, astrocytes produce chondroitin sulfate proteoglycans (CSPGs), particularly neurocan, brevican, and neuron-glial antigen 2 (NG2). The expression of CSPGs creates an inhibitory gradient, with the highest values at the center of lesions and smaller values towards the periphery, which might affect the cytoskeleton and membrane components at the axons' ends [13]. The up-regulation of CSPGs, hyaluronic acid (HA), and tenascin-C leads directly to the inhibition of remyelination and the formation of the glial scar [8, 12]. Additionally, astrocytes release other inhibitory molecules that diminish axonal growth, like Ephrins (Eph), whose expression is increased in MS lesions [13].

At the last stages of demyelinating conditions, astrocytes are hypertrophic, express high levels of glial fibrillary acidic protein (GFAP) [14], overproduce ECM proteins as collagen type IV and within the lesions there are stacks of glial filaments [13]. Astrocytes also start to up-regulate other markers, such as vimentin (Vim), synemin, glutamine synthetase 1 and aldehyde dehydrogenase 1 family, member L1 (ALDH1L1), nestin, S100 and matrix metalloproteinases (MMPs), like the MMP-9 [8, 13]. The activity of MMPs can be counteracted by tissue inhibitors of metalloproteinases (TIMPs) which are also produced by astrocytes. A fine balance between MMPs and TIMPs expression dictates whether astrocytic secretion of these factors is beneficial or inhibitory to remyelination and axonal regeneration. In MS, in opposite to the augmented expression of MMPs, TIMPs' expression remains unaltered or even reduced [15].

Moreover, reactive astrocytes are also immunoreactive and highly express pro- (IL-1β, IL-6, IL-12, IL-17, IL-23, tumor necrosis factor (TNF)-α) and anti-inflammatory cytokines (IL-10, transforming growth factor (TGF)-β, IL-27) [13], chemo-attractant and repellant (e.g. semaphorin) molecules, and trophic factors including vascular endothelial growth factor (VEGF), brain-derived neurotrophic factor (BDNF) and tropomyosin-related kinase (TrkB), ciliary neurotrophic factor (CNTF), insulin-like growth factor-1 (IGF-1), and neurotrophin-3 (NT3) [8].

At the end, the glial scar is not only made of hypertrophic astrocytes [8], but also OPCs, myelin debris and fibromeningeal cells [13] and altogether these factors are believed to contribute to remyelination process failure.

Generally it is considered that it is the balance between myelination-supportive and myelination-inhibitory ECM molecules that dictates the degree of demyelination and remyelination [16]. However, it has also been suggested that remyelination is also dependent on the moment in which these molecules are secreted – "dysregulation hypothesis". In this scenario remyelination can fail because the pro-remyelination environment is not maintained

long enough, or the secretion of pro-differentiation molecules starts before OPCs have migrated to the lesion and matured [10].

During demyelination, the ECM composition is greatly altered which suggests that mechanical properties of the brain may also change. In fact, the combination of different cell-cell interactions and the expression of different ECM proteins and factors at distinct disease stages leads to changes on the biochemical properties of the ECM which in turn have repercussions on the mechanical ones [17]. Currently this is a hot topic on the field and some studies have been reporting that the mechanical properties of the microenvironment can also play a role in the alteration of OPCs behavior and differentiation properties. As a matter of fact, OPC differentiation was reported to be inhibited in stiffer substrates (30 kPa) in comparison with softer ones (around 1kPa) [18].

The effect of the mechanical properties on OPCs behavior is particularly attractive in the study of the glial scar role in MS. Once the scar is highly enriched in ECM proteins that differ from the homeostasis brain's ECM, its rigidity is undoubtedly altered. Glial scar rigidity has in fact emerged as a possibility for its effects of hindering the remyelination process and axonal regeneration [13]. Specifically, it has been suggested that the glial scar region is less rigid than a healthy region control (healthy brain parenchyma elastic moduli around 0.1 – 10 kPa [17]), but at chronic stages in the development of MS the rigidity is higher (Fig. 3) [17].

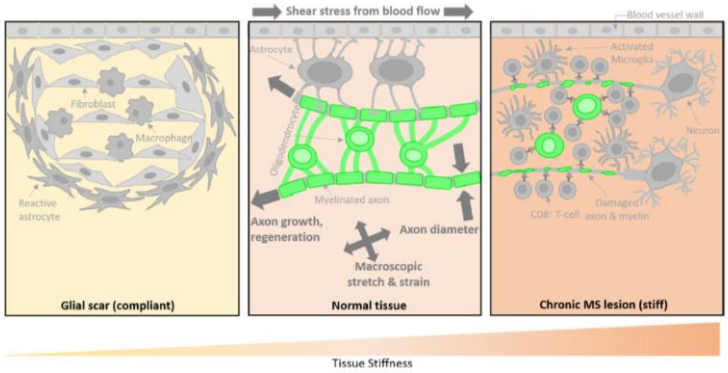

Figure 3 - Comparison of the stiffness of the glial scar in its initial state (left), glial scar in chronic multiple sclerosis (MS) (right) and a health brain (center). Used with permission from Neuroscience Letters [17].

This raises an interesting question regarding the way astrocytes influence the mechanical properties of the ECM and vice-versa, in a MS and glial scar context. Particularly, mechanical properties changes could be the missing key to understand the failure of the remyelination process with time, as well as a possible avenue for an efficient treatment for MS.

1.2. Models to study (de)myelination in the CNS

As the biology behind the complexities of demyelination and remyelination are yet to be fully understood, particularly the role of the glial scar on OL differentiation, *in vivo* and *in vitro* models have become essential tools to help study the evolution of MS, but also its potential treatments.

1.2.1. *In vivo* models of demyelination

Among the rat and murine *in vivo* experimental demyelination models that have been developed, the most used ones are immune-mediated, virus-induced, and toxin-induced models [19].

The experimental autoimmune encephalomyelitis (EAE) model (Fig. 4) is the most common *in vivo* model of MS. It can be established both in rodents and primates. The EAE model can approximate the main pathological characteristics of MS (inflammation, demyelination, axonal loss and gliosis; but also, resolution of inflammation and remyelination) through a range of immunopathological and neuropathological processes. It is a model that can be used to mimic specific aspects of MS pathology by, for instance, varying the induction methodology and the use of knockout animals [20]. The main difference, when compared with human MS, lies on the fact that EAE has to be artificially provoked by inducing sensitization to myelin antigens with the help of an adjuvant. As there is no single antigen that has been identified for MS, this distinction in activating process might result in the differences between the model and the actual clinical condition [20]. Depending on the immunization form, there are two subtypes of EAE: active EAE, where myelin peptide with Freund's adjuvant and pertussis toxin are used; and passive EAE or adoptive cell transfer method, in which lymph node lymphocytes are activated against myelin and injected into the animal [21].

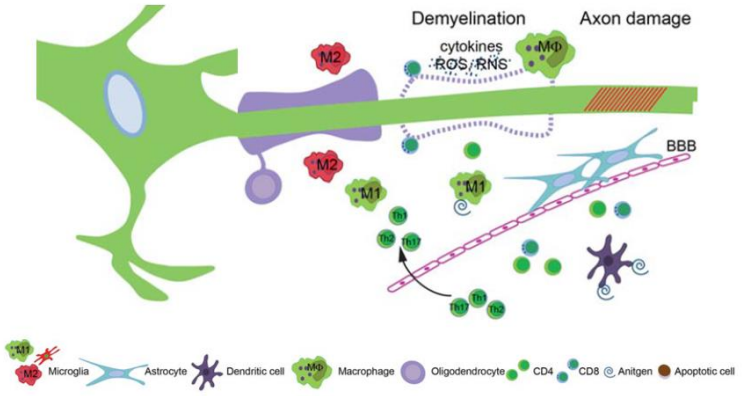

Figure 4 - Schematic representation of the experimental autoimmune encephalomyelitis (EAE) model at the cellular level. Immune cells (dendritic cells and T helper cells) surpass the blood-brain barrier (BBB), gaining access to the central nervous system. The demyelination and axonal damage are consequences of the resident glial cells being activated. Adapted with permission from Journal of Neuroscience Research [19].

Concerning the virus-induced models, the most common one is the Theiler's murine encephalomyelitis virus (TMEV) (Fig. 5), a neurotropic viral infection model. TMEV is a non-enveloped, positive-strand RNA virus [19], of which the most widely used strains are the virulent GDVII and the less virulent Daniels and BeAn strains [21]. The disease manifests in an initially acute phase, three to twelve days after infection. In the gray matter there is an intense and multifocal inflammation, as T-cells, macrophages and B cells are present, the virus replicates fast in neurons and induces neuro-apoptosis, while the white matter and spinal cord are not affected. Thirty to forty days after infection there is chronic demyelination, with inflammatory demyelination, loss of movement control and spastic paralysis. At this moment there is a significant inflammation in the white matter, made of T-cells and monocytes/macrophages, microglial proliferation in the brain stem and thalamus, as well as perivascular inflammation in the spinal cord's white matter. Although this virus model is interesting for MS research, as viral infections are a possible trigger of the disease [19], TMEV does not replicate the cyclical nature of MS, once demyelination and remyelination take place at the same time, which diminish its usefulness.

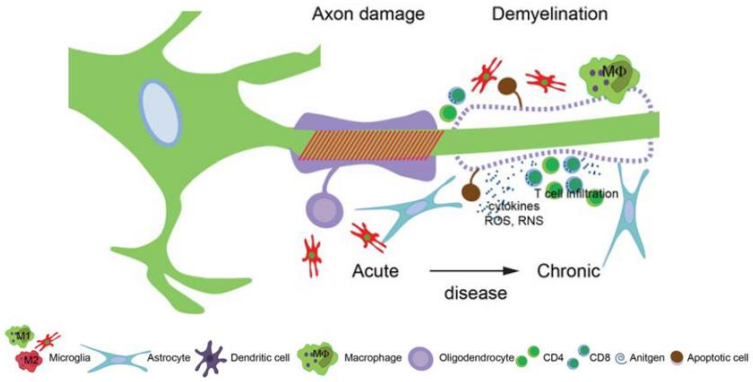

Figure 5 - Schematic representation of the Theiler's murine encephalomyelitis virus (TMEV) model at the cellular level. The infection creates axonal damage, that leads to the immune cells' recruitment of pro-inflammatory mediators, and later creating demyelination. Adapted with permission from Journal of Neuroscience Research [19].

Regarding toxin-induced models (Fig. 6) these explore the direct injection in the white matter of agents in combination with gliotoxins that can create demyelination (ethidium bromide (EtBr) and lysolecithin), while others are administrated systemically (cuprizone). This creates a reproducible model where the location of the lesion is controlled [19].

EtBr is a toxic chemical for the nuclei, which allows the establishment of a focal demyelination lesion. It acts by compromising the transcription of mtDNA in glial cells, but not neurons and endothelial cells. To achieve this, a stereotactic injection is used to deliver it to specific white matter tracts, such as the thoracolumbar dorsal funiculus of the spinal cord or in the caudal cerebellar peduncle. In these lesions, there is a loss of astrocytes and OLs. OLs apoptosis happens three days after injection, after which the remyelination starts, since Schwann cells (myelinating cells in the Peripheral Nervous System (PNS)) have been shown to migrate to the lesion. The advantage of this agent relies on the accurate prediction of the demyelination site

and its size since it is concentration dependent. However, the older the animal is, lower is the level of spontaneous myelin recovery, making age a limiting factor [19].

On the other hand, lysophosphatidylcholine (lysolecithin, LPC) (Fig. 6) solubilizes membranes of myelin-producing cells, which means that the other cellular populations remain relatively unchanged. This allows for the recruitment of immune cells (T and B cells) and microglia/macrophage to clear the myelin debris and secret cytokines and trophic factors. One week after the injection on the spinal cord the remyelination process starts, being completed after a few weeks; in a process faster than with EtBr since the OPCs are not affected, as well as astrocytes and macrophages. The biggest advantage of this model is that it can be used to study both de- and remyelination. On the other hand, demyelination happens in the absence of an inflammatory response, and just like with EtBr the age is an important controlling factor [19].

Cuprizone (oxalic acid bis [cyclohexylidene hydrazide]) (Fig. 6) is a copper-chelating agent toxic to OLs, that creates dysfunction and affect the myelin sheet. Cuprizone is introduced in the diet of the animals and it is usually given during five or six weeks. OLs apoptosis happens after two/three days, when they have pyknotic nuclei, enlarged mitochondria and big vacuoles, which seems to indicate that the apoptosis is caspase-3-dependent. Demyelination becomes visible after three weeks, and is related with immense microgliosis, astrogliosis, and axon damage. After six weeks, demyelination happens generally, but more significantly in the corpus callosum and posterior cerebellar peduncles, creating an acute demyelination model. Afterwards there is spontaneous remyelination, once the cuprizone diet is replaced by normal food. If the exposure to cuprizone is for longer than 12 weeks there is a limited spontaneous remyelination process, or chronic demyelination. In the chronic stages the demyelination occurs in the corpus callosum, cortex, hippocampus, and cerebellum. All in all, cuprizone offers a very simple, reliable and reproducible model, that allows for the study of OLs apoptosis, secondary demyelination and remyelination. Yet, the demyelination level is highly variable, depending on the strain, age, gender of animals, duration of exposure and dosage. Cuprizone model also lacks the presence of infiltration immune cells at the affected area [19].

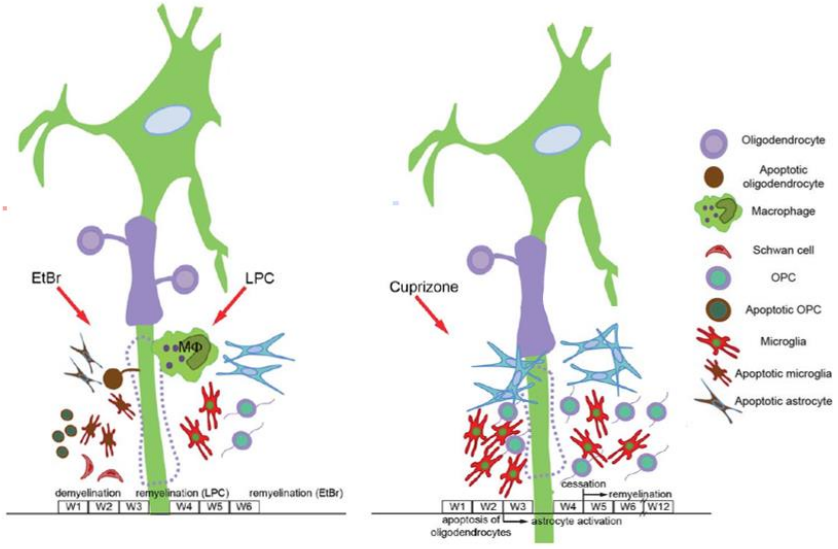

Figure 6 - Schematic representation of the ethidium bromide (EtB)r, lysolecithin (LPC) and Cuprizone models at the cellular level. In the EtB model, astrocyte, oligodendrocytes (OLs) and oligodendrocyte precursor cells' (OPCs) apoptosis is induced during the first week (W1) after injection; at week 6 (W6) remyelination starts. On the other hand, in the LPC model, apoptosis of astrocytes, OLs and OPCs is not induced, and remyelination starts 3 weeks (W3) after injection. Cuprizone) Apoptosis of OLs; microglia is activated at week 2 (W2), and decreases with the progression of remyelination (starts once the cuprizone is no longer given). Adapted with permission from Journal of Neuroscience Research [19].

1.2.2. *In vitro* two-dimensional (2D) models of (de)myelination and glial scar

While *in vivo* models are the most commonly used in (de)myelination studies, they present some challenges due to their inherent complexity, particularly to study the effect of specific structures and mechanisms, like the ECM alterations throughout (de)myelination. As such, different *in vitro* models have been created to replicate in a simpler way the demyelination process and glial scar formation, as well as study the effects of new drugs in a high-throughput manner.

However, these models do not fully eliminate the ethical problem that is also present in *in vivo* models, as primary glial cells are usually derived either from the sacrifice of animals for this specific purpose, or humans (post mortem, surgeries, fetal brain or embryonic stem cells).

1.2.2.1. Cell types

Glial cell cultures often rely on the use of rodent cells, as they can be maintained *in vitro* for long periods of culture. Traditionally, the study of MS has relied on the use of OLs, particularly for the study of mechanisms like myelin maintenance and remyelination, as well as OLs apoptosis and oxidative stress [22]. These cells are usually isolated from brain cortices [22], not only from wild-typ animals, but also from transgenic and knockout ones. While rodent OLs are quite useful due

to their high yield, it is important to keep in mind the differences in behavior between rodent and human OLs, particularly due to their distribution on the brain, time necessary for maturation and long-term culture, and their distinctive responses to different factors [23]. While rat OPCs are easy to isolate and maintain in culture, human OPCs require long culture times, to ensure that they present mature OLs' phenotype [24]. Despite the difficulties associated with obtaining human OLs, studies with human cells are more easily transferred into disease applications [24].

As a result, induced pluripotent stem cells (iPSCs) have become an interesting alternative for obtaining OPCs, as human iPSCs (hiPSCs) can be differentiated into human-derived OPCs, which allow to study specifically the cells of different patients [21]. Notwithstanding, there are also problems inherent with the use of iPSCs, like the epigenetic changes occurring after reprogramming that might interfere with the MS phenotype, as well as long differentiation times [24]. It is also possible to obtain rodent iPSCs. Usually, the latter are extracted from the optic nerve or the brain cortex of both young and adult specimens and can be used to perform differentiation, survival, and proliferation assays, as well as gene expression experiments. Additionally, these cultures are amenable of high-throughput studies, and usually work as the stepping stone into more complex models, as it is possible to study them without the influence of other cells and secreted factors [21].

Besides OPCs and OLs, which are considered the most demanding cells for culturing, neural cells as neurons, microglia and astrocytes have recently emerged as important players in the development of a reliable 2D model of (de)myelination.

Neurons are commonly derived from different primary rodent origins, like embryonal or cortex, or can be derived from progenitor stem cells (neural stem cells, NSCs). Human neurons are usually obtained from surgeries or post-mortems, however they are very difficult to maintain, and availability of these sources is scarce. Immortalized cells lines can be a reliable option, and are often used to study the axonal damage in MS. Nonetheless, neuron cell lines present multiple problems related with dendrite outgrowth and mature neuronal markers expression [22].

Additionally, as microglia activation is a fulcrum outcome of demyelination and remyelination, mimicking microglia cellular changes in morphology, biochemistry and function is undoubtedly significant in the development of an *in vitro* biological relevant model of (de)myelination. Generally, microglia can be isolated form mice, rats, rhesus monkeys or even humans, but cell lines also exist since primary cells have low proliferating rates [22]. Microglia activation status can be mimicked by culturing cells with a variety of different chemical agents, like cuprizone [25, 26], lipopolysaccharide (LPS) or interferon gamma (IFN-γ) [27].

Finally, astrocytes, the golden star of the glial scar, can come from a variety of primarily sources, like mice, rat or human brain tissue, or even stem cells that can be differentiated into an astrocyte lineage [22]. However, it is also necessary for the astrocytes to be activated, to better replicate the glial scar at its different stages. While a comprehensive protocol has yet to be

established, some options have been tested with some success, like the use of LPS [28], microglial conditioned medium [29] or fibroblast conditional medium [30].

LPS has been used alongside with IFN-γ, for example, to induce the overexpression of GFAP, Vim, IL-6, TNF, nitric oxide synthase 2 (NOS-2), and Toll-like receptor 4 (Tlr4) and IFN-γ receptors 1 and 2 (IFNγr1/IFNγr2) in astrocytes derived for mice NSCs, and as such inducing a reactive phenotype [28]. At the same time conditioned medium is interesting as it allows the study of the effects of the cytokines cocktails produced by some cells in others. In particular, the use of microglial conditioned medium of microglia that were previously activated with LPS, showed the capacity to significantly induce a reactive phenotype in astrocytes which in turned inhibited neuronal survival [29]. Moreover, astrocytes cultured with meningeal fibroblast conditioned medium expressed higher levels of glial scar markers, like GFAP, MMPs and collagen type IV [30].

1.2.2.2. Co-cultures

Monocultures are too simple for the study of the intricacy of processes occurring during demyelination and glial scar formation, particularly as these involve the presence of a multitude of cells and cellular products. Hence the use of co-cultures are interesting as slightly more complex methods to evaluate cell interactions. These are used to study how the presence of different cell types, like astrocytes, influences OLs and their responses [22], as well as the effects of the other glial cells have on each other and on neurons. Co-cultures have been used for decades and innumerous studies have relied their conclusions in these types of models. For instance, *Tuinstra et al.* created a co-culture model where an astrocyte cell line and primary neurons were co-cultured in order to examine axonal behavior at the inhibitory barrier created by the glial scar, though it is not clear how the astrocytes were activated in the study. At the end the results showed that while the created astrocyte boundary was probably less dense than the one *in vivo*, there was a significant number of neurites that turned away from the interface or just stopped growing [31].

Fan et al. used a co-culture system of rat neurons and OLs to show that the presence of serotonin leads to a reduction of the number of myelinated internodes, without increase the number of dead OLs [32]. While *Guo et al.* used a mice OPC-dorsal root ganglions (DRG) neuron co-culture to study the effects of vitamin C during myelination/remyelination, showing an increase in length of myelinated axons, as well as of the expression of contactin-associated protein, that marks the point of contact between OLs and neurons and the ensheathment of the axons [33].

1.2.2.3. Microfluidics

A simple co-culture model fails to mimic many structural, physiological, and pathological characteristics of tissues or organs. Microfluidics arises as an interesting approach to precise control cells' microenvironment and mimic molecular gradients found in the majority of tissues. Within these models, the fluids are controlled and manipulated at a submillimeter scale in engineered devices. By taking advantage of microfabrication techniques, like photolithography [34] the devices are usually made of transparent elastomers (as poly(dimethyl)siloxane, PDMS) constituted by one or more microchambers connected via microchannels or microgroove arrays. This structure makes microfluidics especially useful for creating chemical gradients within microchambers or microchannels, but also studying cell differentiation, neurite extension and cell migration [34]. For instance, the channels can be used to physically control the movement of the neurons' cell bodies [35]. Furthermore, in order to recreate more faithfully the microenvironment that cells experience *in vivo,* the surface can be modified with ECM proteins and peptides, the cell ratio can be controlled [36], and hydrogel scaffolds can be injected into the structure [34].

Microfluidics was successfully used by *Kerman et al.* to recreate the myelination process using OLs and neurons derived from mouse embryonic stem cells (ESCs). In this model, there were interactions between the different cell types and OLs were capable of creating myelin sheaths that fully wrapped around the axons. However, the microfluidics design (Fig. 7 A) had to be changed by substituting the compartments by an open well since only a small fraction of neurons remained in the compartments, which translated into a low density of axons to be myelinated [37]. On the other hand, *Chen et al.* developed a microfluidic structure to mimic nerve fibers, using neurons and Schwann cells. This model was able to recreate nerve fibers with nano-orientation and core-shell structure. A triple channel microfluidic system (Fig. 7 B) and alginate-assisted methacrylate hyaluronan/fibrin composite hydrogel were used creating a structure that was biocompatible, and inside which cells were embedded and later able to interact and organized correctly (Schwann cells in the other surface of the nerve fiber and neurons in the core) [38]. Furthermore, *Hyvärinen et al.* used a microfluidic model to simulate the interactions between neuronal axons and reactive astrocytes derived from hiPSCs, as well as make it possible to control the inflammatory environment. Astrocytes obtained a proinflammatory phenotype after being exposed to IL-1β and TNF-α for seven days, which also induced proliferation but hindered their viability. In the microfluidic device the neurons and astrocytes were cultured in separated compartments connected by microtunnels (Fig. 7 C), as well as an axonal compartment, so the astrocytes' processes were able to extend throughout the micro-tunnels and connect with the axons. At the end, the results showed that the proinflammatory environment induced by the presence of reactive astrocytes promoted the axonal density, showing how the astrogliosis can play a role in neuronal response [39].

The main advantages of microfluidic systems relate to the high customizability of their properties, making them tunable for the needs of each cell type, combination of cells and experiments. Another significant pro of this type of model is the fact that it requires significantly less cells and culture medium, when compared with traditional methods; which also translates into less time needed, reduced need for reagents, smaller contamination risk and efficiency in high-throughput assays. Furthermore, one can also include biosensors or electronic systems [34] in the devices, which can be particularly interesting when studying the electrical signals between neurons, as *Jeong et al.* did when studying the BBB. The microfluidic platform included primary mouse endothelial cells and primary astrocytes, a porous membrane that separated the cells where the microchannels intersected, as well as a multielectrode array integrated that allowed for the study of the transendothelial electrical resistance in all points of intersecting microchannels, where the BBB was mimicked. This allowed for the creation of a BBB model that was able to replicate some of the complexity and variation of physiological functions present in this structure, as well as measure many of these aspects [40].

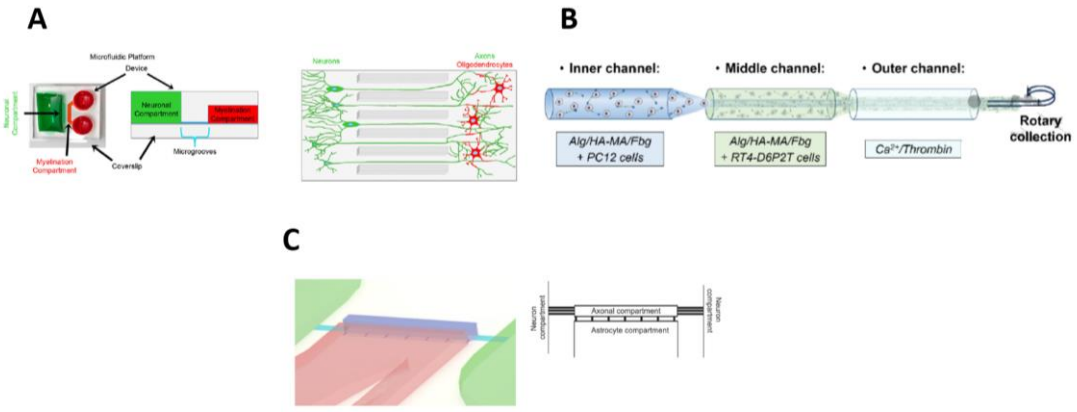

Figure 7 - Schematic representation of microfluidic devices. (A) Schematic representation of the top-view and cross-section of the microfluidic device, as well as a representation of the cells inside it. Neurons and oligodendrocytes (OLs) were cultured separately, but the axons were able to extend through the microgrooves into the region where OLs were. Adapted with permission from Development [37]. (B) Schematic representation of the three microchannels needed to create a core-shell structure of nerve fibers. Adapted with permission from Biofabrication [38]. (C) 3D and 2D schematic representation of a microfluidic device with two compartments for neurons and one for astrocytes all connected to an axonal compartment via microtunnels. Adapted with permission from Scientific Reports [39].

1.2.3. *In vitro* three-dimensional (3D) models of the (de)myelinating environment and glial scar

While 2D models are useful, they lack the ability to recreate the complex microenvironment and mechanical characteristics associated with MS and the glial scar, hindering their applicability as disease models [41]. For this reason, 3D models have emerged as an interesting alternative.

1.2.3.1. Organotypic brain slices cultures

Halfway between an *in vivo* and an *in vitro* model in terms of complexity, there are organotypic brain slices cultures, thin (100-400 µm thick) tissue explants of different rodent or human CNS tissues that can be sustained *ex vivo* and/or *in vitro* for up to a few months [24]. The slices are cultured on porous membranes in cell culture dishes at an air-liquid interface, as the medium below provides nutrients through capillary action and the air above the oxygenation [42]. Additionally, these type of cultures are adaptable, since transgenic mice, transfection or other agents can be used in order to assist in any necessary analysis [24].

In MS research, brain slices are usually isolated form neonatal and/or young tissue (up to one week old), as they undergo developmental myelination *in vitro* [24], and afterwards demyelination can be induced *in vitro* with toxins or immune-mediated insults. Later the slice will spontaneously remyelinate [22, 24].

For example, *Liu et al.* established an antibody-mediated demyelination model using mouse cerebellar slices. This model used monoclonal recombinant antibodies from clonally expanded plasmablasts from the cerebrospinal fluid of MS patients to induce demyelination. The results showed that the antibody primarily bound to OLs' processes and myelinated axons, and that, when combined with human complement, mature OLs' morphology and viability was significantly affected, with total loss of process and hypertrophic cell bodies after 48 hours. Moreover, OPCs were preserved, astrocytes were not affected and microglia was activated [43]. Later the same group used the same model to study glial cell response and myelin integrity during recovery. There was no significant variation on astrocyte number, morphology or network structure during the remyelination period. Nonetheless, the microglia cells were in increased numbers three days after the start of remyelination and presented an activated morphology, while after seven days had returned to a non-activated status. At the same time, by day three of culture OLs started to recover, and by day seven had matured and were presented at the same levels as in the control, with extensive and organized processes, and capable of myelinating axons [44]. These are some of the few studies that use brain slices to study demyelination and highlight their amenability to replicate the changes observed in *in vivo* models due to their intrinsic cellular and structural complexity.

The main advantage of these models relies on the possibility of having all brain cell types present. Additionally, organotypic brain slices are easily accessible and their 3D structure mimic the *in vivo* tissue better than an artificial system, and allow the study of cell-cell interactions in homeostasis and disease conditions [24, 42]. Other advantages relate to the preservation of neurotransmitter release and synaptic transmission, as well as the possibility of producing multiple slices from one brain [42].

However, the lack of a functional blood supply means that brain slices are not useful to study the possible role of the cerebrovasculature or immune cells infiltration in the MS pathology [24].

Additionally, when the age of the cells is an important factor, as it is the case in MS, the use of young animals' brains might constitute a shortcoming, once it has been proved that young and aged animals cells have differences in relation to their structure, function and physiological properties [42].

1.2.3.2. Spheroids and Organoids

Another option is to use spheroids (Fig. 8 A), multicellular aggregates without scaffolds that can be achieved either by spontaneous self-assembly or by forced cell-cell adhesion. In these structures the cells produce their own ECM, which negates the necessity of an artificial matrix that might replicate the native composition. Spheroids are usually used to study cell diversity, electrophysiology, ECM production and mechanical stiffness of the brain, but in combination with other engineering approaches they can be used to recreate neural networks [45]. Concerning demyelination and remyelination studies, mouse telencephalon, embryonic whole rat brain and human fetal brain have been used, with the loss of myelin being activated using antibodies as anti-myelin oligodendrocyte glycoprotein (MOG), -LPC or -IFN-γ [22].

One example of spheroids' application in MS research is the study by *Vereyken et al.* that created whole brain spheroids and used LPC to induce demyelination. Single cell suspension of embryonic rodent brain cell was placed under constant rotation for four weeks so that cells reaggregate and form spheroids, after which LPC was added to the culture. Initially myelin was present in the entirety of the structure in a multilayered fashion. However, seven days after LPC stimulus, myelin presence decreased by more than half, while the one that was still present only lightly covered the axons and was not as even as the control. The number of myelin sheets only returned to normal seven days after the exposure to LPC ended, probably due to the presence of OPCs in the spheroid [46]. This model showed remarkable features of demyelination and remyelination which strengthened the reliability of these type of cultures to be used for (de)myelination studies.

A variation of spheroids are organoids (Fig. 8 B), a type of culture where the tissue grows in 3D, recreating the organs' structure, cell types and functions. Unlike spheroids, in organoids the stem cells self-organize through cell sorting and spatial differentiation, which usually leads to more stable cultures that last for longer periods of time. Moreover, this self-organization capability also means that organoids can better mimic developmental details. However, it also means that organoids can vary significantly in terms of size, shape and composition, particularly when cells form large structures, where the exchange of nutrients and oxygen is difficult, leading to necrosis. Furthermore, a lot of organoids use Matrigel® as a matrix, which is unstable and inconsistent between batches [45]. In particular for demyelination and remyelination studies, organoids were often used until the late 1980s, however, since then not many studies have been

published using these cultures, especially as other more interesting 3D models have emerged, particularly the ones that used biomaterials as scaffolds (see section 1.2.3.3.).

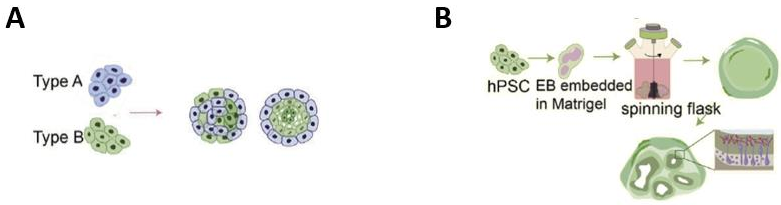

Figure 8 – Formation of spheroids and organoids for in vitro studies. (A) Schematic representation of a spheroid formed with two cell types that can be organized in two ways, mix homogeneously or one cell type in the center and the other in an outer layer. (B) Schematic representation of the formation of a generic organoid. Adapted with permission from Biomaterials [45].

1.2.3.3. Engineered Matrices

The development of synthetic and/or natural hydrogels as scaffolds has offered an interesting opportunity to develop 3D models for MS and glial scar. Hydrogels (water-swollen crosslinked polymer networks [47] can support cell/tissue growth while being tunable, better replicating the physiological properties needed in the specific microenvironment. These changes in properties can be obtained by altering the biodegradability of the material [45] or by functionalizing the polymeric chain with different peptides or proteins that are common in the tissue creating adhesion sites in bioinert hydrogels.

Natural hydrogels are often ECM purified proteins (collagen) or polysaccharides (HA, chitosan, alginate, heparin, dextran), or even a decellularized matrix itself (Matrigel®). Since natural hydrogels originate from ECM components, they can be better recognized by cells, have ligands beneficial for cell attachment, migration and proliferation and be modeled and degraded by cells into amino acids or carbohydrates that can be metabolized [48]. At the same time, synthetic hydrogels, like Poly(ethylene glycol) (PEG) and its derivatives can also be modified to obtain the most desirable characteristics or added to mixes of materials, while also not having significant bat-to-batch variations. These materials will be further discussed in section 1.3.2.1. and 1.3.2.2.

While the usage of these hydrogels scaffolds is still not commonplace in the study of MS, (de)myelination and glial scar, as artificial microfibers [49, 50] or micropillars [51], some researchers have been able to approximate these disease conditions using them.

For instance, *Rocha et al.* used an alginate hydrogel to encapsulate rat astrocytes replicating some of the conditions of the glial scar, that in the future might be useful for drug screening purposes. In this model astrocytes remain viable within alginate hydrogels for seven days *in vitro*. The reactive status was achieved by culturing astrocytes in the presence of meningeal fibroblast conditioned medium and the authors showed that activation of the cells was

dependent on the stiffness of the alginate being mediated by a mechanosensitive signaling pathway. The RhoA/ROCK signaling pathway was pointed as a possible mediator of this effect. Interestingly, astrocytes cultured with meningeal fibroblast conditioned medium were able to alter the mechanical properties of the scaffold [30].

Similarly, *Fang et al.* used a collagen type I scaffold to encapsulate primary mouse astrocytes to simulate the glial scar tissue (Fig. 9A). After eight days in culture the astrocytes had proliferated and presented a stellate morphology and extended process (hypertrophic, hyperplastic and deformed). With time the size of scaffolds with cells contracted and shrank, even changing its shape (smaller on the sides, taller, and gained a more ellipsoid shape) as astrocytes proliferated and migrated and the water content diminished. Moreover, the presence of astrocytes also changed the porous nature of the scaffold making it more compact. Additionally, as the size and cell concentration changed so did the compressive elastic modulus, increasing with it. As such, this model shows how the presence of astrocytes in the glial scar changes the matrix that surrounds them [52].

Simple models can also be just the first iteration of more complex structures, like the one developed by *East et al.* that first started with a simple collagen structure with quiescent rat astrocytes that showed that they were less reactive in 3D than in 2D, mimicking their situation is a healthy CNS [53]. This model later evolved into one also containing DRG cells (neurons and Schwann cells). In this improved model the two different cell populations were embedded separately in hydrogels in different chambers with a physical separation between them (Fig.9 B). Later the separation between the gels was lifted and the hydrogels merged into one, while the cells remained separate. The results showed that in the gels containing both cell populations, the astrocytes were in greater numbers next to the interface and more activated, hypertrophic and expressing higher levels of GFAP, while axon growth was also inhibited in this region. This model allows the monitoring of the culture overtime and can be particularly interesting to study cell-cell interactions and the effects of drugs on cell behavior [54].

Studies more focused on the PNS might also be interesting as they can constitute a blueprint to the development of similar models using astrocytes and neurons, even if their conclusions may not be directly translated into the CNS. Such is the case of the dual scaffold proposed by *Khoshakhlagh et al*. The hydrogels chosen were methacrylated dextran (MeDex) and methacrylated heparin (MeHp) in which rat DRG cells (Schwann cells and neurons) were encapsulated (Fig.9 C). The model needed two distinctive materials because of the different crosslinking process and final objectives: MeDex was crosslinked with visible light and used for immunohistochemistry and histology assays; while MeHp needed ultraviolet (UV) light and was for electrical conduction assays. At the end, and while the combination of both scaffolds proved to be flexible and versatile, it was not possible to study, for example, the effects of conduction velocity or myelin formation at the same time. Moreover this model cannot be translated for

high-throughput assays, as simple histology and nerve conduction assays are not compatible with the need to obtain a significant amount of data [55].

Additionally, these scaffolds can be combined with more traditional 3D models, as *Sharma et al.* did by combining spheroids made of human iPSCs (creating neurons and Schwann cells) and Poly(ethylene glycol) dimethacrylate (PEGDMA) and Matrigel® to create peripheral nerve tissue organ-on-a-chip (Fig.9 D). The results showed that the co-culture formed more compact spheroids and neurons formed spheroids faster in those conditions. The most interesting aspect of this model relies on the use of human cells, as opposed to the traditional animal cells. Furthermore, the reprograming associated with iPSCs did not affect the basic cell functions (myelination and conductivity). On the other hand, the fact that laminar myelin formed without axons and the cells were seeded in Matrigel®, a material derived from animals that has batch-to-batch variations, cannot be ignored and constitute some clear drawbacks of the system [56].

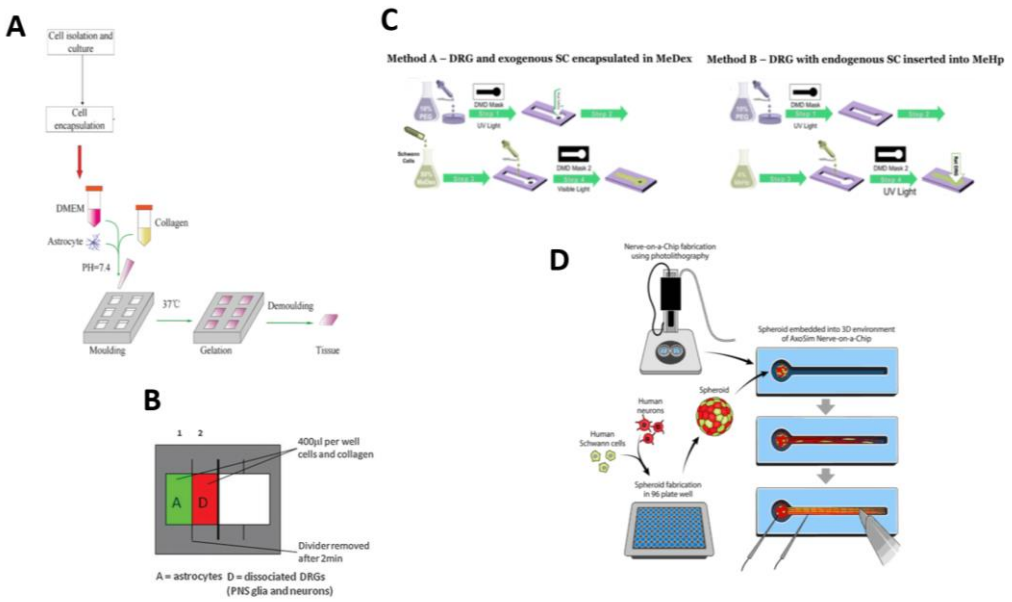

Figure 9 - Schematic representation of the methods used to create hydrogel matrices for mimicking (de)myelinating and glial scar milieu. (A) Astrocytes embedded in collagen type I were molded into different cuboid shaped models depending on the assay that was to be performed. Adapted with permission form International Journal of Bioprinting [52]. (B) Schematic representation of the structure used to physically create the separation between the astrocytes and the dorsal root ganglia (DRG) cells in the collagen matrix. Adapted with permission form Tissue engineering. Part C, Methods [54]. (C) Septs for the production of the two methacrylated dextran (MeDex) and methacrylated heparin (MeHp) matrices using poly(ethylene) glycol (PEG) molds to create structures with defined shapes. Adapted with permission from Journal of Neural Engineering [55]. (D) Design methodology used to create a nerve-on-a-chip structure using spheroids made of human induced pluripotent stem cells (hiPSCs), PEGDMA and Matrigel®. Adapted with permission from Scientific Reports [56].

Table 1 summarizes some 3D models that have been developed using hydrogels as matrices for the study of (de)myelination and glial scar formation.

Table 1 - Summary of studies that explore the development of 3D models of MS, glial scar or myelination using 3D hydrogel matrices.

Study foucus	Biomaterial	Cell type	Scaffold properties	Main conclusions	Model advantages	Model drawbacks	Reference
Glial scar	Alginate	Rat astrocytes	• ↓ concentration → ↓ stiffness • meningeal fibroblasts medium → ↑ astrocytic reactivity	• = C V • Reactive astrocytes → ≠ mechanical properties • Stiffness → ≠ cell activation • V(activation): 1% alginate discs (with CM)	• Tunable alginate mechanical properties • Amenable for drug screening and high-throughput assays	• Use of pure alginate (bioinert) • Cell morphology ≠ from *in vivo*	[30]
Glial scar	Collagen	Mouse astrocytes	• Porous • Stable size and mechanical properties (compressive elastic modulus)	• Astrocytes alter scaffold structure (size, morphology, and shape)	• Feasibility in mimicking astrocyte matrix modulation	• Lack standard size and shape that can be used for testing different conditions	[52]
Interaction between astrocytes and neurons	Collagen	Rat astrocytes and DRG (Schwann cells and neurons)	• One gel, but no mixing of cell populations	• Astrocytes have ↑ presence in the interface; ↑activated • ↓axon growth in the interface	• Cell-cell interactions • Study different cell populations	• Complicated set up • Long culture times	[54]
Myelination PNS	MeDex MeHp	Rat DRG (Schwann cells and neurons)	• MeDex → growth matrix • MeHp → migration and electrodes	• Myelination both hydrogels • MeHp neurons → conductivity	• Flexibility → used for different assays • Versatility → myelination by encapsulated cells or induce migration of others	• Need for two scaffolds • Representation of the PNS and not the CNS	[55]
Organ-on-a-chip – peripheral nerve tissue	Outside: PEGDMA Inside: Matrigel®	Spheroids of human iPSC (neurons and Schwann cells)	• Outside → microphotolithography • Inside → filled with Matrigel®	• Co-culture → neurons form spheroids faster • Co-culture → > compact spheroids • Neurites grew on average 1 mm a week	• Human cells • Significant axonal outgrowth • Can be used for electrical conductivity assays	• Difficult to source cells • Batch variations (Matrigel®) • Laminar myelin without axons • Representation of the PNS and not the CNS	[56]

Symbols: ↑ – higher/high/more significant; ↓ – lower/low/less significant ; → – leads to/after ;V – ideal concentration; = – not affected/remained the same; ≠ – different; > – more/maximum; < – less /minimum; CV – cell viability; CM – conditional medium; CNS – central nervous system; PNS – peripheral nervous system; MeDex – methacrylated dextran; MeHp – methacrylated heparin; PEGDMA – polyethylene glycol dimethacrylate; DRG – dorsal root ganglions; iPSC – induced pluripotent stem cells

1.3. Bioprinting in the development of CNS 3D engineered models

The development of engineered matrices for high-throughput drug screening assays, in particular, can benefit from the creation of complex, precise and reproducible structures through the use of an emerging technology: the bioprinting. This technique can be used not only for drug screening, but also for the development of organ-on a chip devices, simulating neural networks, tissue pattering, disease modelling and neurodevelopment [57]. Moreover, as the properties of the material chosen play a key role in the success of the strategy, bioprinting can be specially interesting in the study of mechanical properties of matrix and its effects, as is the case in (de)myelination and glial scar models.

Conceptually, bioprinting refers to the process of automated and controlled deposition of complex scaffolds (hydrogels – usually referred as the "bioink") [58]. It can encompass cell-laden scaffolds and cell-free scaffolds where the cells are seeded after fabrication [58]. Bioprinting allows the development of prototypes in a fast and dynamic way, where the cells are distributed in the model homogeneously, with standardized spacing and with a significant variety of cell positions [58]. Moreover, models obtained with this technique can help cell attachment and growth, while making it possible to regulate porosity and create interconnected channels [58]. Notwithstanding, bioprinting biggest advantage lies on the possibility of creating automatic and precise cell arrangements with one or more cell types, which does not happen in traditional cell culture methods [45].

1.3.1. Printing methods

The process of bioprinting can be achieved by droplet, extrusion and laser-based methodologies (Fig. 10).

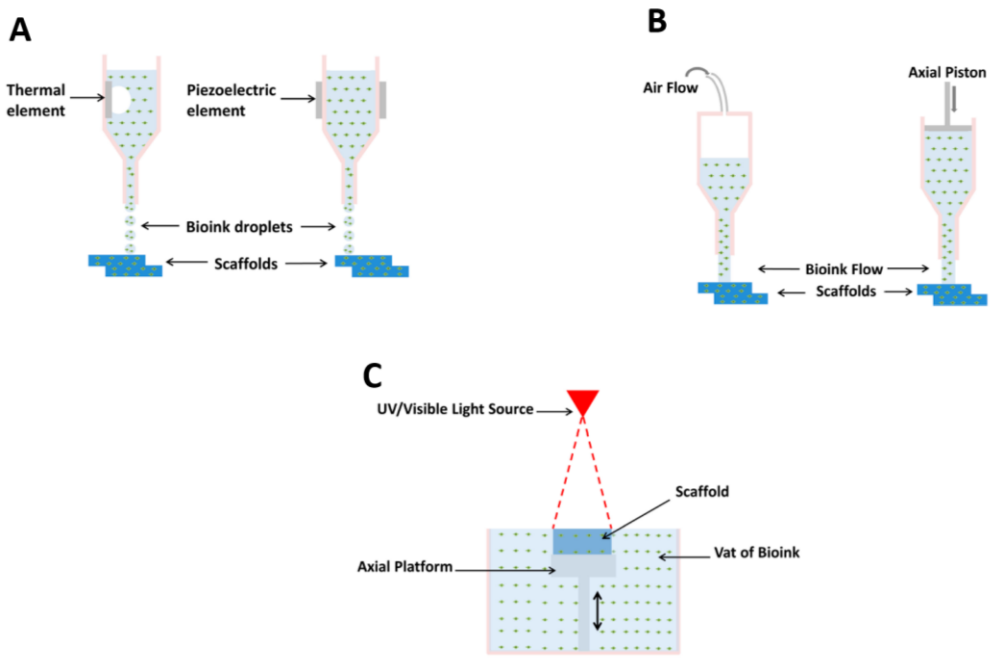

Figure 10 - Schematic representation of the main types of printing methods. In droplet-based/Inkjet bioprinting (A) nucleation bubbles push the ink through a micro-nozzle either by temperature variation or acoustic-waves. In extrusion-based bioprinting (B) filaments are extruded due to compression forces produced by pneumatic or mechanical structures. The laser-based bioprinting or stereolithography (C) uses photopolymerization of light sensitive bioinks. Adapted with permission from Materials [59].

The droplet method (Fig. 10 A) can be used to produce both single independent drops and filaments. However, as it can only be used with low viscosity bioinks (3.5 to 70 mPa.s) [45] the resultant mechanical properties are not ideal, and the produced scaffold might have difficulties in keeping its shape. Furthermore, as it uses small nozzles, cells are often deformed after printing and high concentrations of cells are needed (> 5 million cells/mL) [60].

While there are many distinct types of droplet bioprinting, inkjet printing (thermal, piezoelectric, electro hydrodynamic jetting and electrostatic), acoustic droplet ejection, and micro-valve printing [45], for the CNS studies the majority of studies use only two types: thermal inkjet bioprinting and piezoelectric inkjet bioprinting. Thermal inkjet printing works using an electrical heated printing-head, that creates air-pressure pulses which produces droplets [61] and allows for a resolution of 20-100 µm [47]. In the piezoelectric inkjet bioprinting the drops are made by applying a piezoelectric actuator, in which the voltage excites the piezoelectric crystal (in the printer head). Both the speed of the nozzle and the dimension of the bioprinted construct can be changed by varying the time, pulse and amplitude of the electric current. Since the cells are not exposed to heat or pressure, their viability is higher [47].

On the other hand, extrusion can be performed in two ways, pneumatically or mechanically (Fig. 10 B), with higher viscosity materials (30 to $6x10^7$ mPa s). It is also a simple and cheap method, but it only allows for the production of continuous filaments [45]. Despite this, the accumulation of subsequent layers of bioink gives the structures produced adequate structural integrity. Extrusion is often used in the form of micro-extrusion bioprinting, in which the cells are mixed into the ink and then are dispensed though nozzles or needles. Also, the position in the x-y axis, and then the z axis is given using a CAD-CAM program. While this method allows for the fabrication of structures with high cell density, the applied pressure and the nozzle diameter affect cell viability [47], due to the synergistic effects of compression, tension and shear forces that are created during the printing process. Therefore, on average, to decrease cell loss a larger nozzle diameters, lower hydrogel viscosities and lower printing pressure can be used [45].

Finally, bioprinting can be based on laser system (Fig. 10 C) which, by allowing the manipulation of single cells, is more accurate and precise than the other methods, but also much more expensive [45]. This is possible since the scaffold is produced when the metal surface where the bioink is placed is vaporized by the laser, dropping the precise bioink faction into a receiver structure [59]. Nevertheless, this method has not yet been used with neural cells. Another variation makes it possible to construct multilayered scaffolds by solidifying liquid-based resins using UV photopolymerization, in a process also called stereolithography [61]. Using this technique, it is possible to create scaffolds with high resolution by changing factors like laser power, time of exposure, size of the laser spot, light wavelength value. Moreover, the height of each layer is reliant on the light source energy and time of exposure, while the mechanical performance varies with the post-treatment process that are applied (heating or photocuring) [47].

Additionally, Fused Deposition Modelling (FDM) can also be used to create structures, but due to the high temperatures used, it can only be used to produce a substrate where cells can be seeded on [47]. FDM uses a temperature-controlled extruder to produce filaments of semi-molten thermoplastic polymers in a layer-by-layer structure [61] and to create scaffolds that solidify at room temperature. Furthermore, the direction of the deposition can be changed with each layer (laydown pattern), which allows, with changes of direction in each layer, the creation of scaffolds with uniform internal structures, controlled pore morphology and complete pore interconnectivity [61]. FDM is a cheap, simple and flexible process that does not require the use of solvents [47, 61]. Nevertheless, resultant scaffolds lack mechanical features, poor surface properties and can only be created with a small number of polymers. The mechanical properties of the structure can be tuned by changing the layer thickness, width values, direction of the filaments and air gap within identical layer or between layers, the latter being the major responsible force for mechanical weaknesses of the structure [47].

1.3.2. Bioinks

Regardless of the printing method, the characteristics of the bioink itself are the key element for printability, associated with the viscosity, and then cell viability and cell adhesion [58]. The inks are often hydrogels, synthetic or natural, that create 3D hydrophilic polymer networks after the process of crosslinking [58]. There are a diverse range of materials that have been used for neural 3D models. Among these, alginate, Poly(ethylene glycol) diacrylate (PEGDA), fibrin, chitosan, HA, silk fibroin, gelatin, agarose, methycellulose, and collagen are the ones that have showed more promising results [45].

Generally, a bioink has to fulfill a series of mechanical, rheological, chemical, and biological criteria to be considered ideal [62]. Together these properties should create a material capable of, among others, i) generating tissue constructs with suitable mechanical strength and robustness, though keeping the tissue-matching mechanics, if possible in a tunable manner; ii) adjusting gelation and stabilization to print structures with high shape fidelity; iii) mimicking the natural microenvironment by being biocompatible; and iv) being produced at a large-scale with minimal variations between batches [62].

It is based on these needs that hydrogels have risen as the most studied materials for 3D printing of neural cells. Their high water content creates an appropriate environment for cell embedding and post printing culture [48]. Additionally, hydrogels are highly porous, which allows an easy transport of nutrients, waste and other factors between cells inside the scaffold [57]. Hydrogels can also better simulate the mechanical properties and ECM functionality of neural tissue, since their elastic moduli is low (> 10 Pa) and their properties can be tweaked according to the necessity [48]. However, the same softness that is beneficial to the development of brain models it is not favorable for keeping the structures after printing which are highly prone to deformation, due to gravity or flow forces, related to surface tension and lack of elastic properties [48].

Based on these properties there are several natural and synthetic hydrogels that can be bioprinted for CNS applications. The following sections focus on the main materials used in bioprinting of neural cells, and some examples of applications both in the CNS and the PNS.

1.3.2.1. Natural Hydrogels

Whilst being not often used for bioprinting approaches due to its slow gelation [63] Matrigel®, a mix of ECM proteins derived from the basal membrane of mouse sarcoma, is still sometimes useful [48], due to the high number of Arg-Gly-Asp (RGD) cell binding sites [63] and capacity to support long-term survival of neural cells up to five months. Nonetheless, due to its origin, there are significant variations between batches, which may create inconsistences between experiments, decreasing the efficacy and pharmacological relevance of the results [48]. In the

CNS, Matrigel® has been shown to help axonal growth in a iPSC-derived NPCs and OLs microextrusion model in combination with gelatin and fibrin [64]. Furthermore, when mix with alginate, it allowed for a correct differentiation of iPSCs glial precursors after extrusion [65].

While other CNS decellularized ECM extracts also exist, whether from human or animal cadaveric donor tissues, that are later reconstituted to form hydrogels [48] natural hydrogels used for bioprinting are either ECM purified proteins (collagen and fibrin) or polysaccharides (alginate, chitosan, HA, cellulose and agarose) [48, 57].

Collagen is not a significant component of the brain matrix, thought collagen type IV appears in the interface between the CNS and blood vessels [48]. Despite this, collagen has many characteristics that make it an interesting material for neural system applications, such as the availability of several binding sites that help cell adhesion, migration, proliferation and differentiation, and the non-triggering of a significant immune response post-transplantation [47]. Although collagen can be used for both extrusion and inkjet printing, it also takes a significant amount of time to gel, due to its crosslinking requirements (temperature or pH) [66].

As a denatured form of collagen, gelatin is another natural polymer widely used for bioprinting applications mainly due to its interesting thermoresponsive properties [66]. At lower temperatures, gelatin strands self-associate creating helical structures in a gel-like form, while at higher temperatures the conformation returns to a random coil. Moreover, it keeps the RGD sequence from collagen, creating cell adhesion points in the structure [67]. Gelatin is often mixed with other polymers to improve its mechanical properties, creating bioinks with higher viscosities and better viscoelastic properties [66, 67], particularly as it is often used for inkjet or extrusion bioprinting [47]. A major disadvantage of gelatin relies on the rapid degradation and instability at physiological temperatures [48]. To overcome this, gelatin is often crosslinked with other molecules, like transglutaminase, horseradish peroxidase hydrogen peroxide or glutaraldehyde [67], in order to last longer in culture. A common variation of gelatin is methacryloyl-modified gelatin (GelMA), a photo-crosslinkable type that has been widely used due to rapid crosslinking kinetics and versatile mechanical properties [48]. Once the covalent crosslinking is promoted by UV the extent of crosslinking is easily controlled, as well as its physicochemical properties [62].

Fibrin is a protein derived from the enzymatic reaction between thrombin and fibrinogen that can be used for both extrusion and inkjet printing [66]. The fibrin networks are formed by filaments arrange as a soft complex, capable of a high degree of deformation without breaking [67]. This means that while fibrin is biocompatible, it lacks mechanical properties [66], it is soft and fragile [68], losing its shape, which is why it is usually mix with other polymers to increase its viscosity [66].

Concerning polysaccharides, HA is a non-sulfated glycosaminoglycan [67] that is used in a modified form or as a base for other materials in order to enhance cell adhesion, since it lacks mechanical stability and has slow gelation times [66]. Its structure consists of a series of

repeating disaccharide units of D-glucuronic acid and N-acetyl-D-glucosamine moieties that are linked by alternating β-1,4 and β-1,3 glycosidic linkages. HA has three main functional groups: glucuronic carboxylic acid group, the secondary hydroxyl group and the N-acetyl group, that control its chemical activity [67]. In particular in neural tissue, it has not been widely used *in vitro*, but rather in *in vivo* studies, where it has been shown to alleviate inflammation and decrease glial scar formation [47].

Chitosan is a linear amino-polysaccharide that originates from deacetylation of chitin, having β-(1-4)-linked D-glucosamine residues and randomly placed N-acetyl-D-glucosamine units [68]. As it has unstable mechanical properties, it is not easily printed [67]. Chitosan is only soluble at an acidic pH, hence it is only used in small quantities with other materials as it is not compatible with the pH of most animal tissues [68]. In the neural applications it has been shown to help promoting axonal growth and cell adhesion, as well as improve NSC differentiation *in vitro* [47].

Of all polysaccharides, alginate is perhaps the most versatile. It is a linear copolymer polysaccharide derived from brown algae that while biocompatible, it does not have any adhesive motives. It is composed of long chains of individual sugar residues b-D-mannuronate (M-subunits) and a-L-guluronate (G-subunits) [66]. Alginate crosslinking occurs between two blocks of adjacent polymer chains, in a way that is referred as an “egg-box” formation [69], either between the same type or alternating sub-units, with multivalent cations (i.e. Ca^{2+}, Ba^{2+}, Mg^{+} or Sr^{2+}) [70], based on interactions with the carboxylic groups in the sugars (Fig. 11) [66]. Its viscosity can be manipulated by changing the average molecular weight (MW), MW distribution, average chain subunit ratio (G to M ratio), concentration of the polymer and crosslinker, the pH of the solution, temperature or the presence of other cations besides the crosslinker [71]. Alginate can be used in any of the three main bioprinting techniques (extrusion, inkjet and laser), while offering mechanical protection to cells during extrusion and inkjet bioprinting by avoiding some of the damage caused by extensional flow. Additionally, based on the printing method, characteristics like concentration, temperature, and viscosity can be altered in order to optimize the results. Higher concentrations of high-MW alginates increase the stiffness of the structure, while also increasing the viscosity of the solution before gelation, which is not ideal as it can create high shear forces during printing that damage the cells. One solution is to mix high and low MW alginates, which significantly increases the elastic modulus, while keeping increases in viscosity to a minimum. Other solutions may be to change the degree of crosslinking and the gelation time [66]. Specifically for neural tissue applications alginate is used due to its shear-thinning behavior (the viscosity decreases with the shear stress) and fast gelation kinetics [48]. The problems associated with being bioinert can be overcome by modifying the structure with peptides sequences, like RGD, or add other polymers that improve cell adhesion, degradability or induce cell differentiation [66, 71].

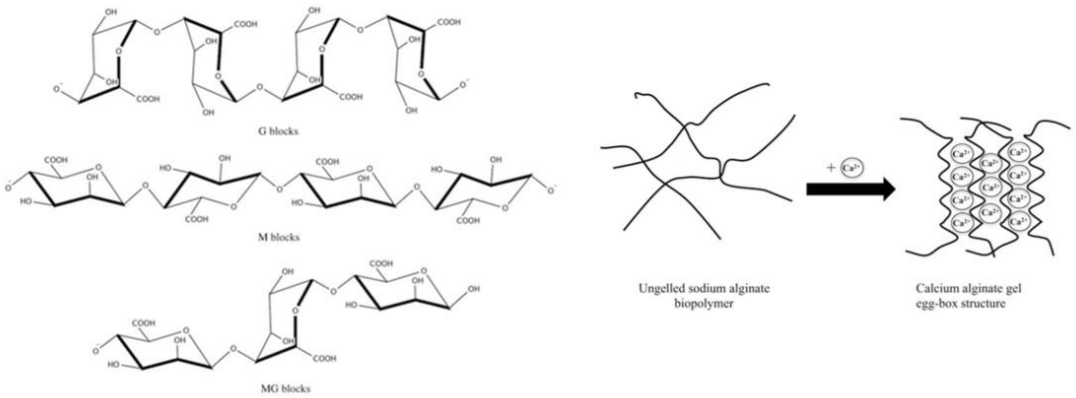

Figure 11 - Sequences of a-L-guluronate (G), b-D-mannuronate (M) and MG blocks (left). Schematic representation of the formation of an alginate gel with an "egg-box" structure in the presence of a divalent ion like Ca^{2+} (right). Adapted with permission from Critical Reviews in Food Science and Nutrition [69].

1.3.2.2. Synthetic and Hybrid Hydrogels

In order to overcome the batch-to-batch variability of natural origin hydrogels, different types of synthetic hydrogel-forming polymers have been developed. These polymers are usually combined with ECM-derived proteins, GAGs, growth factors or biofunctional peptides, creating natural/synthetic hybrid systems that enhance the biological performance and stimulate the embedded cells. Since these systems are completely chemically defined and highly tunable, it is possible to precisely control the physicochemical properties of the hydrogel and the introduction of bioactives cues [48].

For CNS applications, synthetic polymers have not been widely explored, but of those that have been, PEG and its derivatives are most studied [48]. PEG is a polymer that can be either linear or multi-armed, whose mechanical properties are highly tunable and, just like alginate, is bioinert. Notwithstanding this does not constitute a significant problem as PEG can be chemically modified to include different bioactive molecules that mimic cell-matrix adhesion points and signaling cues [66]. Generally, PEG and its derivates have been used for stereolithography, but also inkjet as its low viscosity allows it to be printed while sustaining its shape [66].

1.3.2.3. Advanced materials

More recently there have been some interesting developments related to bioinks, in particular with the production of conductive polymers and carbon-based nanomaterials.

Conductive polymers are attractive when electrochemical impulses are needed, specifically as they are intrinsic to the intercellular communication between nerve cells and have been shown

to play an important role in the targeted differentiation of NSCs. Poly(pyrrole) (PPy) is the most studied one for neural tissue, as it has unique electrochemical and stimulus-responsive properties. Its synthesis process is easy and flexible, allowing its production in large scales, at room temperature, in a variety of solvents, like water [61]. For example, *Zhao et al.* used stereolithography to print a silk fibroin scaffold with PPy coating where Schwann cells were later seeded. The results showed that the electrical conductivity increased with the diameter of the scaffold, a consequence of the presence of more PPy, and that the material was not cytotoxic or affected cell proliferation [72].

Other studies use poly(3,4-ethylenedixoxythiophene) (PEDOT), as it is a material soluble in a many different organic solvents, and suitable for chemical modification. In particular, Poly(3,4-ethylenedixoxythiophene):Poly(styrene sulfonate) (PEDOT:PSS) since it has a low oxidation potential and high electrochemical stability [61]. For example, *Heo et al.* used stereolithography to create an PEDOT:PSS and PEG diacrylate (PEG-DA) scaffold. DRG cell line cells were seeded on the hydrogel or encapsulated into GelMA and then seeded on the hydrogel. The results showed that the electrochemical properties of the hydrogel increased with the concentration of PEDOT:PSS. Cell viability was not affected when cells were cultured directly on the hydrogel. Moreover, when cells were encapsulated electrical stimulation was amenable to be used in order to improve neuronal differentiation [73].

On the other hand, carbon nanotubes (CNTs), have been used to reinforce hydrogel or fibrous scaffolds in order to improve their mechanical properties, particularly when it comes to structural strength and support. Both multiwalled CNT (MWCNT) and single-walled CNT (SWCNT) have been used in combination with both natural and synthetic hydrogels. Additionally, graphene was also been used in neural tissue engineering. Electrical, optical and thermal properties are similar with CNTs, but with more diverse electronic characteristics deriving from its 2D atomic sheet structure. Graphene is also able to be structurally robust and highly flexible at the same time, making it an interesting conductor when thin and flexible materials are needed [61]. For instance, *Zhu et al.* used stereolithography to print a GelMA and graphene scaffold, that was later seeded with NSCs, to create a structure with a defined geometry and that did not interfere with cell viability, proliferation and differentiation [74]. *Bordoni et al.* used extrusion to create cellulose nanofibrils-base, alginate-based and SWCNT-based conductive scaffold where neuroblastoma cells where seeded. The authors were able to produce conductive scaffolds that promoted differentiation with or without differentiation factors, and whose conductivity could be altered by inducing the crosslinking of alginate with calcium [75].

1.3.3. Bioprinting applications for CNS studies

As a new area of interest bioprinting of neural cells is still in the first steps of development. For instance, *Fantini et al.* showed that the extrusion process had no effect on the cell viability of both iPSCs derived from peripheral blood mononuclear cells to produce neurons and NSC, when printed into alginate or gelatin [76]. *Salaris et al.* were also able to prove not only that extrusion of cortical neurons and glial precursors derived from human iPSCs in Matrigel®/alginate did not severally impact cell viability, but also that the cells were able to differentiate, express the respective cellular markers and present membrane potential similar to the ones presented in 2D cultures [65]. More recently, *Ouyang et al.* used pneumatic extrusion to bioprint primary astrocytes in a mix of GelMA and gelatin (used as a thermo-reversible support material), without affecting cellular viability, proliferation capabilities and morphology [77]. Additionally, *Zhou et al.*, created a more complex system by using piezoelectric inkjet bioprinting to embed human NSCs with primary human astrocytes in an outer layer in Matrigel® and a lipid bilayer, without affecting neurons' viability and capability to migrate, with and without astrocytic support [78].

All these studies establish a basis for the development of bioprinted 3D models for demyelinating diseases, as they show that cells can be printed and retained their phenotypes. Nevertheless, a huge room for improvement still exists as myelination was not directly assessed. Consequently, the loss and recovery of myelin could be further investigated in this type of models as these are processes essential for the study of MS.

Besides serving as a very interesting technique to create tissue engineered platforms for demyelinating diseases, bioprinting has been mostly studied with the aim of creating implants that can facilitate the remyelination process, particularly after injury.

Chen et al. developed an extrusion-based collagen/heparin scaffold where NSCs were seeded in order to improve axon growth after spinal cord injury. This resulted in a scaffold with better mechanical properties than one only made of collagen, as heparin helped improve them, and allowed for the growth of cells in its pores [79]. However, the fact that the cells were not embedded in the bioink, but rather seeded over the scaffold might not be as interesting as the cells integration into the structure might be limited.

One the other hand, *Koffler et al.* used a microscale continuous projection printing method (µCPP) to print encapsulate rat NPCs in a PEG-GelMA scaffold which was then implanted in a rat model of complete spinal cord transection. After implantation there was minimal inflammatory response and glial scar formation, and even 6 months after the scaffold still retained their structure. Additionally, the spinal cord axons were remyelinated by Schwann cells and OLs and aligned with the scaffold. However, this axon growth was mostly in the scaffold and not in the adjacent areas [80], which can lead to questions related with its integration within the native tissue.

On other studies the use of the bioprinted structures is not fully determined, whether it is for implantation or not. Nonetheless, bioprinting has a huge potential to be a key technique for nerve tissue engineering. One example is the scaffold created by *Ning et al.* using a mix of alginate modified with RGD peptide, HA and fibrinogen, in which rat Schwann cells were embedded. Afterwards, the hydrogels were bioprinted by extrusion methods. The authors showed that RGD helped cell spreading, although neurite outgrowth was guided in the scaffold with or without this peptide. Additionally, the printing process did not affect cell viability, probably due to the low printing pressure and the low viscosity hydrogels. It was also showed that the concentration of fibrin was related to the stiffness of the structure, as higher concentrations led to stiffer scaffolds. However, probably the most interesting conclusion is that Schwann cells behavior did not significantly change with matrix mechanical properties changes within the range of stiffness tested (low stiffness) [81].

Haring et al. established a free-standing scaffold using micro-extrusion bioprinting, where rodent Schwann cells were encapsulated into Pluronic F-127 with methacrylated gelatin conjugated with dopamine or with HA conjugated with dopamine. These structures could be developed in a series of geometric patterns, and regardless if bioinks were chelated or photocured they did not dissolve in water, as oppose to the partial crosslinked ones that started to dissolve in 24-48 hours. However, the bioinks were not able to be stored, as there was phase separation after one day, and if the crosslinking was not performed completely the structure rapidly dissolved in water. Additionally, bioinks did not affect Schwann cell viability nor did affect their morphology [82].

Espinosa-Hoyos et al. used extrusion-based bioprinting to create PDMS (Young's elastic modulus E = 976 ± 11 kPa; diameter = 10 µm and lengths = 30-200 µm) and two pHEMA-based inks (low E = 88 ± 10 and high E = 333 ± 30 kPa; diameter = 10 µm and lengths = 30-200 µm) fibers. Pprojection micro-stereolithography (PµSL) was also used to create micropillars with two poly(HDDA-co-starPEG) (high E = 140 ± 35 kPa and very low E = 0.42 ± 0.14 kPa polymers; diameter = 10-20 µm and lengths = 70-130 µm). These structures were made to mimic the physical architecture of an axon where OPCs could be seeded. The results showed that OLs reacted differently depending of the stiffness, diameter, and coating of the scaffold: OL engagement increased at higher stiffness and lower diameters, and myelin production was greater when there was a laminin coating. These models are useful to study OPC and OL behavior, whether in healthy or pathological states. Despite their lack of biochemical cues, other different coatings could be applied, overcoming this issue [83].

Wu et al. fabricated an alginate/gelatin scaffold to encapsulate rat Schwann cells, that was later implanted into the back of nude mice. These extrusion-based structures allowed for cells to attach and elongate, connecting with each other, as well as expressing high levels of NGF and mRNA levels of BDNF, glial cell-derived neurotrophic factor (GDNF) and platelet-derived growth factor (PDGF).Moreover, there were no significant changes in properties when the scaffolds

were printed, though there was some swelling after one week. While the geometry is described as remaining unaltered in culture after one week, the material partially collapsed after extrusion, and 4 weeks after implantation the structure disintegrated and lost volume [84].

Table 2 summarizes some examples of bioprinting studies used to mimic the myelination process and the glial scar formation.

Table 2 - Summary of studies that explore bioprinting techniques to recreate the (de)myelinating and the glial scar environment or to be implanted into an injury site to help regeneration, in both CNS and PNS.

Study focus	Biomaterial	Cell type	Printing method	Cell seeding	Scaffold properties	Main conclusions	Model advantages	Model drawbacks	Reference
Implantation	Collagen/Heparin	NSCs	Extrusion	CS	• Compression modulus: ~3,5 MPa • Compressive strength: ~310 kPa	• Cells migrated into the material • Heparin → ↑ mechanical properties of collagen	• Biocompatibility • Suitable mechanical properties	• Cell seeding on the top of the scaffold is not the best approach for implantation purposes	[79]
Implantation	PEG-GelMA	Rat NPCs	µCPP	CE	• Elastic moduli: 260-300 kPa	• < inflammatory response • < glial scar formation • Slow degradation • Cells filled the lesions	• Long-term structure maintenance • < inflammatory response and glial scar formation • Axons aligned with the scaffold • Myelination spinal cord axons by Schwann cells and OLs	• Poor neuronal growth outside the scaffold after implantation	[80]
Create a Schwann cells scaffold	Alginate+RGD peptide/ HA/ Fibrinogen	Rat Schwann cells	Extrusion	CE	• ↓viscosity hydrogels	• CV = after printing • RGD → ↑ Schwann cells function • ↑ fibrin → ↑ stiffness	• Guided growth direction of neurites • ↓printing pressure → ↓process-induced stresses	• Manipulation → partial colapse • Scaffold degradation after 14 days in culture (scaffolds without RGD)	[81]
Create a free-standing scaffold	Pluronic F-127/ DC-gelatin-MA/ DC-HA	Rodent Schwann cell	Microextrusion	CE	• Chelated and photocured hydrogels • ~12 kPa moduli	• Dynamic loading → ↑ material properties • CV = after printing	• Stability of scaffolds under stress • Different geometries	• Impossibility of scaffold storage • Rapid scaffold dissolution if crosslinking is inefficient	[82]

Axon myelination	PDMS pHEMA poly(HDDA-co-starPEG)	OPCs	Extrusion PμSL	CS	• PDMS E ~ 980 kPa; pHEMA low E ~ 90 and high E ~ 350 kPa; poly(HDDA-co-starPEG) E ~ 0,5 and 140 kPa • Laminin surface functionalization	• > stiff axons → > OLs wrapping • < d → > OLs wrapping • ↑ laminin coating → > myelination	• Amenable for functionalization with biological relevant ligands • Possibility to mimic both healthy and disease states	• Lack of biochemical cues • Diameters not comparable with *in vivo* CNS axons' diameters	**[83]**
Implantation	Collagen/Heparin	NSCs	Extrusion	CS	• Compression modulus: ~3,5 MPa • Compressive strength: ~310 kPa	• Cells migrated into the material • Heparin → ↑ mechanical properties of collagen	• Biocompatibility • Suitable mechanical properties	• Cell seeding on the top of the scaffold is not the best approach for implantation purposes	[84]

Symbols: ↑ – higher/high/more significant; ↓ – lower/low/less significant ; → – leads to/after ;v – ideal concentration; CS – cells seeded on the scaffold; CE – cells encapsulated in the scaffold; h – height; d – diameter; E – Young's elastic modulus; = – not affected/remained the same; > – more/maximum; < – less /minimum; CV – cell viability; PEG-GelMA – polyethylene glycol methacryloyl-modified gelatin; HA – hyaluronic acid; DC – dopamine conjugated; PDMS – polydimethylsiloxane; PEG – polyethylene glycol; NSCs – neural stem cells; NPCs – neural progenitor cells; OPCs – oligodendrocyte precursor cells; μCPP – microscale continuous projection printing method; PμSL – projection micro-stereolithography; NGF – nerve growth factor; BDNF – brain-derived neurotrophic factor; GDNF – glial cell-derived neurotrophic factor; PDGF – platelet-derived growth factor

1.3.4. Future perspectives in the bioprinting of neural cells

As bioprinting techniques for the CNS are still in their infancy, a lot of work is still left to be done when one aims to create (de)myelinating and glial scar models.

One of the main questions that is still left to be explored relates to the printing of glial cells like astrocytes and OLs, whether separated or co-printed. The majority of studies in the neural system reported in the open literature were performed with rodent cortical neurons, Schwann cells or NSCs [45], which limits the scope they can reach. Moreover, as the majority of studies have used the PNS or the spinal cord as their target tissue the results and conclusions cannot be directly transposed into the brain, which becomes particularly relevant as the mechanical properties of the material play such an important role in the success of the model. As such there is still a clear need to further explore the printing of brain tissue specifically.

Additionally, there is a need to find an appropriate material for the bioink. Not only it has to be printable, but it also has to hold the structure in place and replicate the specific mechanical conditions of the (de)myelinating or the glial scar environment. The biggest concern is that most materials used to replicate brain conditions do not meet the criteria for printing, particularly the mechanical properties. Some of these problems can be alleviated by starting the crosslinking process before printing, though this can also lead to cell viability problems related to a higher osmotic pressure [45]. Another solution might lay in the usage of a co-axial nozzle, where the solution and the crosslinker are deposited at the same time, which leads to the gelation at the tip of the needle. This allows for the usage of low viscosity materials, but also the formation of hollow tubes and core-shell filaments of multiple materials, simply by changing the configuration of inner and outer nozzles [45].

Concerning the effects of the printing process on cell viability there is still a lot that is not clear. Generally, it has been reported that in extrusion-based methods cell viability is affected by the combination of compression, tension and shear forces that are applied on them during the printing process, and that lowering the viscosity of the hydrogel, using larger nozzle diameters and lowering the used pressure can fix this problem [45]. These generic truths have been used to explain why the cell viability of printed cells is not affected [81]. However, as a significant portion of studies focus on implantation, their goal is to understand if the new structure is biocompatible or not, rather than if the mechanical stress to which cells are exposed during the printing process affects their survival [79, 80]. As a consequence, there is still some uncertainty regarding the effects of the different printing processes on cell viability.

Regardless of the approach, bioprinting can surely become an interesting method to create reproducible 3D models of the glial scar that can later be used for high-throughput assays and drug screening, particularly due to the important role that the mechanical properties play both in the glial scar ECM and in the printing process.

Chapter 2 – Aim of the thesis

Strategies aimed at overcoming the loss of the myelin sheath, in demyelinating diseases, are often unsuccessful due to the lack of knowledge underlying the mechanisms of remyelination failure. Nevertheless, it is now becoming clearer that remyelination failure is intimately connected with the interactions of the different glial cells, as well as with the ECM. Specifically, the formation of a glial scar containing reactive astrocytes is considered a key regulator of the tissue altered biophysical properties. Our working hypothesis is that by tuning the mechanical properties of the lesion one can promote remyelination.

While it is not possible to study all the interactions at the same time, the development of complex 3D models aiming to incorporate the different cellular components and ECM is in the forefront of experimental design innovation. Up until now, there is no model that truly recapitulates the surrounding microenvironment of a demyelinating scenario. The design of a tissue engineered model able to approximate the ECM conditions would also be extremely valuable for drug testing purposes.

The aim of this thesis was to develop a printable alginate matrix with embedded astrocytes that can work as part of a larger system to recreate the glial scar environment observed in a pathological context, and possibly use it for high-throughput drug screening.

To accomplish this, combinations of oxidized alginate modified with a matrix metalloproteinase-sensitive peptide (PVGLIG) and alginate modified with a cell adhesion peptide (RGD) were used as matrices for the culture of rat primary astrocytes. The mechanical properties of these structures were characterized, as well as their influence in cell activity, morphology and survival. Finally, the possibility of automating and standardizing the production process was also explored using an adapted experimental bioprinting arrangement to extrude alginate with embedded

astrocytes[1]. Cellular metabolic activity, survival and morphology were also studied in the bioprinted matrices.

Specific objectives of the work included:

1. Preparation and characterization of cell laden alginate hydrogels with different peptide incorporation and oxidation status. Physical properties including rheological properties and stability of hydrogels as a function of days *in vitro* were assessed.
2. Establishment of rat primary astrocyte cultures in modified alginate hydrogels and evaluation of astrocytic viability and cellular morphology, as a function of hydrogel composition.
3. Optimization of the parameters to bioprint cell laden modified alginate hydrogels. Namely:
    - Automated alginate printing using an adapted extrusion bioprinter. Parameters assessed focused on culture plate and coverslip type, as well as the necessary volume.
    - Automated bioprinting of alginate with embedded astrocytes and characterization of resultant hydrogels properties and evaluation of astrocytic viability and morphology.

[1] Note: This thesis was part of the UT Austin Portugal Program funded project "MECHANO", in the framework of which the *Instituto Politécnico de Leiria (CDRSPP)* is developing a customized bioprinter for alginate extrusion in collaboration with our team. This was the system that was supposed to be tested in the context of the present thesis. However, due to the COVID-19 pandemic, the bioprinter development and set-up was seriously delayed. Consequently, an automatic liquid dispenser was used as an approach to mimic the bioprinting process and assess extrusion parameters, as well as the impact of this process on the cell behavior.

Chapter 3 – Materials and Methods

3.1. Animals

All procedures involving animals and their care were performed in agreement with institutional ethical guidelines (i3S), the EU directive (2010/63/EU) and Portuguese law (DL 113/2013). Animals had free access to food and water, being kept under a 12-h light/12-h dark cycle.

3.2. Cell culture

3.2.1. Brain dissections and collection of cortices

Primary mixed glial cultures (MGCs) were obtained from P1-2 Wistar Han rats by Eva Carvalho and Miguel Morais. All instruments used were sterilized by heat exposure (250°C, 60 s) and cleaned with 70% ethanol. Briefly, neonatal rat pups (8-12 pups) were euthanized through decapitation. The brains were dissected to collect pre-frontal cortices.

Holding the ears with forceps, the skin on top of the head was cut in a caudal-to-rostral direction and removed by pulling each part of the skin to opposite sides. Holding the head with the tweezers (without pressing to avoid brain damage) the underlying cranial bone was cut in a similar fashion. Moreover, small cuts from the middle to the lateral part were done, in order to divide the skull bone into four parts that can be used to separate the skull and expose the brain. The brain was then detached and collected in a Petri dish with Hank's Balanced Salt Solution without calcium and magnesium (HBSS, Sigma H2387-1L) supplemented with 2% (v/v) penicillin/streptavidin (P/S) and maintained on ice (in order to decrease tissue degradation and cell death). Cortex isolation was completed in HBSS 2% (v/v) P/S and under a magnifying glass. Brain hemispheres were separated with thin forceps, and the meningeal tissue removed and discarded. The cerebellum, basal ganglia and hippocampus were removed and discarded. The isolated pre-frontal cortices were maintained in HBSS 2% (v/v) P/S and on ice until dissociation.

3.2.2. Mixed glial cultures

Under a flow hood the HBSS medium was changed to a sterile HBSS 2% (v/v) P/S medium (1 mL per brain). Mechanical digestion was done by pipetting the cortices up and down until obtaining a visibly homogeneous suspension, that was later extruded using a 25G needle. Then the suspension was incubated with DNAse (0.1 mg/mL, Sigma D5025-15KU) and trypsin-EDTA (0.0025%, Gibco 25200) for 15 min, 37°C, flicking the tube every 5 min. This step promotes the enzymatic digestion of the tissue, separation into single cells and the degradation of DNA residues that might have been present due to the mechanical digestion. Afterwards the enzymes were inactivated by the addition of a similar volume of culture medium Dulbecco's Modified Eagle's Medium (DMEM) GlutaMAX™ High Glucose (Gibco 31966-021) supplemented with 10% (v/v) heat-inactivated foetal bovine serum (FBS, Sigma F7524, heat inactivated 30 min 56ºC) and 1% (v/v) P/S, hereby defined as cell culture medium. Finally, the suspension was centrifuged (500 g, 10 min), the supernatant discharged, and the pellet was resuspended in culture medium. The new suspension was transferred through a 70 µm nylon cell strainer (Falcon 352350) and distributed into 100 µg/mL poly-L-lysine (PLL, Sigma P2636, Mw 30 000-70 000) coated T75 flasks (SPL Life Sciences) (2 collected brains per T75 flask) with 10 mL of cell culture medium (37ºC, 5% CO_2). On day 4, 4 mL were changed for new medium. Afterwards the medium was changed every 2 days.

MGCs cultures are made of different glial cells that adhere to the PLL-coated culture flasks differently. The astrocytes adhere fist forming a bottom layer above which microglia and OPCs adhere.

3.2.3. Astrocyte isolation

The first step in obtaining an astrocyte culture consisted on the separation of the top layer of OPCs and microglia.

Around culture day 10-12, cells were totally confluent, and the astrocytic supporting layer was formed. Firstly, MGCs were submitted to a pre-shake (210 rpm, 2h, 37°C) in an Infors AG-4103 shaker, causing detachment of loosely adhered microglia. Medium with detached microglia was removed and cell culture medium was refreshed. Following a 2h incubation period (37°C, 5% CO_2), MGCs were submitted to shake-off (230 rpm, 37°C, overnight), resulting in detachment of OPCs and remaining microglia. The cell suspension was removed, and new cell culture medium was added. This process was repeated once a week for a maximum of 3 times. It is worth noting that during the shake-off procedures the astrocytic layer remained adhered to the bottom of the flasks.

Afterwards the astrocytes were passaged three times before being pure to use. For astrocytic trypsinization the medium was removed, and the cells washed with pre-warmed phosphate buffered saline (PBS). Cells were then incubated with 1 mL 0.25% (v/v) trypsin/EDTA (Gibco 25200, 37°C, 5% CO_2, 5 min) to allow cell detachment and aggregates' separation into single cells. The enzymatic digestion was stopped by adding cell culture medium (double volume of trypsin/EDTA), and the suspension was pipetted against the walls of the flask to help the cell separation process. Then the suspension was centrifuged (500 g, 5 min), the supernatant removed, and the cells resuspended. The cells were later seeded into T75 flasks (SPL Life Sciences) and cell culture medium was changed every 3 days.

To freeze down astrocytes, cells were trypsinized and counted using the Trypan blue exclusion assay. The suspension was then centrifuged (500 g, 5 min), the supernatant removed, and the cells resuspended in 70% (v/v) DMEM GlutaMAX High Glucose, 20% (v/v) FBS and 10% (v/v) dimethyl sulfoxide (DMSO). The resuspended cells ($1x10^6$-$1.5x10^6$ cells/mL) were transferred to cryovials and stored in liquid nitrogen until further use.

Astrocyte thawing was performed by transferring cells to -80°C overnight, and afterwards quickly defrosted at 37°C (1 min). Cell culture medium was gently added to the vial and cells were centrifuged (500 g, 5 min) to remove the excess of DMSO. Astrocytes were plated on T75 flasks ($1x10^6$-$1.5x10^6$ cells/flask) and cell culture medium was added.

3.2.4. Astrocyte culture purity determination

As astrocytes cultures come from MGCs cultures there might be some contamination with other glial cells that were not removed during the isolation process. To quantify astrocyte purity, cells were plated in tissue culture poly(styrene) (TCPS) 24-well-plates (243 cells/mm^2) and fixed after one and three days in culture. For cell fixation, the culture medium was removed, cells were washed twice with PBS (5 min, 37°C) and incubated with 4% fixative microtubule protecting paraformaldehyde (MP-PFA – 65 nM piperazine-N,N'-bis(2-ethanesulfonic acid) (PIPES), 25 mM 4-(2-hydroxyethyl)-1-piperazineethanesulfonic acid (HEPES), 10 mM egtazic acid (EGTA) and 3 mM $MgCl_2$ in PBS [85]) for 20 min at room temperature (RT). Afterwards, cells were washed with PBS (5 min, RT). For long-term storage, samples were kept in PBS containing 0.01% (w/v) sodium azide at 4°C.

Afterwards the permeabilization was performed by incubating the cells with 0.3% (v/v) triton in PBS for 15 min at RT and then blocked with 5% (v/v) normal donkey serum (NDS) in PBS (1h, RT). The primary antibody solution was incubated overnight in 0.15% triton, 1% NDS and PBS (4°C), and then washed three times with PBS (5 min, RT). Cells were then incubated with the secondary antibody (1h, RT, protected from light) diluted in 0.15% (v/v) triton, 1% (v/v) NDS and PBS.

Samples were then washed twice with PBS (5 min, RT, protected from light). Finally, the nuclei were marked with Hoechst (Invitrogen H3570; 1:1000 in PBS, 15 min, RT, protected from light), and washed twice with PBS (5 min, RT). For long-term storage, the samples were kept in PBS with 0.01% (w/v) sodium azide at 4°C.

The following primary antibodies were used: rabbit anti-Olig2 (1:400, Merk Millipore AB9610), rat anti-MBP (1:100, Bio-Rad MCA409S), rabbit anti-GFAP (1:1000, Abcam AB7260), mouse anti-β III tubulin (1:500, BioLegend 801202) and rabbit anti-IBA1 (1:500, Wako 019-19741). The following secondary antibodies were used (1:1000 dilution): Alexa-Fluor (AF) 568 anti-rabbit (Invitrogen A10042), AF 488 anti-rat (Life Technologies A21208), and AF 488 anti-mouse (Life Technologies A21202). Table 3 indicates the combinations of primary and secondary antibodies used.

Table 3 – Antibodies used to determine the presence of specific neural cell types in astrocytic cultures.

Cell type		Primary antibody	Secondary antibody
OLs	Lineage	Olig2 rabbit	568 anti-rabbit
	Differentiation	MBP rat	488 anti-rat
Neurons		β III tub mouse	488 anti-mouse
Astrocytes		GFAP rabbit	568 anti-rabbit
Microglia		IBA-1 rabbit	568 anti-rabbit

Images were later acquired using the INCell Analyzer 2000 (GE Healthcare, acquisition software v4.5) (25 fields per well, 20x objective), and analyzed using CellProfiler (version 3.1.9, https://cellprofiler.org/)) and CellProfiler Analyst (version 2.2.1, https://cellprofiler.org/cp-analyst/). The CellProfiler software was used to segment the images according to the florescent markers they exhibited. The nuclei were identified and segmented, and a radial expansion around it was created, and the intensity measured. Afterwards CellProfiler Analyst was used to classify the cells according to Random Forest algorithm with user-defined classes. The objects were added to each class until at least 100 cells were classified. An accuracy of the algorithm above 85% was accepted. Then the classifier was used for batch processing and data was analyzed using Excel.

3.3. Preparation of alginate discs

Alginate hydrogel discs were produced as described elsewhere [30]. Firstly, ultrapure alginates (NovaMatrix FMC PRONOVA UP LVG – High molecular weight) with a high glucuronic acid content (68%) were dissolved at 1.7% (w/v) in NaCl 0.9% (w/v) solution by mixing at 1400 rpm (Eppendorf Thermomixer comfort) overnight, RT. When needed, the alginate solutions were

sterilized by filtering with a 0.22 µm filter (Millex) and stored at -20°C until further use. Three different alginate units were used (Fig. 12): (i) unmodified alginate; (ii) alginate engrafted with cell adhesion RGD peptide (GGGGRGDSP [86], Mw 758.74 g/mol, peptide incorporation 20 mg/g alginate); and (iii) oxidized alginate, 10% theoretical molar ratio, incorporating the MMP sensitive peptide PVGLIG (GGYGPVG↓LIGGK [86], Mw 1074.23 g/mol, peptide incorporation 69 mg/g). Alginate oxidation and peptide incorporation in alginate was performed by Dr Marco Araújo and Eva Carvalho. Alginate formulations were produced by mixing unmodified alginate, alginate-RGD (final concentration 40 µM) and alginate-PVGLIG (final concentration 200 µM or 400 µM). Hereafter the different alginates will be designated as i) AlgHMW; ii) AlgOx10 200 µM PVGLIG; and iii) AlgOx10 400 µM PVGLIG.

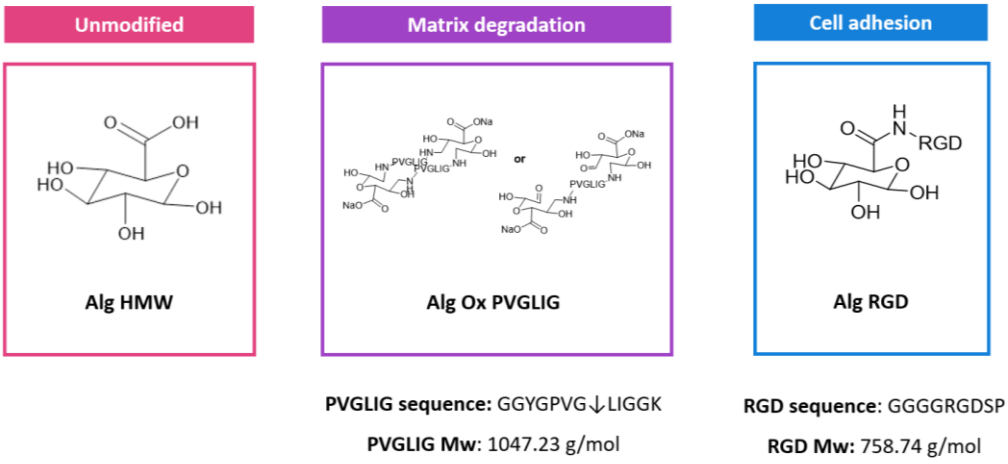

Figure 12 - Chemical structures of the different alginate units used. As alginate is a material without adhesion motives, peptide sequences were added to allow the interaction of the astrocytes and with the matrix. PVGLIG is a matrix metalloproteinase-sensitive peptide that was incorporated in oxidized alginate, creating therefore degradation points in the matrix. RGD is a cell adhesion peptide that was incorporated in pure alginate.

In situ hydrogel discs were prepared by mixing 1.7% (w/v) alginate formulations with $CaCO_3$ (FLUKA) (Ca^{2+}/COO^- molar ratio 0.288); δ-gluconolactone (GDL, Sigma) (Ca^{2+}/GDL ratio 0.125) and primary rat astrocytes in order to obtain a final concentration of 1% (w/v) alginate, 1.02 mg/mL $CaCO_3$, 14.52 mg/mL GDL and 4 million viable cells/mL (determined by Trypan blue exclusion assay). For the control discs, prepared without cells, the cell suspension was substituted with an equivalent volume of cell culture medium.

For the preparation of the $CaCO_3$ solution, the compound was firstly autoclaved and then weighted and dissolved in 0.9% (w/v) NaCl at a final concentration of 130 mg/mL. GDL was prepared at a final concentration of 205.7 mg/mL in NaCl 0.9% (w/v) and sterilized by filtration (0.22 µm filter, GyroDisc Syringe Filter SFPES030022S).

The final disc had a volume of 20 µL and were pipetted into non-cell-culture treated/suspension culture 48 well-plates (Greiner bio-one 677102) with a gel pipette. Crosslinking occurred at 37°C, 5% CO_2 during 30 min. Afterwards, cell culture medium was added to alginate discs and

maintained in culture at 37°C, 5% CO_2 during 1, 3 or 7 days. Cell culture medium was replaced at day 3 *in vitro* (DIV3).

3.3.1. Bioprinting of alginate discs

The production of alginate discs was automated using a liquid dispensing machine as an adaptative extrusion based bioprinting technique (Fig. 13).

Firstly, as explained before, alginate was mixed with primary rat astrocytes and $CaCO_3$ and pipetted into a 384 well-plate (32.9 µL; Costar, Cat. 3657) under sterile conditions and the plate was centrifuged for 20 s, to ensure that the mix was at the bottom of the wells. The GDL (2.5 µL) was added to the final mixture using a Multidrop™ Combi Reagent Dispenser (Thermo-Scientific). GDL was added at the same time to all wells and immediately before the next step, as its addition determines the start of the gelation process.

The plate was then moved to the JANUS with 4 Tip Arm and MDT Arm (PerkinElmer) workstation, a structure an incorporated mechanical arm capable of using 200 µL tips to pipette different volumes automatically. Here the GDL was homogenized into the mixture through up-and-down movements (4 times, 6 µL/s) and then 20 µL of the final solution were removed and extruded into a 3D printed 24 well-plate, made of epoxy resin (designed by Beatriz Custódio), containing Poly(ethylene terephthalate) (PET) coverslips (Sarstedt, 83.1840.002, 9 mm, cut with a metallic puncher) on the bottom of each well.

After alginate crosslinking (30 min, 37°C, 5% CO_2), alginate discs were transferred along with the coverslips to TCPS 24 well-plates (Falcon 353047) and cell culture medium was added. The discs were maintained in culture at 37°C, 5% CO_2 during 1, 3 or 7 days. Cell culture medium was replaced at day 3 of culture *in vitro* (DIV3).

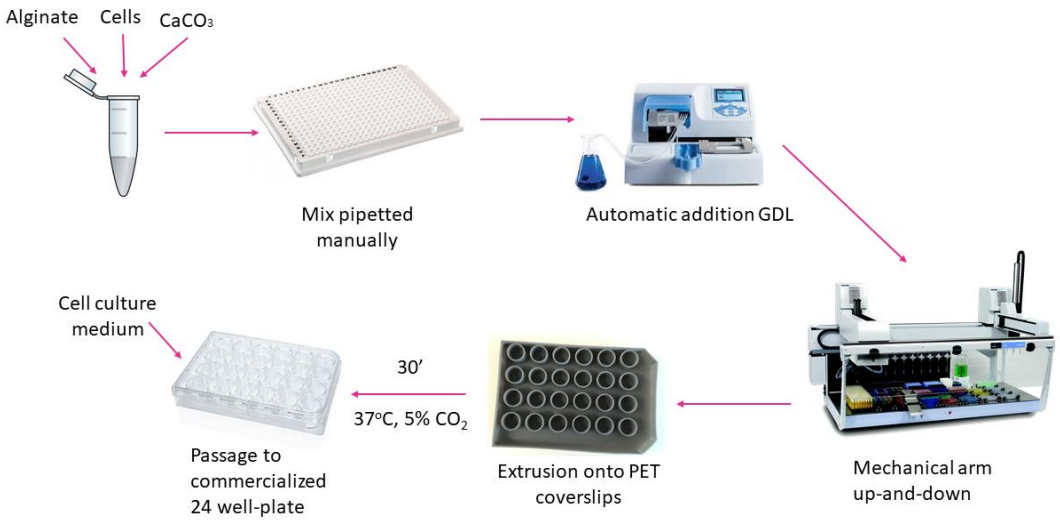

Figure 13 - Schematic representation of the process used to extrude the alginate discs.

In order to sterilize the coverslips and the 3D printed 24 well-plates, both were firstly washed with autoclaved deionized water for 10 min (twice), and then with 70% ethanol for another 10 min (twice). At the end, the materials were again washed with deionized water in order to remove any lixiviated products that might have been left on the wells. Afterwards, both materials were left to dry overnight under a flow chamber.

3.4. Characterization of cell laden alginate hydrogels

3.4.1. Rheological properties

For the characterization of the mechanical properties of the alginate discs (viscoelasticity), rheological measurements were obtained using the Kinexus Rheometer (Malvern Instruments Ltd.). The complex shear modulus (G*), elastic shear modulus (G'), viscous shear modulus (G") and phase angle (δ) were determined.

3.4.1.1. Rheological properties of alginate discs

Alginate discs were manually prepared as described above, with and without cells, and the mechanical properties were assessed after 1, 3 and 7 days in culture. Twenty-four hours before the rheological measurements the cell culture medium was changed to a DMEM Glutamax™ High Glucose containing 25 mM HEPES pH 7.5, in order to stabilize the medium pH at RT.

Four mm-diameter discs were used to perform oscillation tests with 4 mm sandblasted parallel-plate geometries, at 37°C in a humidified environment. Gels were compressed 30% of their height (oscillatory measurement gap). The linear viscoelastic region (LVR) was determined using amplitude sweep tests at a constant oscillation frequency of 0.1 Hz. Once the LVR was determined, oscillation frequency sweep tests were performed. For amplitude sweep tests, samples were submitted to strains in the range of 0.1-100%, at a constant frequency of 0.1 Hz (10 points per decade). For frequency sweep tests, samples were submitted to oscillations in the range of 0.01-0.5 Hz, at a constant strain of 1.5% (10 points per decade). Values of G*, G', G" and δ were determined from the frequency tests, with a tolerance range of around the median value of ± 10%.

The G* values were also used to obtain the Young's modulus (E) of the hydrogels. The E value is usually used to define the stiffness of a material. It can be calculated based on the following equation:

$$E = 2G^*(\upsilon + 1) \quad (1)$$

were G* is the complex modulus and ν is the Poisson's ratio [87] which was assumed 0.5 as alginate hydrogels are considered isotropic (i.e. mechanical properties have identical values in all directions) [88].

3.4.1.2. Mesh size

Rheology can also be used to indirectly determine the average mesh size (ξ) of the hydrogel, and as such determine the impact of the alginate modification and the presence of cells in the hydrogel structure.

According to *Karvinen et al.* definition the average mesh size is the distance between to crosslinking point, and can be calculated in nm as based on the following equation:

$$\xi = \left(\frac{G' N_A}{RT}\right)^{-1/3} \times 10^9 \quad (2)$$

where G' is the storage modulus, N_A is the Avogadro constant (6.022×10^{23}), R is the gas constant (8.314 J/K mol) and T is the absolute temperature (37°C = 310 K) [89].

3.4.1.3. Rheological properties during alginate gelation

The evolution of the viscoelastic properties of alginate hydrogels overtime was assessed using a sandblasted 20 mm parallel plate geometry with frequency and shear strain values within the LVR. Briefly, 170 µL of alginate mix were pipetted to the plate, and the gap was set to 0.5 mm. The frequency was kept constant at 0.1 Hz, shear strain at 1.5% and temperature 37°C, within a humidified environment. Every 30 seconds the G*, G', G'' and δ were determined during a period of 30 minutes.

3.4.2. Alginate disc morphology

Alginate disc morphology was determined by measuring the diameter and the height of the produced discs. To quantify the size of the discs, images were acquired using a Stereomicroscope attached to a camera. Images of the discs at different time-points were then analyzed using ImageJ/Fiji (version 1.52p; Rasband, W.S., ImageJ, U. S. National Institutes of Health, Bethesda, Maryland, USA, http://imagej.nih.gov/ij/, 1997-2016). The diameter of each disc was determined as the average of 6 random measurements.

The height of the discs was determined using a caliper (MHH Engineering Co. Ltd.). Three different measures were performed in each alginate hydrogel (total number of hydrogels five/per condition).

3.5. Cell metabolic activity

Cell metabolic activity was measured by assessing the fluorescence levels of resofurin. Resofurin is the molecule produced by the reduction of resazurin, a non-toxic, cell-permeable, redox-sensitive fluorescent dye that once metabolized creates a change in the color of the solution from purple to pink [90]. This change in color is also accompanied by a change in the fluorescence, which can be measured and used to determine the cellular metabolic activity.

The alginate hydrogels were incubated in a 11% (v/v) solution of resazurin (diluted in cell culture medium) for 3 hours (protected from light, 37ºC, 5% CO_2). Empty wells were also incubated with the resazurin solution to serve as blanks. Afterwards the medium was pipetted into a black 96 well-plate (Greiner Bio-one 655096). Fluorescence was measured at 530/590 nm using a fluorometer Synergy Mx (BioTek Instruments, GenX software). The metabolic activity of astrocytes was inferred by analyzing three alginate discs per condition and the fluorescence values for each alginate hydrogel were measured in technical triplicates. Since the fluorescence values obtained for the wells containing alginate without cells were similar to the blanks, the formers were used to remove the effects of the external factors that could be interfering with effective cellular fluorescence levels.

3.6. Live/dead assay

At a defined time-point, cells were washed with pre-warmed tris-buffered saline (TBS)-$CaCl_2$ (15 mM) (37ºC, 5 min, under agitation), and incubated with calcein-AM (1:250 diluted in TBS-$CaCl_2$ 15 mM) at 37ºC 5% CO_2, during 20 min. Afterwards cells were washed with TBS-$CaCl_2$ (15 mM) (37ºC, 5 min, under agitation), and incubated with propidium iodide (PI, 1:250 in TBS-$CaCl_2$ 15 mM, RT, 5 min). The excess of PI was removed by rinsing the discs with TBS-$CaCl_2$ 15 mM. The discs were immediately imaged using a confocal microscope (SP5, Leica, Germany,). Three different fields per hydrogel were acquired using a 10x objective (Numerical aperture – NA 0.4) and an average z-size of 350 mm (z-step size 5 mm).

The number of cells either alive, whose cytosol was market with calcein, or dead, whose DNA was marked with PI, was determined using the image analysis software Bitplane Imaris (version 9.5.1.; Oxford Instruments, Belfast, United Kingdom, https://imaris.oxinst.com/). For this purpose, cellular cytoplasm marked with calcein was segmented using the tool “Surfaces” and PI labelling was segmented using the tool “Spots”. Additionally, as there were cells sained with

both dyes a third category was created using “Surfaces” to mark the cells that had measurable intensity on both channels. Afterwards the automatic function that counts the number of each structure was used. To the total number of dead cells, and the total number of live cells, the number of cells marked with both dyes was subtracted. This step was necessary, since the cells could not be considered as healthy, since PI was able to stain the nuclei, i.e. the cell membrane was compromised; but the cells were still able to metabolize calcein, something that is not possible for dead cells.

3.7. Immunocytochemistry

For experiments involving immunocytochemistry analysis, before fixation, the cell culture medium was removed, and cells were washed twice with TBS-$CaCl_2$ 15 mM (10 min, 37ºC, under agitation). Afterwards, cells were fixed with 4% (v/v) MP-PFA diluted in TBS-$CaCl_2$ 15 mM (20 min, RT) and washed again twice with TBS-$CaCl_2$ 15 mM (10 min, RT, agitation). For long-term storage, samples were kept in TBS-$CaCl_2$ 15 mM supplemented with 0.01% sodium azide at 4°C.

Subsequently, cells were permeabilized by incubation with 0.3% triton in TBS-$CaCl_2$ 15 mM (75 min, RT, under agitation) and blocked using 1% (v/v) bovine serum albumin (BSA) diluted in TBS-$CaCl_2$ 15 mM (1h, RT, under agitation). Later the alginate hydrogels were incubated with the primary antibody (1:8000 GFAP in TBS-$CaCl_2$ 15 mM, 1% (v/v) BSA and 0.15% (v/v) triton; overnight, 4ºC, under agitation). The discs were washed three times with 0.05% (v/v) triton in TBS-$CaCl_2$ 15 mM (30 min, RT, agitation) and incubated with the secondary antibody (1:500 488 anti-rabbit) diluted in TBS-$CaCl_2$ 15 mM , 1% (v/v) BSA and 0.15% (v/v) triton for 5h at RT under agitation and protected from light. The discs were washed three times with 0.05% triton in TBS-$CaCl_2$ 15 mM (30 min, RT, under agitation and protected from light) and finally the nuclei was stained with Hoechst (1:1000 in TBS-$CaCl_2$ 15 mM) for 15 min at RT under agitation and protected from light. Finally, alginate hydrogels were washed once with 0.05% (v/v) triton in TBS-$CaCl_2$ 15 mM (15 min, RT, under agitation and protected from light), and stored in 0.01% (w/v) sodium azide in TBS-$CaCl_2$ 15 mM at 4ºC.

Images were acquired using a confocal microscope (SP5, Leica, Germany), 20x objective (NA 0.7) and an average z-size of 177 mm (z-step size 2.0 mm), and analyzed using ImageJ/Fiji (version 1.52p; Rasband, W.S., ImageJ, U. S. National Institutes of Health, Bethesda, Maryland, USA, http://imagej.nih.gov/ij/, 1997-2016).

3.8. Statistical analysis

Statistical analysis was performed using GraphPad Prism (version 7.03, www.graphpad.com). Data are shown as mean ± standard deviation (SD). All datasets included in this report were in the interval between the average and twice the standard deviation. Statistical differences between groups were calculated based on two-way ANOVA (influence of two factors), followed by Tukey's multiple comparisons test. A p-value below 0.05 was considered statistically significant.

Chapter 4 – Results and Discussion

4.1. Alginate hydrogels remain morphologically stable overtime

In order to recapitulate the astrocytic microenvironment, astrocyte laden alginate hydrogels were formed through internal gelation using calcium as the crosslinker. Different alginate discs were produced, varying the concentration of oxidized alginate with engrafted PVGLIG and maintaining constant the concentration of the cell adhesion peptide RGD. Unmodified alginate was used as a control.

Alginate was chosen as the matrix to mimic the 3D environment of astrocytes as its gel structure is structurally similar to that of the components of the ECM [91]. Despite the fact that alginate has no cell adhesive motives, it can be chemically altered to include different peptide sequences that can improve its interactions with the cells [71]. This polymer is also stiffness-tunable, which means that one can easily change its stiffness by, for instance, change ionic crosslinking concentration or alginate content [66, 71] and specifically study the effect of the viscoelastic properties on cellular behavior. Additionally, alginate is biocompatible, easy to produce and work with, and produced matrices are highly reproducible. Alginate also has low cellular toxicity associated and relatively low costs [91]. Moreover, the crosslinking process also allows the recovery of the cells after culture through the use of chelators [69], thus further biochemical or cellular analysis can be performed.

Before any other analysis, a characterization of the morphology of the alginate formulations overtime, and their stability is imperative. Particularly, if their macrostructure evolves with time as a function of peptide modifications and cell presence.

Therefore, the evolution of the discs' diameter was assessed by measuring the diameters of the hydrogels using images taken with a stereomicroscope (Fig. 14). The disc height was inferred using a caliper.

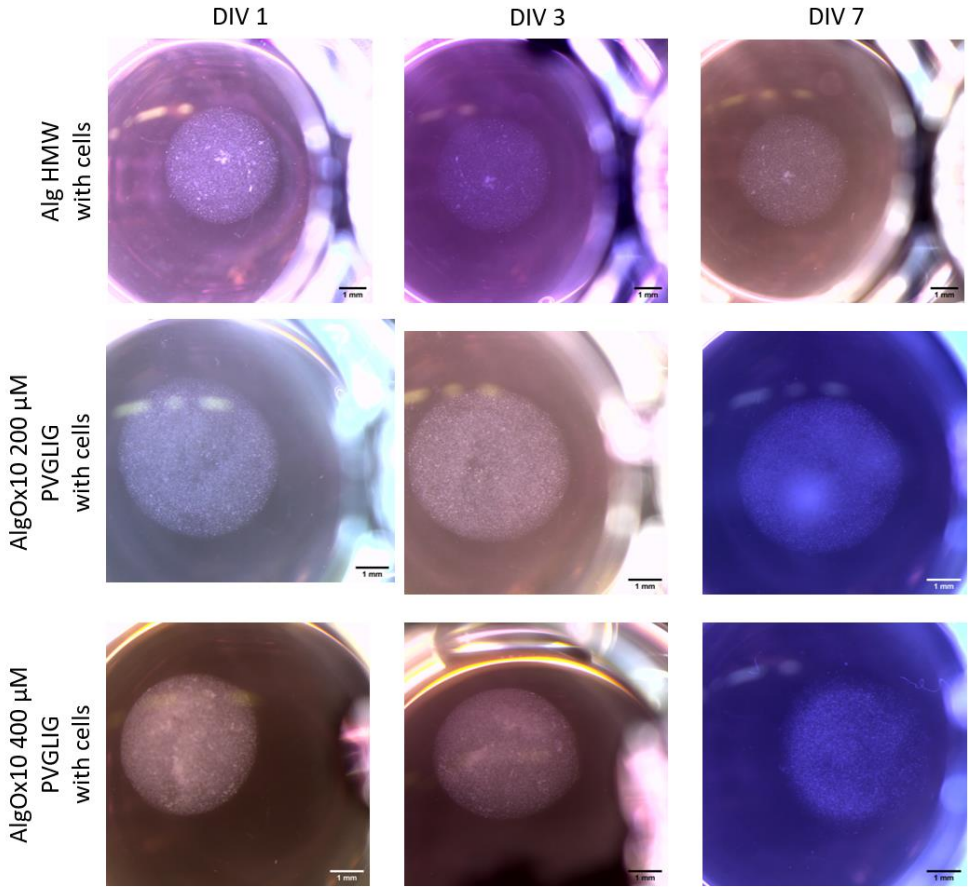

Figure 14 - Representative images of alginate discs with embedded astrocytes at different incubation times. Scale bar: 1 mm. (DIV: days in vitro).

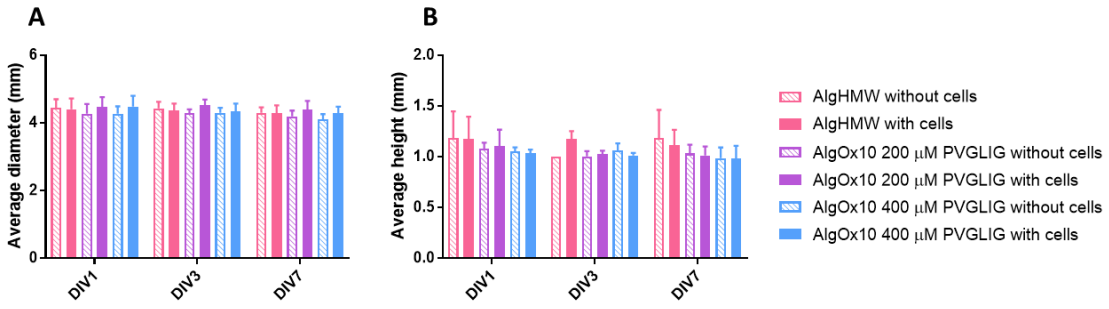

Figure 15 – Alginate hydrogels diameter and height as a function of days in vitro (DIV). Disc diameter (A) was determined to be around 4.3 – 4.4 mm. n = 3 independent experiments, 6 measurements of 1 technical replicate. Statistical analysis was performed using Two-way ANOVA and Tukey's multiple comparisons test, and there were no statistically significant differences between the conditions. Disc height (B) was determined to be around 1 – 1.2 mm. n > 4 technical replicates from 2-3 independent experiment. Statistical analysis was performed using Two-way ANOVA, Tukey's multiple comparisons test. No statistically significant differences between the conditions were observed.

The obtained results show (Fig. 15) that there is no significant difference between the discs' diameter and height regardless of the variable changed (incubation time, presence of cells or alginate modifications).

The discs' diameter varied between 4.2 – 4.5 mm, which is particularly interesting because in a previous study with alginate modified with RGD and PVGLIG, there was a decrease in the size of

the discs, laden with cells, after one week [86]. However, it should be noted that in the study by *Fonseca et al.* the team used twice the concentration of human mesenchymal stem cells (hMSCs) in relation to the present study. Moreover, it is possible that these cells produce more and distinct MMPs then astrocytes, the molecules responsible for the cleavage of PVGLIG, though this should be more thoroughly studied. Taken together, these reasons might explain the different outcome observed in both situations. Additionally, the study of the effects of the alginate modifications on the astrocyte MMPs production, while not performed, is an interesting aspect to be assessed in the future, as this might also influence the stability of the disc.

Moreover, the fact that the disc height also remained reasonably unchanged (around 1 – 1.2 mm) is also interesting, as the process associated with its determination was not as straightforward as the process used for disc diameter evaluation. The heigh was assessed as part of the essential step in the rheological assays: the measurement of the gap parameter for each hydrogel. In order to perform these measurements, the discs were removed from the well, cut, and then transferred to a spatula and their height measured with a caliper. During this process, especially for softer hydrogels, the discs might be deformed or damaged which compromised the precision of the measurement.

The stability of all discs, whether in diameter or height, overtime is a good starting point for the following rheological assays, as they rely on comparable size samples.

4.2. Evaluation of the mechanical properties of different alginate hydrogels

4.2.1. Modified alginate matrices are softer than unmodified alginate

In the development of biological relevant tissue engineered matrices it is of utmost importance to understand their mechanical properties as they play a critical role in modulating cellular behavior, and more accurately recreating the cellular structures present *in vivo*. Moreover, mechanical properties are also an indicator of the cellular activity since the cells themselves produce factors, enzymes and ECM proteins, that can physically and chemically reshape their surroundings, so the influence of astrocytes was also studied.

Taking this into consideration, a rheometer was used to perform oscillations assays (amplitude and frequency) in 4 mm discs. The objective was to understand how the alginate type (unmodified, oxidized alginate modified with 200 µM of PVGLIG and 40 µM of RGD, and oxidized alginate modified with 400 µM of PVGLIG and 40 µM of RGD), time of culturing (1, 3 or 7 days *in vitro*) and the presence of astrocytes affected the stiffness of the hydrogels.

Firstly, samples were subjected to amplitude sweep tests to determine the LVR, i.e., the range in which the test can be carried out without destroying the structure of the sample. Figure 16 shows a representative graph of one of amplitude sweep tests.

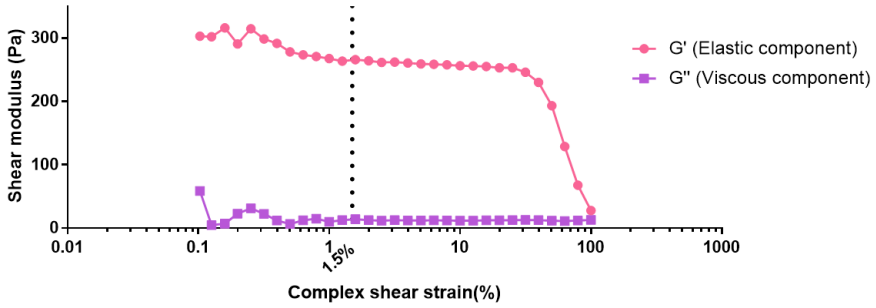

Figure 16 – Representative graph of an amplitude sweep test (shear strain 0.1-100%, 0.1Hz, 10 points per decade) for AlgHMW with cells (DIV 1). G' (elastic component) stabilized in the 1-16% shear strain range.

As an example, in the case of AlgHMW with cells at DIV 1, the elastic shear modulus stabilizes around 260 Pa between 1-16% shear strain, and then starts to decrease significantly. This means that the material stops being able to return to its original form and stars to break down, i.e. 16% is the threshold when the deformation stops having an elastic behavior and stars to have a plastic one.

The determination of this interval was necessary for performing frequency sweep tests, used to analyze the viscoelastic properties of the material. For this type of assays a shear strain was chosen from the LVR, to ensure that the results are not affected by changes/deformation of the structure. Hence, after some iterations for the frequency (5% and 1.5% shear strains were tested) the value chosen was 1.5%, as it was a common denominator for the different conditions.

The values of G* (complex modulus – measures the total stiffness or resistance to deformation), G' (storage/elastic modulus – measures energy storage, or the elastic contribution to G*), G'' (loss/viscous modulus – measures energy loss, or the viscous contribution to the G*), and δ (phase angle – measures the difference between the input stress and the measured strain) were determined from frequency sweep measurements [92]. Moreover, based on Equation 2 it was possible to determine ξ (mesh size – measures the distance between two crosslinking points) [89]. Figure 17 presents the average values of these parameters for each tested condition.

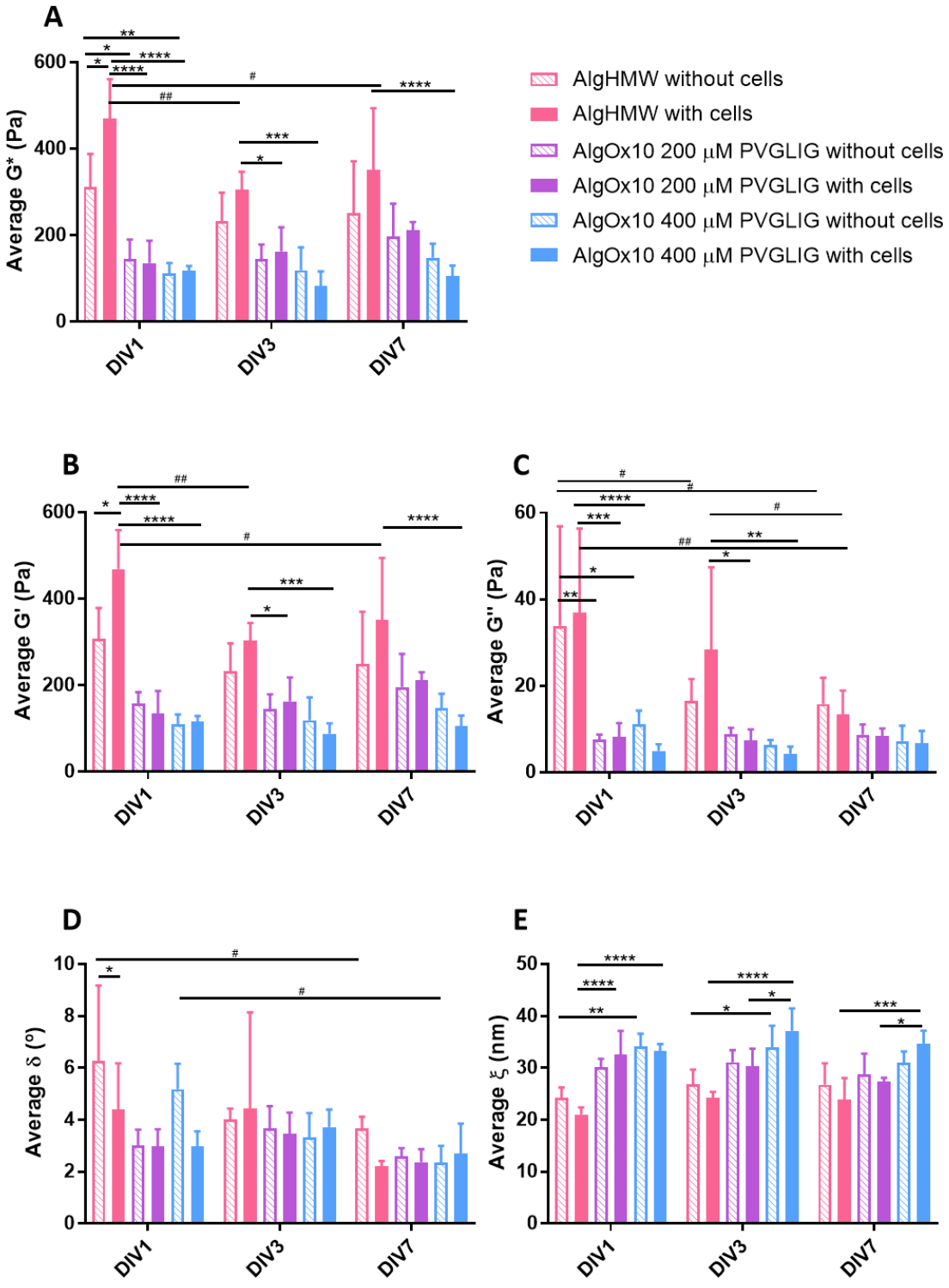

Figure 17 – Rheological properties of alginate hydrogels as a function of the days in vitro (DIV). Graphs show the average values of G (A), G' (B), G'' (C), δ (D) and ξ (E). The effects of the alginate modifications, presence of cells, and culture time are presented. The frequency varied between 0.01-0.5 Hz, and the shear strain was kept constant at 1.5%. n=3-4 alginate discs from 1 independent experiment. Results show mean ±SD. Statistical analysis performed using Two-way ANOVA and Tukey's multiple comparisons test. Symbols for comparison between conditions at the same time point are indicated by '*' and between same conditions but at different time points are noted by '#'. *p<0.05, **p<0.004, ***p<0003, **** p<0.0001.*

Solid structures with viscoelastic properties, like it is the case for hydrogels, present a G'>G'' and δ closer to 0°. More liquid-like structures present G'' values higher than G', and δ closer to 90° [93]. Therefore, it was expectable that the fully formed alginate discs would present, regardless of modifications, lower values for δ, and significant differences between G' and G''. Moreover, as the modified alginates were, empirically, softer, it was to be expected that these would have a smaller difference between G' and G'', in comparison to the unmodified control.

Generally, it has been shown that chemical modifications to the alginate's network induces changes in its mechanical properties [94]. Specifically, *Dalheim et al.* used 8% oxidized alginate modified with methyl tyrosine ester, the hexapeptide GRGDSP involved in cell adhesion and β-cyclodextrin in order to study how these alterations changed the mechanical properties of the alginate. The results showed that oxidation led to low values of Young's Modulus (E) (a measure of stiffness related with G*, Equation 1) and that the increase concentration of modifications lowered the values even more [95].

Similarly, in this study, the presence of oxidized alginate modified with PVGLIG and RGD lead to a significant reduction of the stiffness of the matrix, as expected. The presence of the modifications, and to a lesser extent the increase of the PVGLIG concentration, led to a reduction of the G* in the absence of cells, at DIV 1, from 311.0 ± 77.1 Pa in the unmodified alginate to 145.7 ± 44.5 Pa and 112.2 ± 24.0 Pa, for AlgOx10 200 µM PVGLIG and AlgOx10 400 µM PVGLIG, respectively. A possible explanation is that the modifications in the alginate interfered with the normal packing of the polymeric network. Particularly, the alginate oxidation leads to a chain scission on its network, and, consequently, a reduction of the calcium crosslinking points. This creates more space inside the polymeric network, decreasing the stiffness. Moreover, the usage of oxidize alginate itself, has been shown to creates more space in the alginate network and, consequently, softer structures [96], which is in line with these results.

Additionally, the increase of the concentration of the PVGLIG, while not being statistically significant, led to a slightly reduction of the G*, as the presence of more modifications interferes more with the packing of the polymeric network. It should be highlighted that the specific effects of the presence of RGD alone were not studied in the framework of this project.

Furthermore, the presence of astrocytes, in the modified alginates, did not change the mechanical properties of the material, unlike in the unmodified control alginate where there was an increase of stiffness, observed in G* (Fig. 17 A) and G' (Fig. 17 B), at DIV 1. As previously explained, PVGLIG is a proteolytical-degradable peptide sequence, thus, by producing MMPs (peculiarly MMP-2 and -9), cells have the capacity to remodel their environment by the cleavage of its structure [71]. The increase in cellular activity and activation, created by the interaction with the matrix also leads to an increased production of other matrix components that can also influence the general properties of the matrix. These new matrix components are a probable explanation for the mechanical properties' stability of the discs overtime, even if the PVGLIG

had been cleaved. The absence of significant variations within days of culturing even in the absence of cells, again suggested that the material is stable overtime

At the same time, the mesh size (Fig. 17 E), was also stable overtime for all conditions tested but varied with the modifications. Expectedly, the alginate oxidation and the introduction of the PVGLIG sequence led to a slightly higher, though not statistically significant, mesh size values, due to their interference in the polymeric network. Furthermore, when astrocytes were embedded within modified alginate formulations, there was a significant increase of the mesh size of the hydrogel network, particularly at DIV 1, in comparison with the control. Apart from the role of the alginate modifications on mesh size values, the presence of cells also influences this parameter once they create physical barriers that reduce the crosslinking points, leading to bigger spaces in the polymer network.

Specially as the mesh size is determined based on indirect measurements of rheological data, it might not be entirely accurate as far as the influence of the cells overtime is concerned. Astrocytes in modified alginate have the ability to both cleave the alginate, and produce new ECM components, which changes the characteristics of the matrix. Moreover, as they are able to adhere to it, they might also help with the "crosslinking" of its structure. As such, while the mesh size might, overall, not vary significantly with time, the composition of the matrix is significantly distinct. Therefore, it would be important to, in addition, study these hydrogels using scanning electron cryomicroscopy (cryo-SEM), in order to observe the matrix at the microscopic level. Moreover, matrix composition could be characterized by immunocytochemistry that allow specific quantification of the components.

Additionally, by using the values of G* to estimate the Young's module (E) (Table 4), based on Equation 1, it was possible to compare the stiffness of the alginate discs with the stiffness of the healthy brain parenchyma (0.1–10 kPa [17]). The fact the alginate hydrogels have a value of E inside the range supports the hypothesis that these are suitable to be used in tissue engineered brain models.

Table 4 - Calculated values of the Young's modulus (E) based on the rheological properties of the alginate hydrogels. All values are presented in Pa (mean ± SD). n = 3 or 4 alginate discs from 1 independent experiment. (DIV: days in vitro).

		DIV 1	DIV 3	DIV 7
Alg HMW	Without cells	(9.33 ± 2.31) x10^2	(6.99 ± 1.97) x10^2	(7.52 ± 3.62) x10^2
	With cells	(14.1 ± 2.73) x10^2	(9.18 ± 1.24) x10^2	(10.5 ± 4.29) x10^2
Alg Ox10 200 µM PVGLIG	Without cells	(4.37 ± 1.34) x10^2	(4.38 ± 0.99) x10^2	(5.90 ± 2.30) x10^2
	With cells	(4.07 ± 1.56) x10^2	(4.89 ± 1.68) x10^2	(6.34 ± 0.58) x10^2
Alg Ox10 400 µM PVGLIG	Without cells	(3.36 ± 0.72) x10^2	(3.58 ± 1.59) x10^2	(4.44 ± 0.99) x10^2
	With cells	(3.54 ± 0.35) x10^2	(2.5 ± 1.01) x10^2	(3.15 ± 0.75) x10^2

4.2.2. The gelation process of the hydrogels is delayed in modified alginates

Since one of the major aims of this project is to understand the ability of the different alginate formulations to be printed by extrusion processes, with crosslinking happening through internal gelation, it is relevant to understand the way the gelation process occurs. When gelation starts, the properties of the material also start to change. Consequently, resistance to the printing process is expected to increase, and cells might incur in more damage. For this reason, the moment in which a bioink stops behaving like a liquid and starts to adopt a more solid-like structure, becoming more resistant to deformation, is a key moment to be determined.

Hence, the gelation profiles of the different alginate formulations were assessed using a rheometer at a constant shear strain of 1.5% and a frequency of 0.1 Hz (inferred from the oscillation measurements, explained in section 4.2.1). For this assay, the mechanical properties of the different alginates without cells were measured for 30 minutes (the established gelation time *in vitro* for all the experiments described).

The results are presented in Figure 18.

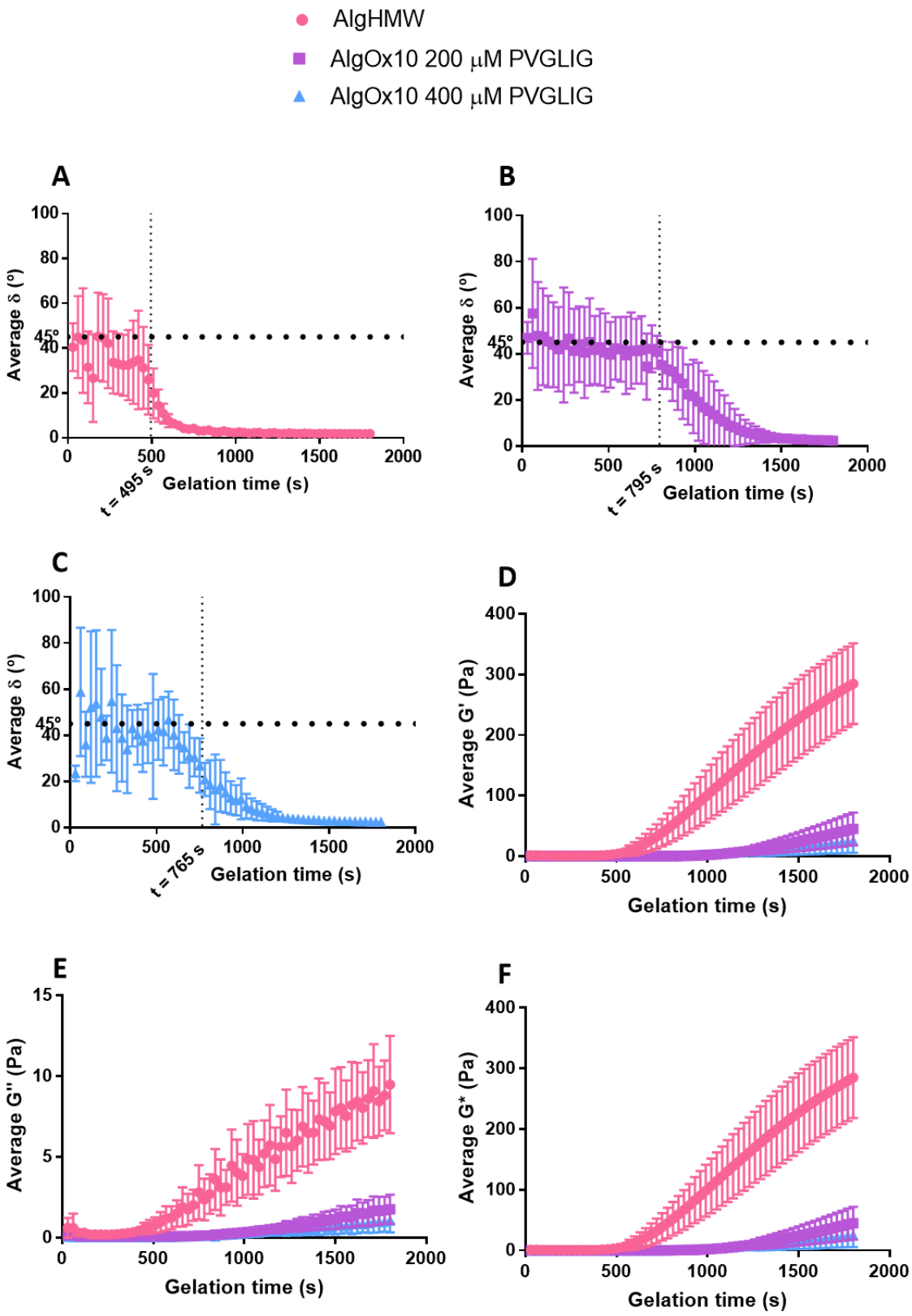

Figure 18 - Evolution of δ (A, B, C), G' (D), G''(E) and G (F) over the gelation time. n = 3 or 4 technical replicates from 1 independent experiment. The gel started to solidify once the δ was above 45º, which coincides with the moment when the other values start to increase. These intervals were determined using the lowest first derivative value of the δ. Graphs show mean ±SD.*

The determination of the gelation starting point is linked to the moment the material stops behaving like a liquid and starts to behave like a solid. Although generally a material is classified as viscoelastic/solid when G'>G'' and δ<45^{o} [93], the results of the alginate gelation profile show that for the entire assay G' was always higher than G'', even if marginally in the initial minutes. This is a consequence of the polymer intrinsic viscosity properties, therefore, the most important variable when determining the point when the gelation starts to take place is the δ.

Taking the unmodified alginate as an example, it is observable that the phase angle values started around 45^{o} and stayed relatively stable until the 480-510 seconds (8 minutes). After this point, the value of the δ decreases significantly, at the end stabilizing at around 2^{o}. This inversion point, when the δ starts to have a tendency to 0, also coincides with when G', G'' and G* start to increase, clearly indicating that this is the moment when stiffness begins to increase. Moreover, this relation is also valid for the modified alginates, although it happens later (AlgOx10 200 µM PVGLIG at 780-810 seconds, and AlgOx10 400 µM PVGLIG at 750-780 seconds), and the increase in G', G'' and G* is not as significant, as it was expected based on the mechanical properties previously determined (section 4.2.1.). This delay in gelation is most likely related with the smaller number of crosslinking sites due to the oxidation and modifications, as explained before.

Moreover, the general behavior of the G' and G'' is consistent with what was been previously reported for alginate [97, 98].

The determination of the moment when the mechanical properties start to change offers some insights into the process associated with the formation of the discs that might be useful when trying to keep an internal crosslinking process for bioprinting. The critical point is the moment the hydrogel starts to gel and offer resistance to the printing process, regardless of the chosen method for loading of the bioink (whether by pipetting it into a syringe or by tip suctioning). As it becomes harder to print the hydrogels, the pressure exerted on the material and the embedded cells, increases. Thus, it would be interesting to test the gelation process with astrocytes, as cells may affect the gelation time, as they occupy space in the polymeric network, possibly limiting the number of available sites for crosslinking.

Overall, these results showed that there is a safety interval that can be used to print the alginate hydrogels without any significant increase in resistance to the printing. Moreover, modified alginates present delayed gelation times which might be beneficial for the printing process.

4.3. Astrocytes survive and have a similar morphology to *in vivo* in modified alginate discs

4.3.1. Evaluation of astrocytic cultures purity

Primary astrocytes were isolated from a mixed neuronal cell population derived from Wistar Han P1-2 cortices (MGCs, as described in chapter 3.2). The protocol used to isolate astrocytes is based on the differential adherent properties of the cells: while microglia and OPCs are loosely attached cells, astrocytes tightly attach to the surface of the PLL-coated flasks. Through a series of shake-offs the majority of the microglia and OPCs are removed, and after some passages it is possible to obtain mostly astrocytes.

To determine the purity of the cultures, astrocytes were seeded on 2D cell culture plates and labelled for characteristic neuronal markers, at DIV 1 and 3. The results presented (Fig. 19) depict the number of cells classified using CellProfiler Analyst software.

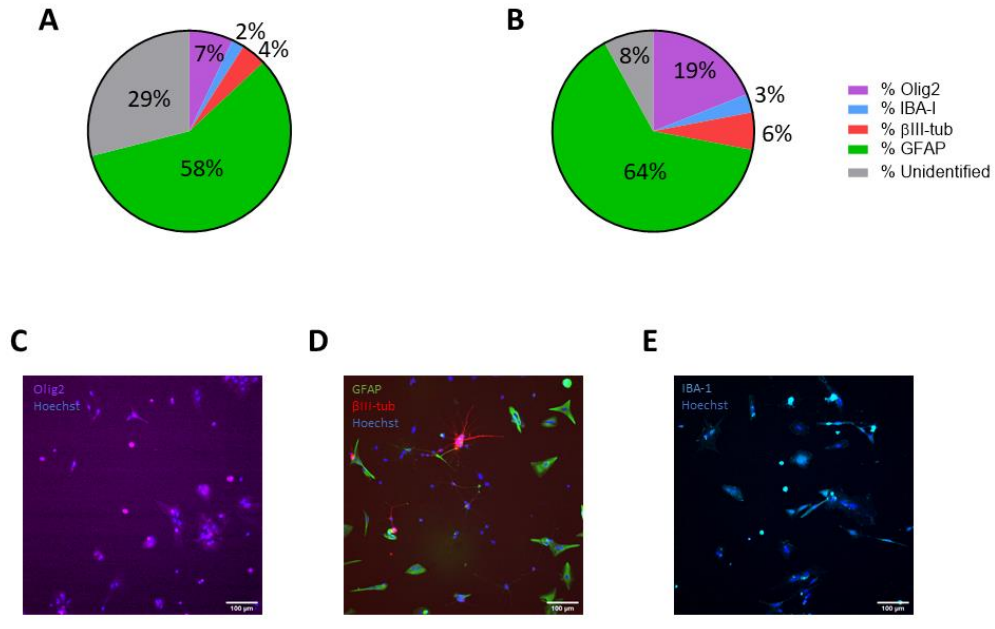

Figure 19 - Astrocytic culture purity as determined in 2D in percentage of each cellular marker, as function of days in vitro (DIV). DIV 1 (A) and 3 (B). n=1 independent experiment, 1 technical replicate. 2013 total cells counted at DIV 1, and 1987 at DIV 3. Representative images of cells stained with Olig2 (magenta, oligodendrocytes) (C), GFAP (green, astrocytes) and βIII-tub (red, neurons) (D) and IBA-I (cyan, microglia/macrophages) (E), and nuclei counterstained with Hoechst (blue). Scale bars: 100 µm.

Since only one experiment was performed the results cannot be generalized, but some initial conclusions can be stated.

Because immature astrocytes might not express or express very low levels of GFAP, this marker might be not detected through ICC means. Hence, the astrocytic culture purity was determined by subtracting to the global cell number the percentage of cells that stained positive to Olig2,

βIII-tubulin and IBA-1. Astrocytic culture purity was determined to be 87% and 72% at DIV 1 and 3, respectively. These values suggest that this passage it is still not ideal, and further passages should be used, particularly due to the presence of OPCs (7 and 19% at DIV 1 and 3, respectively). The fact that the percentage of OPCs increased overtime might be due to the secretion of factors like FGF by astrocytes [13], even if the culture conditions used are not ideal for OPC proliferation. However, further studies of the purity overtime, until DIV 7, should be performed to confirm this tendency.

The presence of neurons probably reflects experimental difficulties in separating the neurons from the MGCs during the initial isolation of these cells from the cortices.

It should be noted that a manual count should also be performed to determine the accuracy of these results determined by the automatic pipeline classification (an 20% variation between the two methods is acceptable). Notwithstanding the purities here presented are in line with previously reported by the group [99] and the presence of non-astrocytic cells at low percentages would not influence further studies on cellular behavior within alginate hydrogels.

4.3.2. Astrocytes survive and have increased metabolic activity in alginate hydrogels

To create a biological relevant matrix for astrocytic environment, these cells should be able to survive, extend processes and express functional markers, mimicking, as far as possible, the *in vivo* homeostasis scenarios. Aiming to understand astrocytic behavior and morphology within the tissue engineered alginate hydrogels, cellular survival and metabolic activity were assessed at DIV 1, 3 and 7.

To determine astrocytic survival as a function of the alginate formulation a live/dead assay, using calcein and PI as dyes, was performed. Calcein AM, a cell-permeant dye, is supplied to the cells. In live cells the non-fluorescent calcein AM is converted to a green-fluorescent calcein after acetoxymethyl ester hydrolysis by intracellular esterases. PI stains the nuclei of cells with a compromised cellular membrane, which means that these cells are considered non-viable or dead [100, 101]. However, in some cases, cells may stain for both probes. In this case, cells are still functional and able to metabolize calcein AM but might have a compromised membrane (for e.g. due to manipulation). With time these cells will either die or recover [101].

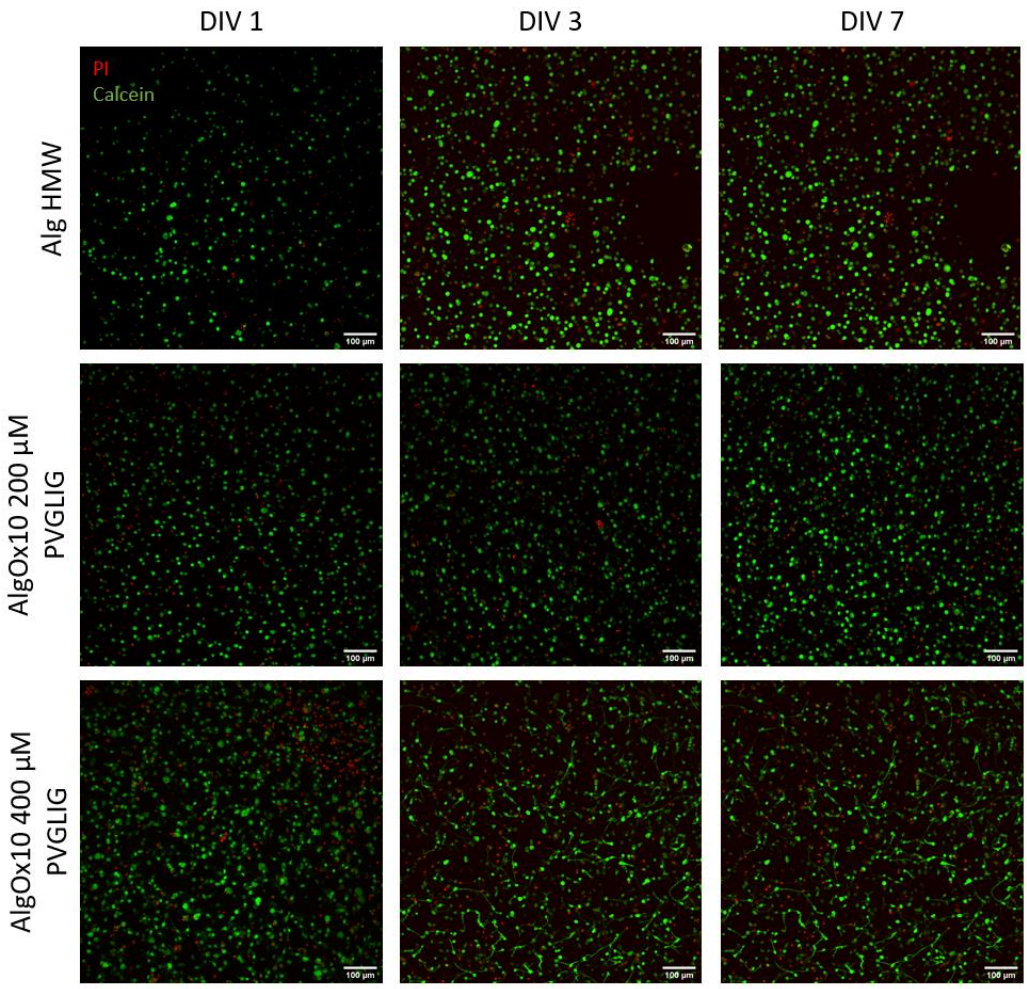

Figure 20 - Representative confocal microscopy images of astrocytes stained with propidium iodide (PI) and Calcein in alginate discs as a function of days in vitro (DIV). PI (red) represents dead cells and Calcein (green) denotes live cells. Scale bars: 100 µm.

Using the confocal microscope images obtained (Fig. 20), cells were counted and divided into three distinct categories: (i) those only stained with PI (non-viable/dead), (ii) those only stained with calcein (viable) and (iii) those stained with both dyes. With Imaris imaging software it was possible to create algorithms that allowed for automated determination of the number of cells that fitted within each category. It should be pointed out that a manual validation of the algorithms should be performed (a maximum of 20% variation between automated and manual counting methods should be accepted to ensure the reliability of the algorithms).

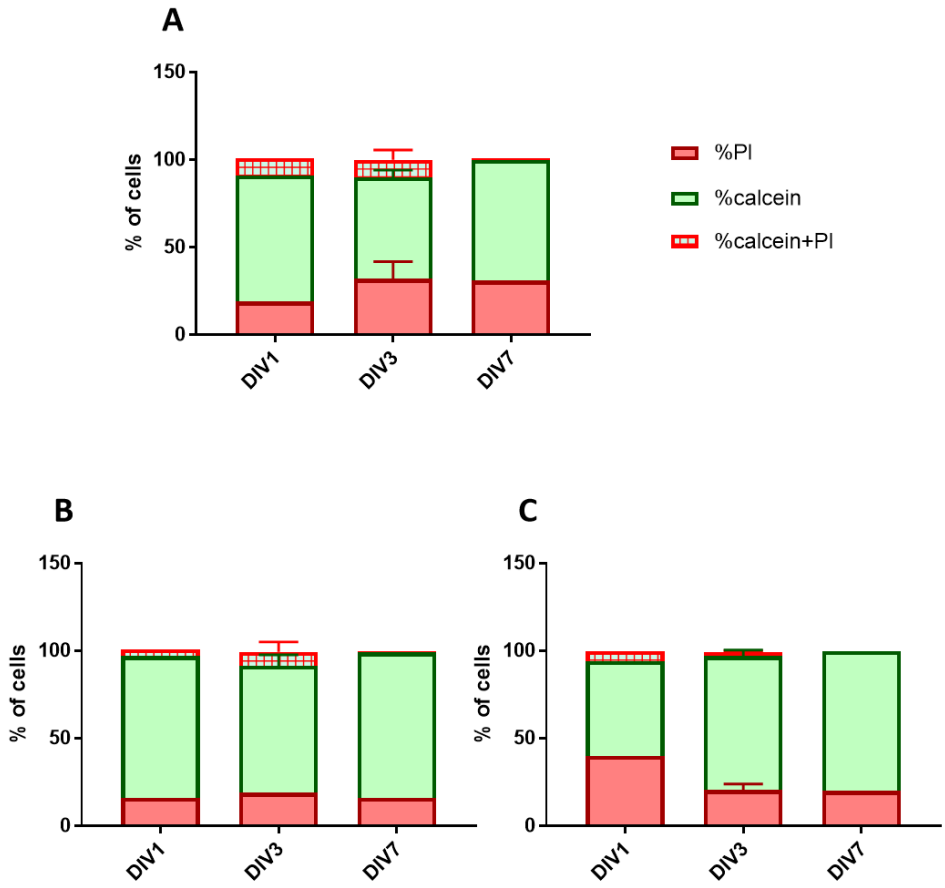

Figure 21 – Astrocytic survival within AlgHMW (A), AlgOx10 200 µM PVGLIG (B) and AlgOx10 400 µM PVGLIG (C) as a function of days in vitro (DIV). Cells were stained with calcein and propidium iodide (PI) and counted using Imaris imaging software. n=1-2 technical replicates from 1 independent experiment (three different regions analyzed per hydrogel) with frozen cells.

The obtained results show that astrocytic survival was similar for the three tested alginate hydrogels (Fig. 21). Nevertheless, it could be observed that the dead cells are higher (around 40%) for modified alginate with high concentration of PVGLIG at DIV1. The slightly higher values of dead cells in the AlgOx10 400 µM PVGLIG might be explained by the presence of non-reactive aldehyde groups in the alginate backbone (Fig. 12), that could be toxic to the cells [102]. These highly reactive groups are created during the oxidation process [103], and are later used to modify the alginate [104] with the PVGLIG sequence. As not all these groups are used, some remain free and are able to interact with the astrocytes. Nevertheless, overtime of culture, it could be observed that the percentage of dead cells in this condition decreases to 20%, showing that the cells that were viable in the start of the culture are able to proliferate. Previously, *Rocha et al.* showed that 1% (w/v) alginate hydrogels, composed by a mix of HMW and low molecular height alginate, did not induce significant astrocytic death overtime of culturing (DIV 1, 3 and 7) [30]. This reiterates that the negative effect on astrocytic death observed in modified alginates were mostly due to the oxidation process, as explained before. Nevertheless, in the study from *Rocha et al*., the PI positive cells were evaluated through flow cytometry. This technique allows for a more precise determination of the percentage of death cells, as it is less likely to be

influenced by human errors. This option should be explored in the future, to ensure more precise results.

On the contrary, for unmodified alginate the percentage of dead cells increased overtime of culture, from 19 to 31%. This suggests that the absence of matrix anchoring points exerted a negative effect on the cells, in time leading to an increase in cellular death.

While these experiments need to repeated to increase the number of independent experiments, overall the results show that the number of live astrocytes were always significantly higher than the number of dead ones, which constitutes a good indicator towards the non-toxicity of the alginates.

Additionally, the analysis of the images obtained (Fig. 20) also allowed for the determination of the total number of cells present in each disc (Table 5). Generally, the total number of cells was higher than the one that was seeded (4 $x10^3$ cell/mm^3), suggesting that the cells were able to proliferate, particularly in the modified alginates. This increase is probably a result of the interactions that are established between the cells and the matrix in these alginates, as oppose to the control. However, in order to verify this hypothesis, proliferation and migration studies should be performed.

Table 5 - Calculated values of the total number of cells present in the alginate discs as a function of days in vitro (DIV). For each disc, 3 images were taken, and the values were determined based on the total number of cells present in the total volume of each image. All values are presented in cells/mm^3 (mean ± SD for DIV 3). n = 1 or 2 alginate discs from 1 independent experiment.

	DIV 1	**DIV 3**	**DIV 7**
Alg HMW	6.310 $x10^3$	(5.852 ± 1.583) $x10^3$	5.448 $x10^3$
Alg Ox10 200 µM PVGLIG	1.230 $x10^4$	(8.725 ± 1.539) $x10^3$	8.254 $x10^3$
Alg Ox10 400 µM PVGLIG	1.054 $x10^4$	(7.754 ± 0.101) $x10^3$	7.583 $x10^3$

The resazurin assay can be used as quantifiable way to determine the effects of the cell culturing time and the alginate modifications on the astrocytic metabolic activity. Hence, alginate discs with and without astrocytes were incubated in cell culture medium with 11% (v/v) resazurin for 3 hours, at the end of which the medium was removed and the produced fluorescence quantified.

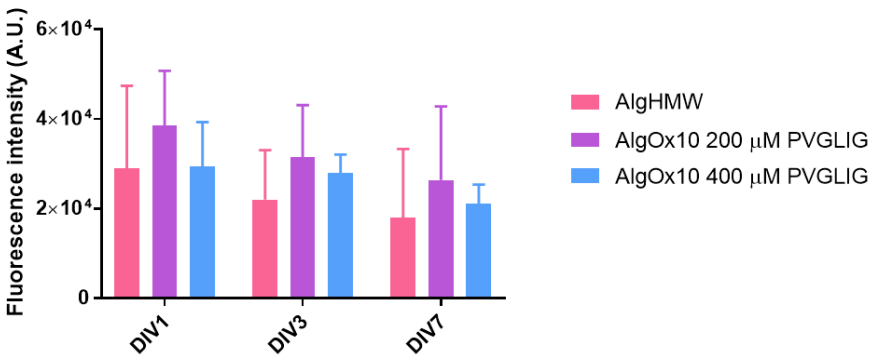

Figure 22 - Metabolic activity of astrocytes embedded within alginate hydrogels as a function of days in vitro (DIV). The results show the difference between alginate discs with cells and the respective discs without cells. n = 3 independent experiments, 3 technical replicates (one experiment was performed with frozen cells). Statistical analysis was performed using Two-way ANOVA and Tukey's multiple comparisons test, and there were no statistically significant differences between the conditions. Results are represented as mean ± SD.

Firstly, it was clear that the presence of alginate itself had no effect on the levels of fluorescence, as the results without cells and the blanks (resazurin incubated in empty wells) were the same.

While the differences observed between the conditions and overtime are not statistically significant, generally some trends can be observed (Fig. 22), particularly regarding the increase of cellular activity in the presence of the alginate modifications. As previously mentioned, PVGLIG is a MMP-sensitive peptide, so after MMP secretion by cells (namely, MMP-9) the alginate is degraded [105]. The cleavage of the matrix not only increases cellular interactions with the microenvironment, but also opens the alginate polymeric network favoring its remodeling by the cells. While MMP production by astrocytes was not directly assessed in the framework of this project, it has been reported that these cells are able to secrete them [106], which justifies the tendency for increased cellular activity for cells within modified alginates. Specifically, for AlgOx10 200 μM PVGLIG there was an average of 1.4x fold increase in the fluorescence levels, while for AlgOx10 400 μM PVGLIG there is an average 1.2x fold increase in comparison to the control. It should also be highlighted that there was a slightly decrease on the cellular metabolic activity for high PVGLIG content alginate in comparison with the lower PVGLIG concentration formulation. This could be due to the possible toxic effect that oxidation exert on cells, as previously explained.

Moreover, taking together the cellular viability and the metabolic activity assays, one can conclude that due to the stability of the percentage of live cells regardless of the alginate formulation, the differences observed in cellular activity are solely related to the effects of the matrix on the cells themselves. This is particularly relevant for the case of the modified alginates that contain peptide sequences with which cells are able to interact.

4.3.3. Astrocytes have morphologies similar to *in vivo* in modified alginate hydrogels

Like most cells, astrocytes react to their environment, presenting different morphologies according to the different stimulus. In the CNS, astrocytes present a complex branched out, star-like appearance, full of bigger and smaller processes that are able to interact with the neurons' synapses [107, 108], and are part the BBB. However, these characteristics can change in case of disease (enlargement of the cell stroma and reduced density of processes [7]), or if they are not able to interact with their environment correctly.

Therefore, the effects of the alginate modifications and the culture time on the cellular morphology were studied to determine the capability of the alginate matrices to mimic the brain microenvironment. For this reason, cells were fixed and labelled with GFAP, a typical astrocytic marker [107].

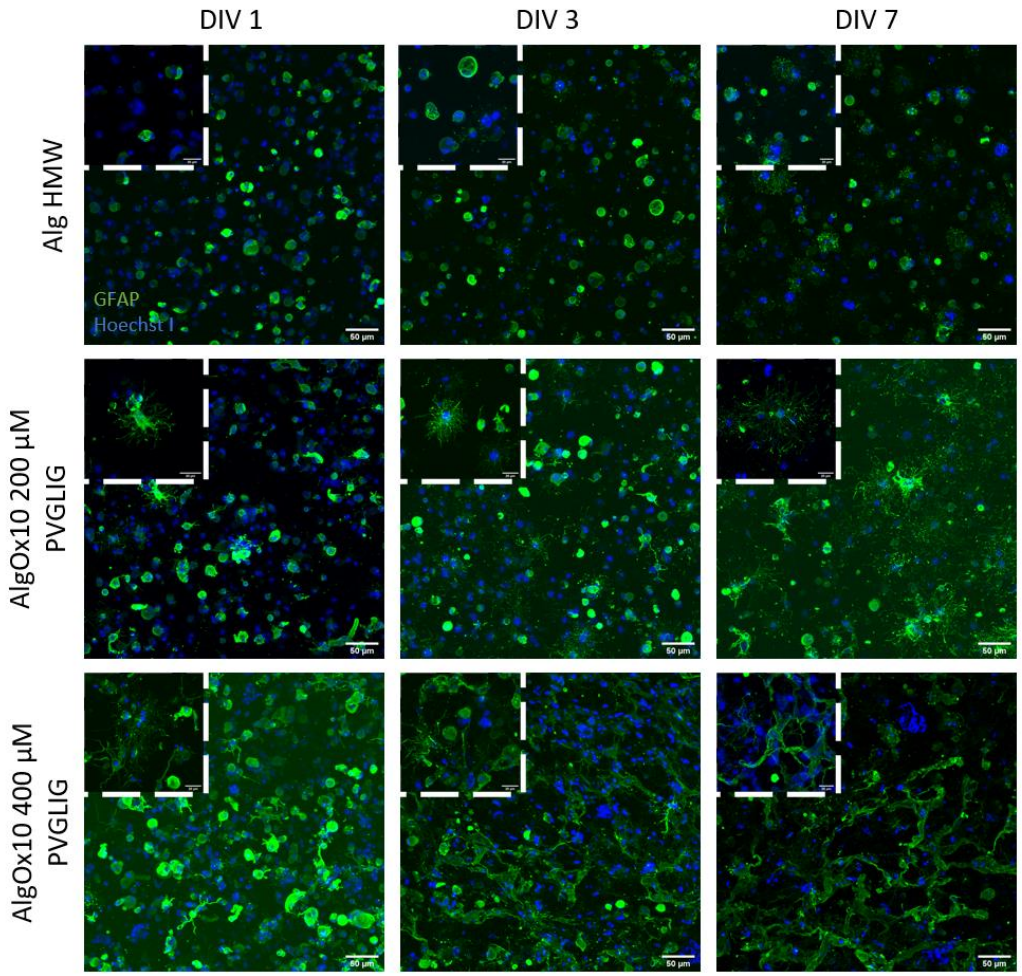

Figure 23 - Confocal microscopy representative images of astrocytes after culture in alginate discs. Astrocytic cell processes were labelled with GFAP (glial fibrillary protein, green) and nuclei counterstained with Hoechst (blue). Scale bars: 50 µm. (DIV: days in vitro).

In unmodified alginate the cells have a spherical morphology once these matrices do not present cell adhesive domains, and the cells are not able to directly interact with the matrix. It could also be observed that astrocytes were not able to interact with each other, as the alginate polymeric network could physically limit the space occupied by the cells as well as their movement. On the other hand, due to RGD and PVGLIG introduction in alginate, the cells are able to adhere to the matrix and degrade it (production of MMPs by astrocytes [15]), creating space to grow and extend processes. This also enables astrocytes to start interacting with each other. Moreover, the oxidation of alginate, as previously explained, opens the polymeric network (higher mesh size values) giving cells more space to extend processes. Therefore, astrocytes end up presenting a more spread and branched out morphology. Overtime in culture, cells are even able to form networks, particularly in, the AlgOx10 400 µM PVGLIG (Fig. 23), as it has a higher concentration of degradable peptides. These results qualitatively show the reliability of the modified alginate matrices to serve as an *in vitro* model to culture astrocytes as their morphology closely resembles the one *in vivo*.

Moreover, these changes in morphology are similar to what has been previously described in hMSCs [86] embedded within alginate matrices modified with PVGLIG and RGD, after 1 week. Likewise, in other matrices that also have cell adhesion and cleavage points, astrocytes have also presented this morphology *in vitro*, such as collagen after a week [52], fibrin [109], collagen type I, collagen+HA and collagen+HA+Matrigel® after 24 hours in culture [110].

4.4. Alginate hydrogels can be printed using an extrusion-based bioprinter

4.4.1. Optimization of the extrusion process

One of the initial aims of this project was to optimize a customized bioprinter for the bioprinting of alginate hydrogels with embedded astrocytes (please refer to Chapter 2 – Aim of the Thesis). However, due to the impossibility of testing the custom-made bioprinter, an automatic dispenser was explored to assess important parameters of bioprinting processes.

4.4.1.1. Printing process setup

The automatic dispenser set-up that was explored was a liquid dispenser JANUS with a 4 Tip dispensing arm and a Modular Dispense Technology™. The pipette tips that fit the mechanical arm have an arrangement compatible with a 96 TCPS well-plate. Although there was the possibility of performing the experiments with these plates, the shape of the discs would be compromised due to the confined space of the wells. Additionally, due to the spatial

arrangement of the tips, it was also impossible to use the 48 TCPS well-plates chosen for the experiments involving the manually prepared alginate discs.

While the 24 well-plates commercially available were more compatible with the tips positioning, the reality showed that only four of the six wells per line were usable, as in the middle wells the discs ended up being pipetted into the walls.

Therefore, a specially designed epoxy 24 well-plate that perfectly fitted with the tips positioning was developed. Due to the inherent roughness of the surfaces of the epoxy plates, commercially available plastic cell-culture coverslips were used to serve as the surface where the discs were printed. Table 6 refers to the options tested and the respective evaluation of alginate disc formation, swelling and compatibility with experimental assays. It should be noted that this optimization was performed both with AlgHMW and the modified alginates.

Table 6 – Evaluation of the different well-plates in terms of alginate disc formation, hydrogel spreading and compatibility with experimental assays.

Surface material	Hydrogel formation	Hydrogel spreading	Compatibility with experimental assays
TCPS 24wp	✓	++	✓
Epoxy 24wp	✓	+	×
Epoxy 24wp with PP coverslips	✓	+	✓
Epoxy 24wp with PET coverslips	✓	+	✓

Symbols: ✓ – compatible; x – not compatible; + – apparent hydrogel spread; ++ – considerable hydrogel spread

Poly(propylene) (PP) and PET coverslips were tested and no observable differences in terms of hydrogel formation and swelling were detected between them. Due to the low thickness of the PP coverslips and, consequently, their fragility, practical difficulties were found during coverslip manipulation. Therefore, PET coverslips were used to proceed for further studies. In future studies, a contact angle assay could be performed in order to asses the hydrophobicity of the coverslips, as this is a determining factor in the hydrogel spreding, as discussed in section 4.4.2.

4.4.1.2. The epoxy well-plate, as cell culturing plate for printed alginate discs, affects astrocytic metabolic activity

Initial studies involved the culture of printed alginate hydrogels on the PET coverslips with astrocytes in the epoxy 24 well-plates until DIV 7. Although hydrogels remained morphologically stable overtime, cellular viability was severely affected (Fig. 24).

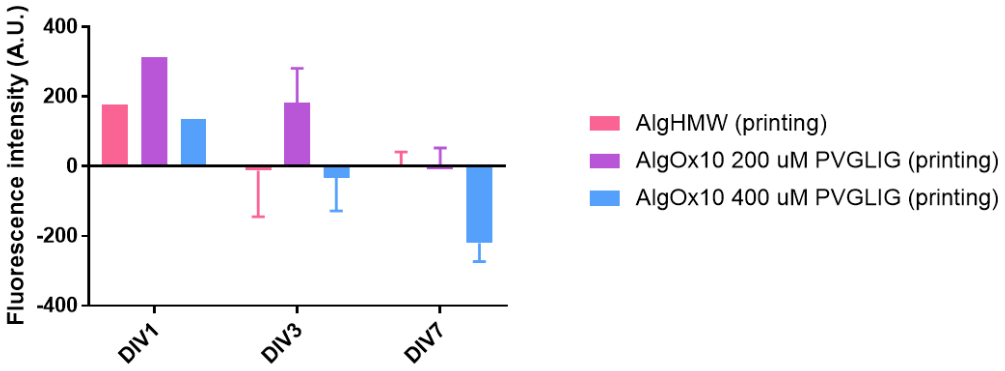

Figure 24 - Metabolic activity of astrocytes embedded within printed alginate hydrogels as a function of days in vitro (DIV). The cultures were conducted in the epoxy 24 well plates, with the coverslips with the discs only being transferred to a TCPS plate for the metabolic activity measurement. n=1 technical replicate form 1 independent experiment (DIV1), n=2-3 technical replicates form 1 independent experiment (DIV3), n=4 technical replicates form 1 independent experiment (DIV7).

The results show that the cellular metabolic activity was very low or residual (Fig. 24). While the extrusion process is expected to influence astrocytic behavior, other hypotheses were assessed first due to the unexpected negative impact on cell activity that was observed. The use of an epoxy resin to construct the designed 24 well-plate, once in contact with the cell culture medium, might have led to the leaching of some components from the resin that might have been toxic to the cells. At the same time, the sterilization process used (described in section 3.3.1.) might have increased the possibility of toxic elements being at the surface of the material, and not correctly removed (originally the last step of the sterilization was with an organic solvent, ethanol).

For this reason, it was decided that in subsequent experiments, after the 30 minutes incubation necessary for the crosslinking of the alginate hydrogels occur, the discs were immediately transferred along with the coverslips to commercially available TCPS well-plates and then the cell culture medium was added. This extra step allowed the possible toxicity of the epoxy well-plate to be eliminated, as will be discussed in the following section.

4.4.2. Printed alginate discs have higher diameters in comparison to manually prepared ones

After the printing process being optimized, the morphology of the extruded discs was analyzed by discs diameter measurements overtime of culture (Fig. 25).

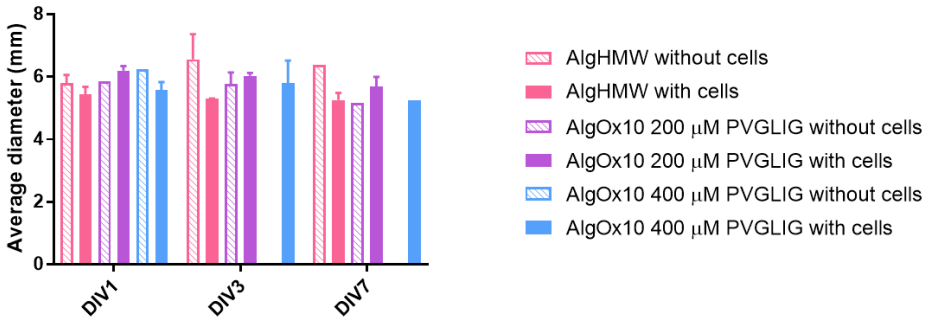

Figure 25 - Printed alginate hydrogels diameter as a function of time of culture. Disc diameter was determined as ranging from 5.8-6.4 mm. n=1-3 discs (technical replicates) from 1 independent experiment. In the case of the AlgOx10 400 μM PVGLIG at DIV 3 and 7 it was not possible to observe the discs due to technical issues.

There were no significant differences between discs' diameter. The values were around 5.8 and 6.2 mm, regardless of culture time, presence of cells or alginate modifications. However, when compared with the manually produced discs these were clearly bigger, with a 1.5-fold maximum increase.

The most probable explanation for this increase in diameter relates to the surface material in which the alginate discs were cultured. Alginate has a high-water content [71], meaning that the hydrogels interact more with hydrophilic materials, having more points of contact and resulting in more fragile discs with larger diameters. The culture plates that were used when the discs were made manually were non-treated cell culture dishes (i.e. more hydrophobic), which allowed for the formation of smaller and more well-defined discs. However, for printing purposes, the used plastic coverslips were cell culture treated (more hydrophilic), which might explain this increase in diameter.

4.4.3. Astrocytic survival, metabolic activity and morphology is altered in alginate hydrogels after printing

After observing that the morphological behavior of the discs was constant overtime of culturing, and eliminating the possible toxic effects of the epoxy 24 well-plate on cells, astrocytic behavior was assessed in printed alginate discs in terms of survival, metabolic activity and morphology.

Concerning the cell survival assay, just by simple observation of the calcein/PI images showed in Figure 26, it is possible to see the clear increase in the number of dead cells present in these

discs, particularly at DIV 1 and 3. Moreover there was a significant number of cells stained with both calcein and PI. These results are corroborated by a more quantitative determination (Fig. 27), that show that the printing process, and probably also the extra handling, had a significant impact on the astrocytic viability. It should also be noted that due to experimental difficulties it was not possible to obtain the results for the AlgOx10 200 µM PVGLIG at DIV 7.

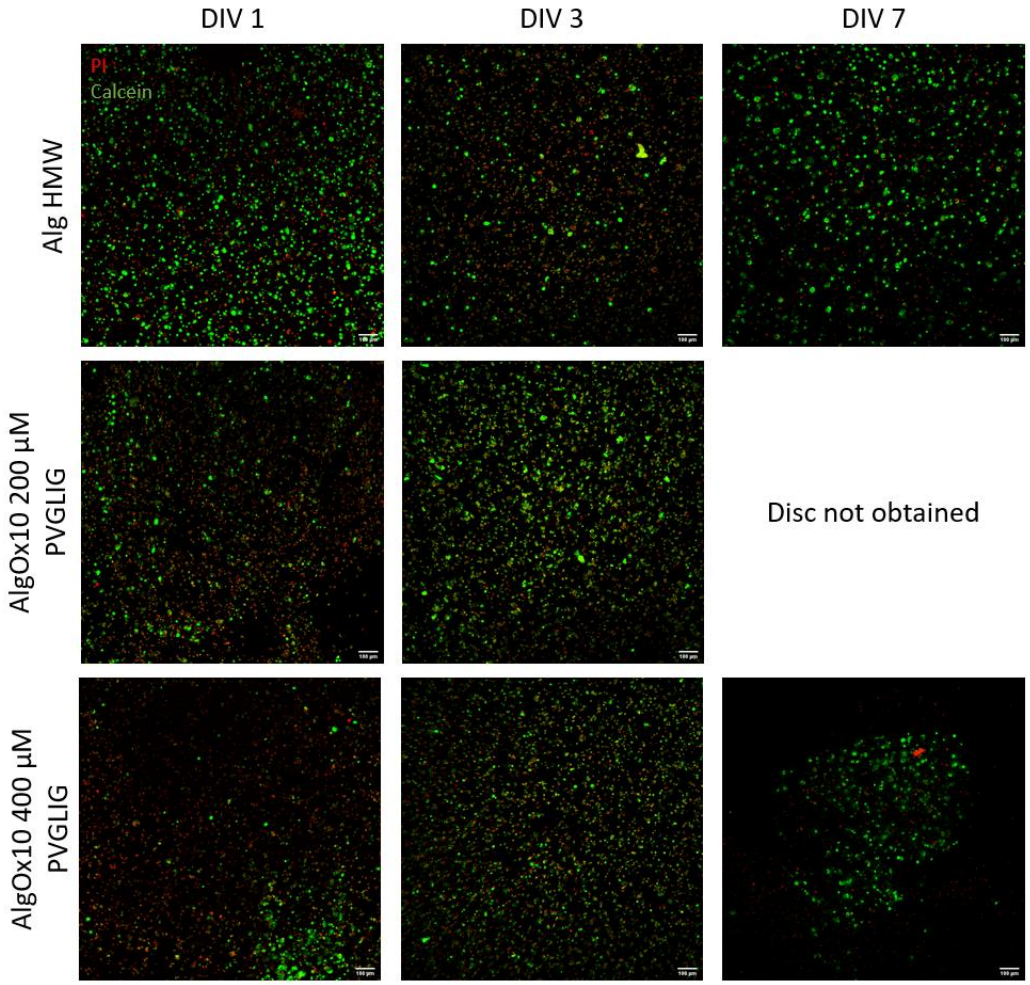

Figure 26 - Representative confocal microscopy images of astrocytes stained with propidium iodide (PI) and Calcein in printed alginate discs as a function of days in vitro (DIV). PI (red) represents dead cells and Calcein (green) denotes live cells. Scale bars: 100 µm.

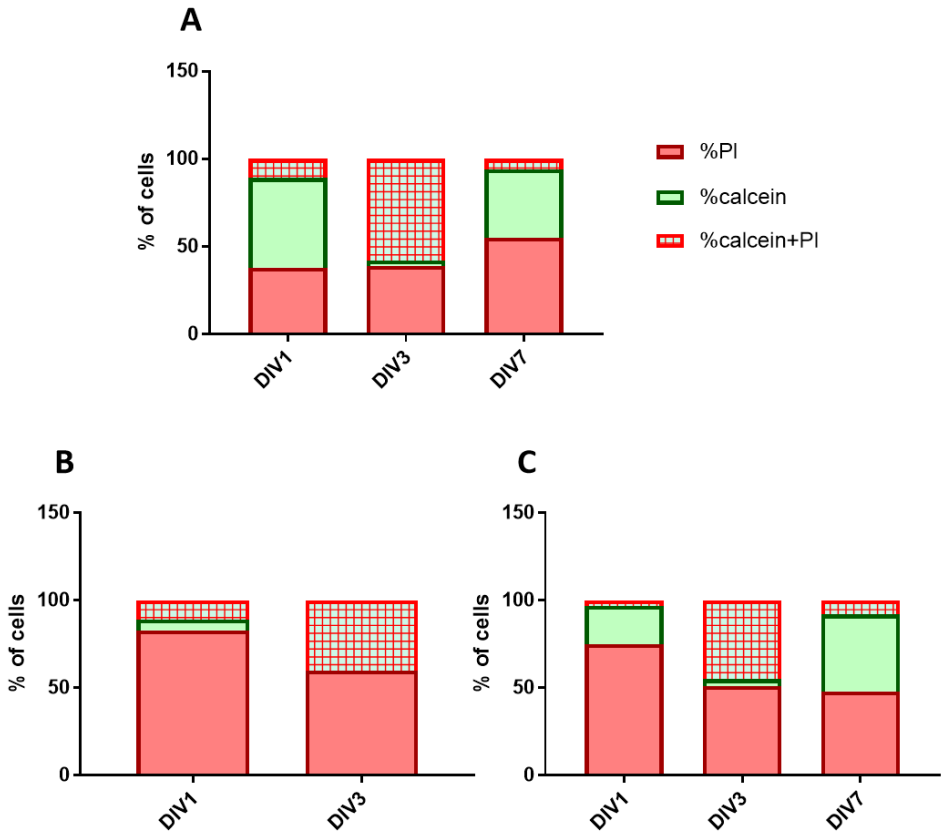

Figure 27 - Astrocytic survival within printed AlgHMW (A), AlgOx10 200 µM PVGLIG (B) and AlgOx10 400 µM PVGLIG (C) as a function of days in vitro (DIV). Cells were stained with calcein and PI and counted using Imaris imaging software. n=1 technical replicate from 1 independent experiment (three different regions analyzed per hydrogel).

For all alginate formulations tested there was a clear increase in the percentage of dead cells or with a compromised membrane in comparison with the percentage of alive cells (Fig. 27). While at DIV 1 there was still a relatively small percentage of cells with a compromised cell membrane, this number increased dramatically at DIV 3, regardless of the alginate formulation. At DIV 7 there was an enhancement of the number of live cells, which suggests that at this time-point the astrocytes that survived the printing process might have been able to recover from some of the damage of the printing process and even proliferate.

Moreover, astrocytes appear to have been more affected, at DIV 1, in the AlgOx10 200 µM PVGLIG than in the other formulations, particularly in comparison with the unmodified control. A possible explanation might relate to the gelation characteristics of each alginate, as described in section 4.2.2. As AlgHMW gels faster than the AlgOx10 200 µM PVGLIG, the polymeric network of this formulation involved the astrocytes in a protective way, which might have counteracted some of the negative effects that the printing process had on the cells, improving their survival chances.

However, as only one disc was analyzed for each condition, these results should not be generalized, and further replicates are necessary to infer with more certainty the effect of the printing process.

Interestingly, the total number of astrocytes present in the printed alginate discs (Table 7), was in line with the values observed in the manual discs. This suggests that the final mix printed has similar in terms of cellular dispersion to that of the manually mix, and that there was no sedimentation of the astrocytes at the bottom of the 384 well-plate.

Table 7 - Calculated values of the total number of cells present in the bioprinted alginate discs as a function of days in vitro (DIV). For each disc, 3 images were taken, and the values were determined based on the total number of cells present in the total volume of each image. For AlgOx10 400 µM PVGLIG at DIV 7 only one image was taken, and the total number of cells was calculated based on the area where the cells occupied, and not the total image. Originally seeded 4x10³ cells/mm³. All values are presented in cells/mm³. n = 1 alginate discs from 1 independent experiment.

	DIV 1	DIV 3	DIV 7
Alg HMW	8.539 x10³	7.032 x10³	4.469 x10³
Alg Ox10 200 µM PVGLIG	9.424 x10³	9.041 x10³	Disc not obtained
Alg Ox10 400 µM PVGLIG	5.297 x10³	8.628 x10³	4.997 x10³

At the same time, the cellular activity as a consequence of printing (Fig. 28) was clearly reduced. However, no definite conclusions can be made, as only one assay was performed.

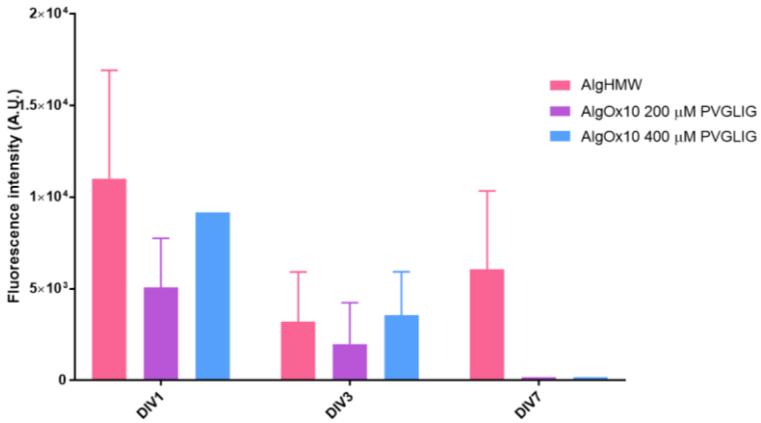

Figure 28 - Metabolic activity of printed astrocyte laden alginate hydrogels as a function of days in vitro (DIV). n = 1-3 technical replicates form 1 independent experiment.

During the printing process, in particular extrusion, the bioinks, and in this case the cells themselves, are exposed to a series of forces of compression, tension and shear stress that might affect their viability [45, 47]. Consequently, some decline in cellular metabolic activity was expected, which in this case was particularly significant at DIV 3 and 7.

Additionally, the cells cultured in the unmodified control and the AlgOx10 400 μM PVGLIG, specially at DIV 1, presented higher levels of metabolic activity, probably due to the presence of a higher percentage of live cells, than in the AlgOx10 200 μM PVGLIG. At DIV 3 it is possible to observe the overall decrease of metabolic activity in all conditions, most likely as a result of the significant number of astrocytes either dead or with a compromised cell membrane. At DIV 7, while cells in the AlgHMW partially recover their metabolic activity, as the percentage of metabolic active cells increases again, the same does not happen in the AlgOx10 400 μM PVGLIG. This might indicate that while cells were able to recover their membrane structure at DIV 7, they had not yet recovered at a metabolic level.

However, most likely, these results are derived from experimental errors, in the cell viability assay or in the cell metabolic activity assay, and more discs should be analyzed before general conclusions are made.

Moreover, in terms of astrocyte morphology the changes are also significant (Fig. 29).

An important factor that plays a crucial role in the analysis of these results was the difficulty in manipulating the alginate discs during the experimental process, due to their fragility. Hence, it was impossible to keep the alginate discs of the conditions AlgOx10 200 μM PVGLIG and AlgOx10 400 μM PVGLIG until DIV 7 for evaluating astrocytic morphology.

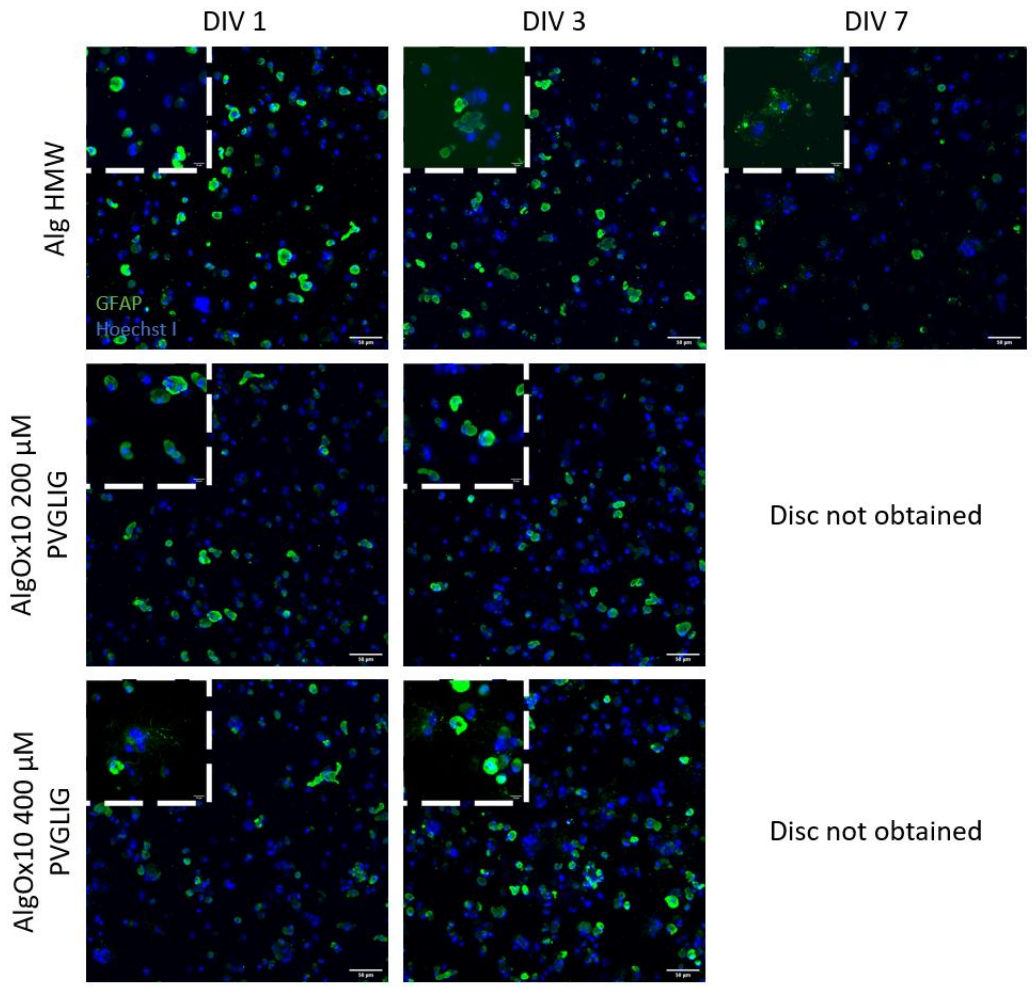

Figure 29 - Representative confocal images of astrocytes after culture in printed alginate discs. Astrocytic cell processes were labelled with GFAP (glial fibrillary protein, green) and nuclei counterstained with Hoechst (blue). Scale bars: 50 µm. (DIV: days in vitro).

A qualitative analysis of the images allowed to conclude that regardless of the alginate type, astrocytes always presented a more spherical morphology in comparison with previously observed with the manual discs. The exceptions are some cells in the AlgOx10 400 µM PVGLIG at DIV 1 that appear to branch out slightly, but it is not clear that this is still the case at DIV 3. . In the future, a quantification of process extension would be interesting to assure a more objective and quantitative analysis of the astrocytic morphology.

The increase in the percentage of cells either dead or with a compromised cell membrane, the decrease in cellular activity and the changes in morphology in the astrocytes cultured in the extruded discs are, most likely, a consequence of the printing process itself. Based on the presence of a significant number of cells with a compromised membrane it is possible that this process has affected the integrity of the cell membrane, affecting the presence of integrins and other cell receptors at its surface. The absence of these molecules affects the cells' capacity to interact with the RGD present in alginate, hence astrocytic morphology changed to a more

spherical one in modified alginates. Consequently, it also affects their metabolic capabilities as explained in section 4.3.2.

As stated before in the Chapter 1 - Introduction, the bioprinting of astrocytes, or other glial cells, is still underdeveloped. However, some attempts have been made to change this situation. For example, *Zhou et al.* were able to use piezoelectric inkjet bioprinting to create Matrigel® droplets involved in a lipid bilayer. Inside these droplets were a co-culture system with an outer layer of primary human astrocytes involving human NSCs, that was able to support neuron migration [78]. While *Salaris et al.* used extrusion of neurons and glial progenitor derived iPSCs in alginate/Matrigel®. The results showed that neither the cellular viability, differentiation capabilities and ability to express cellular markers, like GFAP, were affected by the printing process [65]. More recently *Ouyang et al.* were able to pneumatically extrude primary astrocytes in a mix of GelMA, at low concentrations and gelatin. The gelatin worked as a thermo-reversible support material, ensuring that concentrations that were compatible with cell culture were also viable to be printed, without significant damaged to cell viability, cell metabolic activity or morphology [77].

Accordingly, it is possible to conclude that it is conceivable to successfully print astrocytes without affecting their cellular survival and behavior, which suggests that in the case here presented there is a lot of optimization that is still left to be done.

Furthermore, studies with alginate have shown that its printability is inherently connected with its rheological properties. For instance, *Gao et al.* showed that by varying the concentration of a mix of gelatin and alginate it was possible to vary the G’ and G’’ with various degrees of printability success. When G’’/G’ was higher, this led to more uniform structures, while a lower ratio created more structurally stable scaffolds. The group also showed that it is possible to use the G’ and G’’ of the bioink to estimate the pressure applied during extrusion [111]. In order to control the rheological properties, *Tabriz et al.* used a three-step crosslinking process, ensuring that each step of the extrusion process had the necessary conditions to print the alginate structure and then keep it viable in culture. At the end, the scaffold was stable, and when a human brain tumor cell line was added to the bioink, the process had no effect on cell viability right after printing, or after 11 days in culture [112].

In this specific project, the need to develop an alginate matrix compatible with the culture of astrocytes led to the creation of alginate discs orders of magnitude softer than usually studied [77, 111], even in the limit for what is reported for brain [112]. This in turn, creates additional challenges when trying to understand how the properties of the material might affect the embedded cells during extrusion. While more viscous/stiff materials offer more resistance to the printing process, which in turn negatively affects cells, very soft materials leave the cells unprotected from the forces exerted during the process. This fragile balance might be a possible explanation to why the cells embedded in modified alginate ended up more affected by the extrusion, since these were also softer materials.

The most discussed mitigating options for improving cell compatibility with bioprinting usually are the pressure applied on the material during the extrusion process and the characteristics of the nozzle. If the nozzle is too small, there is the creation of different flow patterns and velocities within the bioink, that can lead to significant damages in the cells and cellular loss. Bigger nozzles (> 800 μm) diminish this effect, and as such improves cell viability [113]. However, ideal nozzle sizes have not been described for the printing of neural cells.

Since the original purpose of the system used in this project to print alginate is not to dispense a viscous material, the control of the nozzle/tip diameter is a complex matter. While the velocity was possible to control (6 μL/s), the pressure was not as straightforward. The biggest problem could be attributed to the area in which the machine arm force was being applied. As only 24 of the 96 tips were used, the force that originally was designed to be applied uniformly was only being applied in ¼ of the surface. Because of this, slower printing velocities should be tested in order to diminish the pressure exerted on the astrocytes.

Moreover, the system uses specific 200 μL tips that cannot easily be changed, making the possibility of changing the nozzle diameter difficult.

Although not as obvious, using hydrophilic coverslips significant altered the conformation of the discs which in turn could have affected the astrocytic behavior. The increase in disc diameter created structures that were empirically more fragile, softer and tougher to work with, particularly in the case of the modified alginates. Additionally, when cell culture medium had to be added or removed during the culturing process parts of the softer discs were removed, leaving the remaining segments fragmented, or not even leaving nothing behind. These practical problems difficulted the maintenance of intact alginate discs until the end of the culture period. Thus, the results might be negatively affected not only by the loss of technical replicates, but also by possibly inducing some additional stresses on the cells. This was more significant with the modified alginates, which might also explain why the difference between the results by hand and printed are not as glaring for the non-modified alginate.

Notwithstanding all the above-mentioned problems, alginate discs from unmodified and modified alginates were successfully created and maintained in culture until DIV7 with the presence of functional astrocytes (observed by the expression of the astrocytic marker, GFAP).

Altogether these preliminary results confirm the successfully printability of alginate and consist an excellent starting point towards the development of a high-throughput system to mimic the astrocytic environment.

Chapter 5 – Conclusions and future perspectives

Understanding the intricacies of the remyelination failure processes is still a challenge. While some therapies have been proposed for OPC differentiation induction, the remaining CNS glial cells and the surrounding microenvironment of the lesion have been undervalued. Notwithstanding, astrocytes were already proved to play multiple roles on demyelinating pathologies being considered the main responsible cells for the formation of a glial scar. Whether the astrocyte-OPC crosstalk has been already studied, the ECM alterations due to the glial scar formation have been neglected, peculiarly due to the lack of a suitable experimental models to mimic different diseases' states.

Consequently, 3D engineered matrices have been pointed as interesting models to replicate the physical structure of the CNS and manipulate the surrounding environment of the cells in a controlled manner. 3D models avoid the complexity of animal models and the oversimplified view of the traditional 2D models. Nevertheless, up until now there is no model capable of truly recapitulating *in vitro* the microenvironment of a demyelinating lesion and at the same time function as a high-throughput screening model.

Consequently, the work here presented aimed to explore a novel *in vitro* high-throughput tissue engineered platform composed by a 3D alginate hydrogel with embedded astrocytes for mimicking the astrocytic microenvironment.

The results suggest that the alginate modifications with cell adhesion and matrix metalloproteinase peptides (RGD and PVGLIG, respectively) led to the formation of softer matrices (consistent with the Young modulus of the brain) that maintained the mechanical properties during culture (tested up to 7 days). Moreover, the modifications in the polymer also

led to delayed gelation times which constitutes an advantage towards the development of a printing-like protocol to produce alginate discs.

Astrocytic impact on hydrogel stiffness as a function of culture time was found to be minimal, which indicates that a balance between alginate matrix degradation and astrocytic own ECM production might happen. On a cellular level the introduction of the PVGLIG sequence, and the increase in its concentration, allowed astrocytes to adopt a branched out morphology, consistent with their appearance *in vivo*, as they are able to interact with the matrix and with each other. The presence of the peptide sequences also led to an increase in cellular metabolic activity, that was not related with a higher cell viability, indicating that the presence of an environment in which they are able to interact has significant effects on cellular behavior. Nevertheless, it should also be highlighted that all the experiments described in this thesis should be repeated to increase the number of independent experiments and to strengthen the reliability of the presented data.

Moreover, a more detailed study on the morphological characterization of the different alginate formulations should be conducted (for example, by evaluation by cryo-SEM the microstructure of the discs). A composition characterization of the matrix by immunocytochemistry or quantification assays of matrix components produced by astrocytes, would also help better understand the effects of the different alginate formulations on cells and vice versa. At later stages, it would be also interesting to study the activation of the astrocytes and observe how astrocytes cultured at different activation stages may impact the alginate properties, and how those compare with what has been reported *in vivo* at distinct disease stages.

Additionally, in this work, a bioprinting-like approach to automatically create 3D matrices based on alginate for the growing of astrocytes was explored. Hydrogels from all alginate formulations were successfully produced using an automatic solution dispenser, although discs were more fragile and swollen from previous ones. The astrocytic viability and metabolic activity were affected as well as their morphology with less visible process extension. Nevertheless, cells were functional overtime of culturing which was confirmed by the expression of an astrocytic characteristic marker (GFAP).

Several reasons might be behind these changes, and all of them should be tested independently to better optimize the process. In extrusion-based bioprinting some reasons that might be associated with the decrease in cell viability and cell activity relate to the pressure exerted on the cells and the nozzle diameter. In this particular system, in the future, lower velocities should be tested both during the alginate mix homogenization process, and the extrusion itself. Once hydrogel diameter was enhanced in discs produced by printing, changing the substrate onto which the alginate is dispensed is of utmost importance. Specifically, this change should occur to a more hydrophobic surface to avoid alginate interaction with it.

Furthermore, after optimizing the printing process understanding the astrocytic response in terms of reactivity state might be of interest. For instance, performing quantitative real time

polymerase chain reaction (qRT-PCR) assays for evaluation of the gene expression of genes involved in astrocytic activation and ECM production as GFAP, lipocalin 2, vimentin and collagen type IV. Moreover, it would also be interesting to determine if the printing process had any effect on the mechanical properties of the discs by performing similar rheological assays to those that were presented here.

Overall, by allowing the recreation of some of the brain's matrix characteristics, peculiarly the modulation of the ECM composition and its mechanical properties, the creation of alginate discs with embedded astrocytes here described is an important step forward in the development of a 3D engineered matrix for the screening of biological targets or drugs for MS treatment. Furthermore, by proving the printability of alginate with astrocytes, a major hurdle to the development of a high-throughput assay has been overcame.

Bibliography

1. Correale, J., M.I. Gaitán, M.C. Ysrraelit, and M.P. Fiol *Progressive multiple sclerosis: from pathogenic mechanisms to treatment*. Brain, 2016. **140**, 527-546 DOI: 10.1093/brain/aww258.
2. Wallin, M.T., W.J. Culpepper, E. Nichols, Z.A. Bhutta, T.T. Gebrehiwot, S.I. Hay, I.A. Khalil, K.J. Krohn, X. Liang, and M. Naghavi *Global, regional, and national burden of multiple sclerosis 1990–2016: a systematic analysis for the Global Burden of Disease Study 2016*. The Lancet Neurology, 2019. **18**, 269-285 DOI: 10.1016/S1474-4422(18)30443-5.
3. Kawano, H., J. Kimura-Kuroda, Y. Komuta, N. Yoshioka, H.P. Li, K. Kawamura, Y. Li, and G. Raisman *Role of the lesion scar in the response to damage and repair of the central nervous system*. Cell and Tissue Research, 2012. **349**, 169-180 DOI: 10.1007/s00441-012-1336-5.
4. Olsen, J.A. and E.M. Akirav *Remyelination in multiple sclerosis: Cellular mechanisms and novel therapeutic approaches*. Journal of Neuroscience Research, 2015. **93**, 687-696 DOI: 10.1002/jnr.23493.
5. Chamberlain, K.A., S.E. Nanescu, K. Psachoulia, and J.K. Huang *Oligodendrocyte regeneration: Its significance in myelin replacement and neuroprotection in multiple sclerosis*. Neuropharmacology, 2016. **110**, 633-643 DOI: 10.1016/j.neuropharm.2015.10.010.
6. Society, N.M.S. *Types of MS*. [cited 2020 14 Oct]; Available from: https://www.nationalmssociety.org/What-is-MS/Types-of-MS.
7. Ponath, G., C. Park, and D. Pitt *The role of astrocytes in multiple sclerosis*. Frontiers in Immunology, 2018. **9**, 217 DOI: 10.3389/fimmu.2018.00217.
8. Ludwin, S.K., V.T. Rao, C.S. Moore, and J.P. Antel *Astrocytes in multiple sclerosis*. Multiple Sclerosis Journal, 2016. **22**, 1114-1124 DOI: 10.1177/1352458516643396.
9. Franklin, R.J. *Remyelination in the CNS: from biology to therapy*. Nature Reviews Neuroscience, 2008. **9**, 839-855 DOI: 10.1038/nrn2480.
10. Fancy, S.P., J.R. Chan, S.E. Baranzini, R.J. Franklin, and D.H. Rowitch *Myelin regeneration: a recapitulation of development?* Annual Review of Neuroscience, 2011. **34**, 21-43 DOI: 10.1146/annurev-neuro-061010-113629.
11. Lampron, A., A. Larochelle, N. Laflamme, P. Préfontaine, M.-M. Plante, M.G. Sánchez, V.W. Yong, P.K. Stys, M.-È. Tremblay, and S. Rivest *Inefficient clearance of myelin debris by microglia impairs remyelinating processes*. Journal of Experimental Medicine, 2015. **212**, 481-495 DOI: 10.1084/jem.20141656.
12. Rawji, K.S., G.A.G. Martinez, A. Sharma, and R.J. Franklin *The Role of Astrocytes in Remyelination*. Trends in Neurosciences, 2020. DOI: 10.1016/j.tins.2020.05.006.
13. Correale, J. and M.F. Farez *The role of astrocytes in multiple sclerosis progression*. Frontiers in Neurology, 2015. **6**, 180 DOI: 10.3389/fneur.2015.00180.
14. Molina-Gonzalez, I. and V.E. Miron *Astrocytes in myelination and remyelination*. Neuroscience Letters, 2019. 134532 DOI: 10.1016/j.neulet.2019.134532.
15. Nair, A., T.J. Frederick, and S.D. Miller *Astrocytes in multiple sclerosis: a product of their environment*. Cellular and Molecular Life Sciences, 2008. **65**, 2702 DOI: 10.1007/s00018-008-8059-5.

16. de Jong, J.M., P. Wang, M. Oomkens, and W. Baron *Remodeling of the interstitial extracellular matrix in white matter multiple sclerosis lesions: Implications for remyelination (failure)*. Journal of Neuroscience Research, 2020. DOI: 10.1002/jnr.24582.
17. Makhija, E.P., D. Espinosa-Hoyos, A. Jagielska, and K.J. Van Vliet *Mechanical regulation of oligodendrocyte biology*. Neuroscience Letters, 2019. 134673 DOI: 10.1016/j.neulet.2019.134673.
18. Urbanski, M.M., L. Kingsbury, D. Moussouros, I. Kassim, S. Mehjabeen, N. Paknejad, and C.V. Melendez-Vasquez *Myelinating glia differentiation is regulated by extracellular matrix elasticity*. Scientific Reports, 2016. **6**, 1-12 DOI: 10.1038/srep33751.
19. Bjelobaba, I., V. Begovic-Kupresanin, S. Pekovic, and I. Lavrnja *Animal models of multiple sclerosis: Focus on experimental autoimmune encephalomyelitis*. Journal of Neuroscience Research, 2018. **96**, 1021-1042 DOI: 10.1002/jnr.24224.
20. Constantinescu, C.S., N. Farooqi, K. O'Brien, and B. Gran *Experimental autoimmune encephalomyelitis (EAE) as a model for multiple sclerosis (MS)*. British Journal of Pharmacology, 2011. **164**, 1079-1106 DOI: 10.1111/j.1476-5381.2011.01302.x.
21. Osorio-Querejeta, I., M. Sáenz-Cuesta, M. Muñoz-Culla, and D. Otaegui *Models for Studying Myelination, Demyelination and Remyelination*. NeuroMolecular Medicine, 2017. **19**, 181-192 DOI: 10.1007/s12017-017-8442-1.
22. Kipp, M., B. van der Star, D.Y. Vogel, F. Puentes, P. van der Valk, D. Baker, and S. Amor *Experimental in vivo and in vitro models of multiple sclerosis: EAE and beyond*. Multiple Sclerosis and Related Disorders, 2012. **1**, 15-28 DOI: 10.1016/j.msard.2011.09.002.
23. Bradl, M. and H. Lassmann *Oligodendrocytes: biology and pathology*. Acta Neuropathologica, 2010. **119**, 37-53 DOI: 10.1007/s00401-009-0601-5.
24. Madill, M., D. Fitzgerald, K.E. O'Connell, K.K. Dev, S. Shen, and U. FitzGerald *In vitro and ex vivo models of multiple sclerosis*. Drug Discovery Today, 2016. **21**, 1504-1511 DOI: 10.1016/j.drudis.2016.05.018.
25. Voet, S., M. Prinz, and G. van Loo *Microglia in central nervous system inflammation and multiple sclerosis pathology*. Trends in Molecular Medicine, 2019. **25**, 112-123 DOI: 10.1016/j.molmed.2018.11.005.
26. Luo, C., C. Jian, Y. Liao, Q. Huang, Y. Wu, X. Liu, D. Zou, and Y. Wu *The role of microglia in multiple sclerosis*. Neuropsychiatric Disease and Treatment, 2017. **13**, 1661 DOI: 10.2147/NDT.S140634.
27. Koss, K., M.A. Churchward, C. Tsui, and K.G. Todd *In vitro priming and hyper-activation of brain microglia: an assessment of phenotypes*. Molecular Neurobiology, 2019. **56**, 6409-6425 DOI: 10.1007/s12035-019-1529-y.
28. Smith, J.A., A. Braga, J. Verheyen, S. Basilico, S. Bandiera, C. Alfaro-Cervello, L. Peruzzotti-Jametti, D. Shu, F. Haque, and P. Guo *RNA nanotherapeutics for the amelioration of astroglial reactivity*. Molecular Therapy-Nucleic Acids, 2018. **10**, 103-121 DOI: 10.1016/j.omtn.2017.11.008.
29. Liddelow, S.A., K.A. Guttenplan, L.E. Clarke, F.C. Bennett, C.J. Bohlen, L. Schirmer, M.L. Bennett, A.E. Münch, W.-S. Chung, and T.C. Peterson *Neurotoxic reactive astrocytes are induced by activated microglia*. Nature, 2017. **541**, 481-487 DOI: 10.1038/nature21029.
30. Rocha, D.N., J.P. Ferraz-Nogueira, C.C. Barrias, J.B. Relvas, and A.P. Pêgo *Extracellular environment contribution to astrogliosis—lessons learned from a tissue engineered 3D model of the glial scar*. Frontiers in Cellular Neuroscience, 2015. **9**, 377 DOI: 10.3389/fncel.2015.00377.
31. Tuinstra, H.M., M.M. Ducommun, W.E. Briley, and L.D. Shea *Gene delivery to overcome astrocyte inhibition of axonal growth: an in vitro model of the glial scar*. Biotechnology and Bioengineering, 2013. **110**, 947-957 DOI: 10.1002/bit.24750.
32. Fan, L.W., A. Bhatt, L.T. Tien, B. Zheng, K.L. Simpson, R.C. Lin, Z. Cai, P. Kumar, and Y. Pang *Exposure to serotonin adversely affects oligodendrocyte development and*

myelination in vitro. Journal of Neurochemistry, 2015. **133**, 532-543 DOI: 10.1111/jnc.12988.

33. Guo, Y.e., N. Suo, X. Cui, Q. Yuan, and X. Xie *Vitamin C promotes oligodendrocytes generation and remyelination*. Glia, 2018. **66**, 1302-1316 DOI: 10.1002/glia.23306.
34. Osaki, T., Y. Shin, V. Sivathanu, M. Campisi, and R.D. Kamm *In vitro microfluidic models for neurodegenerative disorders*. Advanced Healthcare Materials, 2018. **7**, 1700489 DOI: 10.1002/adhm.201700489.
35. Lopes, C.D., C.P. Gomes, E. Neto, P. Sampaio, P. Aguiar, and A.P. Pêgo *Microfluidic-based platform to mimic the in vivo peripheral administration of neurotropic nanoparticles*. Nanomedicine, 2016. **11**, 3205-3221 DOI: 10.2217/nnm-2016-0247.
36. Yi, Y., J. Park, J. Lim, C.J. Lee, and S.-H. Lee *Central nervous system and its disease models on a chip*. Trends in Biotechnology, 2015. **33**, 762-776 DOI: 10.1016/j.tibtech.2015.09.007.
37. Kerman, B.E., H.J. Kim, K. Padmanabhan, A. Mei, S. Georges, M.S. Joens, J.A. Fitzpatrick, R. Jappelli, K.J. Chandross, and P. August *In vitro myelin formation using embryonic stem cells*. Development, 2015. **142**, 2213-2225 DOI: 10.1242/dev.116517.
38. Chen, S., C. Wu, A. Liu, D. Wei, Y. Xiao, Z. Guo, L. Chen, Y. Zhu, J. Sun, and H. Luo *Biofabrication of nerve fibers with mimetic myelin sheath-like structure and aligned fibrous niche*. Biofabrication, 2020. DOI: 10.1088/1758-5090/ab860d.
39. Hyvärinen, T., S. Hagman, M. Ristola, L. Sukki, K. Veijula, J. Kreutzer, P. Kallio, and S. Narkilahti *Co-stimulation with IL-1β and TNF-α induces an inflammatory reactive astrocyte phenotype with neurosupportive characteristics in a human pluripotent stem cell model system*. Scientific Reports, 2019. **9**, 1-15 DOI: 10.1038/s41598-019-53414-9.
40. Jeong, S., S. Kim, J. Buonocore, J. Park, C.J. Welsh, J. Li, and A. Han *A three-dimensional arrayed microfluidic blood–brain barrier model with integrated electrical sensor array*. IEEE Transactions on Biomedical Engineering, 2017. **65**, 431-439 DOI: 10.1109/TBME.2017.2773463.
41. Rocha, D.N., E.D. Carvalho, and A.P. Pêgo *High-throughput platforms for the screening of new therapeutic targets for neurodegenerative diseases*. Drug Discovery Today, 2016. **21**, 1355-1366 DOI: 10.1016/j.drudis.2016.05.005.
42. Tan, G.A., K.L. Furber, M.P. Thangaraj, L. Sobchishin, J.R. Doucette, and A.J. Nazarali *Organotypic cultures from the adult CNS: a novel model to study demyelination and remyelination ex vivo*. Cellular and Molecular Neurobiology, 2018. **38**, 317-328 DOI: 10.1007/s10571-017-0529-6.
43. Liu, Y., K.S. Given, D.E. Harlow, A.M. Matschulat, W.B. Macklin, J.L. Bennett, and G.P. Owens *Myelin-specific multiple sclerosis antibodies cause complement-dependent oligodendrocyte loss and demyelination*. Acta Neuropathologica Communications, 2017. **5**, 25 DOI: 10.1186/s40478-017-0428-6.
44. Liu, Y., K.S. Given, G.P. Owens, W.B. Macklin, and J.L. Bennett *Distinct patterns of glia repair and remyelination in antibody-mediated demyelination models of multiple sclerosis and neuromyelitis optica*. Glia, 2018. **66**, 2575-2588 DOI: 10.1002/glia.23512.
45. Zhuang, P., A.X. Sun, J. An, C.K. Chua, and S.Y. Chew *3D neural tissue models: From spheroids to bioprinting*. Biomaterials, 2018. **154**, 113-133 DOI: 10.1016/j.biomaterials.2017.10.002.
46. Vereyken, E., D. Fluitsma, M. Bolijn, C. Dijkstra, and C. Teunissen *An in vitro model for de-and remyelination using lysophosphatidyl choline in rodent whole brain spheroid cultures*. Glia, 2009. **57**, 1326-1340 DOI: 10.1002/glia.20852.
47. Bedir, T., S. Ulag, C.B. Ustundag, and O. Gunduz *3D bioprinting applications in neural tissue engineering for spinal cord injury repair*. Materials Science and Engineering: C, 2020. 110741 DOI: 10.1016/j.msec.2020.110741.

48. Qiu, B., N. Bessler, K. Figler, M.-B. Buchholz, A.C. Rios, J. Malda, R. Levato, and M. Caiazzo *Bioprinting Neural Systems to Model Central Nervous System Diseases*. Advanced Functional Materials, 2020. **n/a**, 1910250 DOI: 10.1002/adfm.201910250.
49. Ong, W., J. Lin, M.E. Bechler, K. Wang, M. Wang, and S.Y. Chew *Microfiber drug/gene delivery platform for study of myelination*. Acta Biomaterialia, 2018. **75**, 152-160 DOI: 10.1016/j.actbio.2018.06.011.
50. Lee, S., M.K. Leach, S.A. Redmond, S.C. Chong, S.H. Mellon, S.J. Tuck, Z.-Q. Feng, J.M. Corey, and J.R. Chan *A culture system to study oligodendrocyte myelination processes using engineered nanofibers*. Nature Methods, 2012. **9**, 917-922 DOI: 10.1038/nmeth.2105.
51. Mei, F., S.P. Fancy, Y.-A.A. Shen, J. Niu, C. Zhao, B. Presley, E. Miao, S. Lee, S.R. Mayoral, and S.A. Redmond *Micropillar arrays as a high-throughput screening platform for therapeutics in multiple sclerosis*. Nature Medicine, 2014. **20**, 954-960 DOI: 10.1038/nm.3618.
52. Fang, A., Z. Hao, L. Wang, D. Li, J. He, L. Gao, X. Mao, and R. Paz *In vitro model of the glial scar*. International Journal of Bioprinting, 2019. **5**, DOI: 10.18063/ijb.v5i2.235.
53. East, E., J.P. Golding, and J.B. Phillips *A versatile 3D culture model facilitates monitoring of astrocytes undergoing reactive gliosis*. Journal of Tissue Engineering and Regenerative Medicine, 2009. **3**, 634-646 DOI: 10.1002/term.209.
54. East, E., J.P. Golding, and J.B. Phillips *Engineering an integrated cellular interface in three-dimensional hydrogel cultures permits monitoring of reciprocal astrocyte and neuronal responses*. Tissue Engineering Part C: Methods, 2012. **18**, 526-536 DOI: 10.1089/ten.tec.2011.0587.
55. Khoshakhlagh, P., A. Sivakumar, L.A. Pace, D.W. Sazer, and M.J. Moore *Methods for fabrication and evaluation of a 3D microengineered model of myelinated peripheral nerve*. Journal of Neural Engineering, 2018. **15**, 064001 DOI: 10.1088/1741-2552/aae129.
56. Sharma, A.D., L. McCoy, E. Jacobs, H. Willey, J.Q. Behn, H. Nguyen, B. Bolon, J.L. Curley, and M.J. Moore *Engineering a 3D functional human peripheral nerve in vitro using the Nerve-on-a-Chip platform*. Scientific Reports, 2019. **9**, 1-12 DOI: 10.1038/s41598-019-45407-5.
57. de la Vega, L., C. Lee, R. Sharma, M. Amereh, and S.M. Willerth, *3D bioprinting models of neural tissues: the current state of the field and future directions.* Brain Research Bulletin, 2019.
58. Knowlton, S., S. Anand, T. Shah, and S. Tasoglu *Bioprinting for neural tissue engineering*. Trends in Neurosciences, 2018. **41**, 31-46 DOI: 10.1016/j.tins.2017.11.001.
59. Kačarević, Ž.P., P.M. Rider, S. Alkildani, S. Retnasingh, R. Smeets, O. Jung, Z. Ivanišević, and M. Barbeck *An introduction to 3D bioprinting: possibilities, challenges and future aspects*. Materials, 2018. **11**, 2199 DOI: 10.3390/ma11112199.
60. Thomas, M. and S.M. Willerth *3-D bioprinting of neural tissue for applications in cell therapy and drug screening*. Frontiers in Bioengineering and Biotechnology, 2017. **5**, 69 DOI: 10.3389/fbioe.2017.00069.
61. Lee, S.J., T. Esworthy, S. Stake, S. Miao, Y.Y. Zuo, B.T. Harris, and L.G. Zhang *Advances in 3D bioprinting for neural tissue engineering*. Advanced Biosystems, 2018. **2**, 1700213 DOI: 10.1002/adbi.201700213.
62. Gungor-Ozkerim, P.S., I. Inci, Y.S. Zhang, A. Khademhosseini, and M.R. Dokmeci *Bioinks for 3D bioprinting: an overview*. Biomaterials Science, 2018. **6**, 915-946 DOI: 10.1039/c7bm00765e.
63. Cui, X., J. Li, Y. Hartanto, M. Durham, J. Tang, H. Zhang, G. Hooper, K. Lim, and T. Woodfield *Advances in Extrusion 3D Bioprinting: A Focus on Multicomponent Hydrogel-Based Bioinks*. Advanced Healthcare Materials, 2020. 1901648 DOI: 10.1002/adhm.201901648.

64. Joung, D., V. Truong, C.C. Neitzke, S.Z. Guo, P.J. Walsh, J.R. Monat, F. Meng, S.H. Park, J.R. Dutton, and A.M. Parr *3D Printed Stem-Cell Derived Neural Progenitors Generate Spinal Cord Scaffolds*. Advanced Functional Materials, 2018. **28**, 1801850 DOI: 10.1002/adfm.201801850.
65. Salaris, F., C. Colosi, C. Brighi, A. Soloperto, V. de Turris, M.C. Benedetti, S. Ghirga, M. Rosito, S. Di Angelantonio, and A. Rosa *3D Bioprinted Human Cortical Neural Constructs Derived from Induced Pluripotent Stem Cells*. Journal of Clinical Medicine, 2019. **8**, 1595 DOI: 10.3390/jcm8101595.
66. Camacho, P., H. Busari, K.B. Seims, J.W. Tolbert, and L.W. Chow, *Materials as Bioinks and Bioink Design*, in *3D Bioprinting in Medicine*. 2019, Springer. p. 67-100.
67. Hospodiuk, M., M. Dey, D. Sosnoski, and I.T. Ozbolat *The bioink: A comprehensive review on bioprintable materials*. Biotechnology Advances, 2017. **35**, 217-239 DOI: 10.1016/j.biotechadv.2016.12.006.
68. Aljohani, W., M.W. Ullah, X. Zhang, and G. Yang *Bioprinting and its applications in tissue engineering and regenerative medicine*. International Journal of Biological Macromolecules, 2018. **107**, 261-275 DOI: doi.org/10.1016/j.ijbiomac.2017.08.171.
69. Ching, S.H., N. Bansal, and B. Bhandari *Alginate gel particles–A review of production techniques and physical properties*. Critical Reviews in Food Science and Nutrition, 2017. **57**, 1133-1152 DOI: 10.1080/10408398.2014.965773.
70. Rastogi, P. and B. Kandasubramanian *Review of alginate-based hydrogel bioprinting for application in tissue engineering*. Biofabrication, 2019. **11**, 042001 DOI: 10.1088/1758-5090/ab331e.
71. Neves, M.I., L. Moroni, and C.C. Barrias *Modulating alginate hydrogels for improved biological performance as cellular 3D microenvironments*. Frontiers in Bioengineering and Biotechnology, 2020. **8**, DOI: 10.3389/fbioe.2020.00665.
72. Zhao, Y.-H., C.-M. Niu, J.-Q. Shi, Y.-Y. Wang, Y.-M. Yang, and H.-B. Wang *Novel conductive polypyrrole/silk fibroin scaffold for neural tissue repair*. Neural Regeneration Research, 2018. **13**, 1455 DOI: 10.4103/1673-5374.235303.
73. Heo, D.N., S.-J. Lee, R. Timsina, X. Qiu, N.J. Castro, and L.G. Zhang *Development of 3D printable conductive hydrogel with crystallized PEDOT: PSS for neural tissue engineering*. Materials Science and Engineering: C, 2019. **99**, 582-590 DOI: 10.1016/j.msec.2019.02.008.
74. Zhu, W., B.T. Harris, and L.G. Zhang *Gelatin methacrylamide hydrogel with graphene nanoplatelets for neural cell-laden 3D bioprinting*. 2016 38th Annual International Conference of the IEEE Engineering in Medicine and Biology Society (EMBC), 2016. 4185-4188 DOI: 10.1109/EMBC.2016.7591649.
75. Bordoni, M., E. Karabulut, V. Kuzmenko, V. Fantini, O. Pansarasa, C. Cereda, and P. Gatenholm *3D Printed Conductive Nanocellulose Scaffolds for the Differentiation of Human Neuroblastoma Cells*. Cells, 2020. **9**, 682 DOI: 10.3390/cells9030682.
76. Fantini, V., M. Bordoni, F. Scocozza, M. Conti, E. Scarian, S. Carelli, A.M. Di Giulio, S. Marconi, O. Pansarasa, and F. Auricchio *Bioink Composition and Printing Parameters for 3D Modeling Neural Tissue*. Cells, 2019. **8**, 830 DOI: 10.3390/cells8080830.
77. Ouyang, L., J.P. Armstrong, Y. Lin, J.P. Wojciechowski, C. Lee-Reeves, D. Hachim, K. Zhou, J.A. Burdick, and M.M. Stevens *Expanding and optimizing 3D bioprinting capabilities using complementary network bioinks*. Science Advances, 2020. **6**, eabc5529 DOI: 10.1126/sciadv.abc5529.
78. Zhou, L., A.C. Wolfes, Y. Li, D.C. Chan, H. Ko, F.G. Szele, and H. Bayley *Lipid-bilayer-supported 3D printing of human cerebral cortex cells reveals developmental interactions*. Advanced Materials, 2020. **32**, 2002183 DOI: 10.1002/adma.202002183.
79. Chen, C., M.l. Zhao, R.k. Zhang, G. Lu, C.y. Zhao, F. Fu, H.t. Sun, S. Zhang, Y. Tu, and X.h. Li *Collagen/heparin sulfate scaffolds fabricated by a 3D bioprinter improved mechanical*

properties and neurological function after spinal cord injury in rats. Journal of Biomedical Materials Research Part A, 2017. **105**, 1324-1332 DOI: 10.1002/jbm.a.36011.

80. Koffler, J., W. Zhu, X. Qu, O. Platoshyn, J.N. Dulin, J. Brock, L. Graham, P. Lu, J. Sakamoto, and M. Marsala *Biomimetic 3D-printed scaffolds for spinal cord injury repair*. Nature Medicine, 2019. **25**, 263-269 DOI: 10.1038/s41591-018-0296-z.
81. Ning, L., H. Sun, T. Lelong, R. Guilloteau, N. Zhu, D.J. Schreyer, and X. Chen *3D bioprinting of scaffolds with living Schwann cells for potential nerve tissue engineering applications*. Biofabrication, 2018. **10**, 035014 DOI: 10.1088/1758-5090/aacd30.
82. Haring, A.P., E.G. Thompson, Y. Tong, S. Laheri, E. Cesewski, H. Sontheimer, and B.N. Johnson *Process-and bio-inspired hydrogels for 3D bioprinting of soft free-standing neural and glial tissues*. Biofabrication, 2019. **11**, 025009 DOI: 10.1088/1758-5090/ab02c9.
83. Espinosa-Hoyos, D., A. Jagielska, K.A. Homan, H. Du, T. Busbee, D.G. Anderson, N.X. Fang, J.A. Lewis, and K.J. Van Vliet *Engineered 3D-printed artificial axons*. Scientific Reports, 2018. **8**, 1-13 DOI: 10.1038/s41598-017-18744-6.
84. Wu, Z., Q. Li, S. Xie, X. Shan, and Z. Cai *In vitro and in vivo biocompatibility evaluation of a 3D bioprinted gelatin-sodium alginate/rat Schwann-cell scaffold*. Materials Science and Engineering: C, 2020. **109**, 110530 DOI: 10.1016/j.msec.2019.110530.
85. Ristola, M., L. Sukki, M.M. Azevedo, A.I. Seixas, J.B. Relvas, S. Narkilahti, and P. Kallio *A compartmentalized neuron-oligodendrocyte co-culture device for myelin research: design, fabrication and functionality testing*. Journal of Micromechanics and Microengineering, 2019. **29**, 065009 DOI: 10.1088/1361-6439/ab16a7.
86. Fonseca, K.B., S.J. Bidarra, M.J. Oliveira, P.L. Granja, and C.C. Barrias *Molecularly designed alginate hydrogels susceptible to local proteolysis as three-dimensional cellular microenvironments*. Acta Biomaterialia, 2011. **7**, 1674-1682 DOI: 10.1016/j.actbio.2010.12.029.
87. Hearn, E., *CHAPTER 14 - COMPLEX STRAIN AND THE ELASTIC CONSTANTS*, in *Mechanics of Materials*. 1997, Butterworth-Heinemann: Oxford. p. 361-400.
88. Ahearne, M., Y. Yang, A.J. El Haj, K.Y. Then, and K.-K. Liu *Characterizing the viscoelastic properties of thin hydrogel-based constructs for tissue engineering applications*. Journal of the Royal Society Interface, 2005. **2**, 455-463 DOI: 10.1098/rsif.2005.0065.
89. Karvinen, J., T.O. Ihalainen, M.T. Calejo, I. Jönkkäri, and M. Kellomäki *Characterization of the microstructure of hydrazone crosslinked polysaccharide-based hydrogels through rheological and diffusion studies*. Materials Science and Engineering: C, 2019. **94**, 1056-1066 DOI: 10.1016/j.msec.2018.10.048.
90. Kumar, P., A. Nagarajan, and P.D. Uchil *Analysis of cell viability by the alamarBlue assay*. Cold Spring Harbor Protocols, 2018. **2018**, pdb. prot095489 DOI: 10.1101/pdb.prot095489.
91. Lee, K.Y. and D.J. Mooney *Alginate: properties and biomedical applications*. Progress in Polymer Science, 2012. **37**, 106-126 DOI: 10.1016/j.progpolymsci.2011.06.003.
92. Instruments, M., *A Basic Introduction to Rheology.* 2016.
93. Yan, C. and D.J. Pochan *Rheological properties of peptide-based hydrogels for biomedical and other applications*. Chemical Society Reviews, 2010. **39**, 3528-3540 DOI: 10.1039/b919449p.
94. Bidarra, S.J., C.C. Barrias, and P.L. Granja *Injectable alginate hydrogels for cell delivery in tissue engineering*. Acta Biomaterialia, 2014. **10**, 1646-1662 DOI: 10.1016/j.actbio.2013.12.006.
95. Dalheim, M.Ø., L.A. Omtvedt, I.M. Bjørge, A. Akbarzadeh, J.F. Mano, F.L. Aachmann, and B.L. Strand *Mechanical Properties of Ca-Saturated Hydrogels with Functionalized Alginate*. Gels, 2019. **5**, 23 DOI: 10.3390/gels5020023.

96. Wright, B., P.A. De Bank, K.A. Luetchford, F.R. Acosta, and C.J. Connon *Oxidized alginate hydrogels as niche environments for corneal epithelial cells*. Journal of Biomedical Materials Research Part A, 2014. **102**, 3393-3400 DOI: 10.1002/jbm.a.35011.
97. Hashemnejad, S.M. and S. Kundu *Rheological properties and failure of alginate hydrogels with ionic and covalent crosslinks*. Soft Matter, 2019. **15**, 7852-7862 DOI: 10.1039/c9sm01039d.
98. Moxon, S.R., N.J. Corbett, K. Fisher, G. Potjewyd, M. Domingos, and N.M. Hooper *Blended alginate/collagen hydrogels promote neurogenesis and neuronal maturation*. Materials Science and Engineering: C, 2019. **104**, 109904 DOI: 10.1016/j.msec.2019.109904.
99. da Rocha Mar, D.N., *Impact of Mechanotransduction in the Context of Central Nervous System Diseases*. 2015.
100. Giordano, G., S. Hong, E.M. Faustman, and L.G. Costa, *Measurements of cell death in neuronal and glial cells*, in *In Vitro Neurotoxicology*. 2011, Springer. p. 171-178.
101. Hiraoka, Y. and K. Kimbara *Rapid assessment of the physiological status of the polychlorinated biphenyl degrader Comamonas testosteroni TK102 by flow cytometry*. Applied and Environmental Microbiology, 2002. **68**, 2031-2035 DOI: 10.1128/AEM.68.4.2031–2035.2002.
102. Pizzimenti, S., E.S. Ciamporcero, M. Daga, P. Pettazzoni, A. Arcaro, G. Cetrangolo, R. Minelli, C. Dianzani, A. Lepore, and F. Gentile *Interaction of aldehydes derived from lipid peroxidation and membrane proteins*. Frontiers in Physiology, 2013. **4**, 242 DOI: 10.3389/fphys.2013.00242.
103. Gomez, C., M. Rinaudo, and M. Villar *Oxidation of sodium alginate and characterization of the oxidized derivatives*. Carbohydrate Polymers, 2007. **67**, 296-304 DOI: 10.1016/j.carbpol.2006.05.025.
104. Szabó, L., S. Gerber-Lemaire, and C. Wandrey *Strategies to Functionalize the Anionic Biopolymer Na-Alginate without Restricting Its Polyelectrolyte Properties*. Polymers, 2020. **12**, 919 DOI: 10.3390/polym12040919.
105. Fonseca, K.B., F.R. Maia, F.A. Cruz, D. Andrade, M.A. Juliano, P.L. Granja, and C.C. Barrias *Enzymatic, physicochemical and biological properties of MMP-sensitive alginate hydrogels*. Soft Matter, 2013. **9**, 3283-3292 DOI: 10.1039/c3sm27560d.
106. Jha, M.K., J.-H. Kim, G.J. Song, W.-H. Lee, I.-K. Lee, H.-W. Lee, S.S.A. An, S. Kim, and K. Suk *Functional dissection of astrocyte-secreted proteins: Implications in brain health and diseases*. Progress in Neurobiology, 2018. **162**, 37-69 DOI: 10.1016/j.pneurobio.2017.12.003.
107. Khakh, B.S. and M.V. Sofroniew *Diversity of astrocyte functions and phenotypes in neural circuits*. Nature Neuroscience, 2015. **18**, 942 DOI: 10.1038/nn.4043.
108. Oberheim, N.A., T. Takano, X. Han, W. He, J.H. Lin, F. Wang, Q. Xu, J.D. Wyatt, W. Pilcher, and J.G. Ojemann *Uniquely hominid features of adult human astrocytes*. Journal of Neuroscience, 2009. **29**, 3276-3287 DOI: 10.1523/JNEUROSCI.4707-08.2009.
109. Seyedhassantehrani, N., Y. Li, and L. Yao *Dynamic behaviors of astrocytes in chemically modified fibrin and collagen hydrogels*. Integrative Biology, 2016. **8**, 624-634 DOI: 10.1039/c6ib00003g.
110. Placone, A.L., P.M. McGuiggan, D.E. Bergles, H. Guerrero-Cazares, A. Quiñones-Hinojosa, and P.C. Searson *Human astrocytes develop physiological morphology and remain quiescent in a novel 3D matrix*. Biomaterials, 2015. **42**, 134-143 DOI: 10.1016/j.biomaterials.2014.11.046.
111. Gao, T., G.J. Gillispie, J.S. Copus, A.K. PR, Y.-J. Seol, A. Atala, J.J. Yoo, and S.J. Lee *Optimization of gelatin–alginate composite bioink printability using rheological parameters: a systematic approach*. Biofabrication, 2018. **10**, 034106 DOI: 10.1088/1758-5090/aacdc7.

112. Tabriz, A.G., M.A. Hermida, N.R. Leslie, and W. Shu *Three-dimensional bioprinting of complex cell laden alginate hydrogel structures*. Biofabrication, 2015. **7**, 045012 DOI: 10.1088/1758-5090/7/4/045012.
113. Cidonio, G., M. Glinka, J. Dawson, and R. Oreffo *The cell in the ink: Improving biofabrication by printing stem cells for skeletal regenerative medicine*. Biomaterials, 2019. **209**, 10-24 DOI: 10.1016/j.biomaterials.2019.04.009.